

Recognising surface versus sub-surface deformation of soft-sediments: Consequences and considerations for palaeoseismic studies

G.I. Alsop^{a,*}, S. Marco^b, T. Levi^c

^a Department of Geology and Geophysics, School of Geosciences, University of Aberdeen, Aberdeen, UK

^b Department of Geophysics, Tel Aviv University, Israel

^c Geological Survey of Israel, Jerusalem, Israel

ARTICLE INFO

Keywords:

Mass transport deposit
Fold and thrust system
Soft-sediment deformation
Dead sea

ABSTRACT

Soft-sediment deformation structures associated with slumps and mass transport deposits (MTDs) are generally considered to form at the surface when un lithified sediment moves downslope under the influence of gravity. Where stratigraphic sequences contain several deformed horizons, the question arises as to whether repeated slope failure at the sediment surface has systematically built-up multiple MTDs in the stratigraphic record in a 'sequential failure model'. Alternatively, a single failure event may concurrently create surficial and sub-surface deformed 'intrastratal' horizons at different stratigraphic levels in a 'synchronous failure model'. The implications of these differing models are important as sub-surface deformation can be significantly younger than the depositional age of beds it affects thereby weakening age-depth correlations used to estimate the timing of palaeo-earthquakes. In order to investigate the potential for sub-surface deformation, we examine the late Pleistocene Lisan Formation exposed around the Dead Sea Basin that contains numerous MTDs and gravity-driven fold and thrust systems. Surficial deformation is recognised by identifying irregular erosive surfaces above MTDs that are overlain by sedimentary caps deposited out of suspension following the failure event. Such surficial deformation is also characterised by thickened sedimentary successions that create 'growth' sequences. Conversely, sub-surface intrastratal deformation is typified by detachment-bound folds and thrusts that are marked by repetitions of stratigraphy across the upper detachment surface, fluidised sediment that intrudes upwards into the overlying sequence, together with abrupt truncations of older faults developed in overburden above the detachment. MTDs created at the surface form relatively competent horizons when subsequently buried as they are internally disrupted and lack 'layer-cake' geometries, while repeated seismicity can lead to dewatering and compaction resulting in 'seismic strengthening'. Later sub-surface deformation may therefore be focussed adjacent to earlier MTDs that influence the mechanical stratigraphy, leading to secondary failures and complications when attempting to 'balance' extension and contraction that may be of different ages. Sub-surface deformation is localised along discrete detachments that carry the overlying sequence downslope as relatively intact slides, affecting what appear to be 'undeformed' beds between individual MTDs. As sub-surface deformation does not directly correlate with sedimentary caps, the rates of movement on deeper detachments remain unconstrained and may be significantly slower than surficial deformation resulting in downslope creep of the sediment pile.

1. Introduction

The downslope movement of subaqueous sediments to create mass transport deposits (MTDs) is increasingly documented across a range of m-km scales in both outcrop-based studies (e.g. Gibert et al., 2005; Garcia-Tortosa et al., 2011; Sharman et al., 2015; Korneva et al., 2016; Sobiesiak et al., 2017; Cardona et al., 2020) and seismic analysis from

offshore areas (e.g. Reis et al., 2016; Scarselli et al., 2016; Jolly et al., 2016; Kumar et al., 2021). MTDs have been recognised from subaqueous settings varying from lacustrine (e.g. Van Daele et al., 2015; Sammartini et al., 2020; Liang et al., 2021) to deep marine (e.g. Huhn et al., 2020), resulting in a number of recent collections of papers (e.g. Van Loon, 2014; Krastel et al., 2014; Lamarche et al., 2016; Ogata et al., 2020; Georgiopolou et al., 2020).

* Corresponding author.

E-mail address: ian.alsop@abdn.ac.uk (G.I. Alsop).

<https://doi.org/10.1016/j.jsg.2021.104493>

Received 10 September 2021; Received in revised form 3 December 2021; Accepted 11 December 2021

Available online 14 December 2021

0191-8141/© 2021 Elsevier Ltd. All rights reserved.

MTDs incorporate several processes including creep, (which is defined as “the slow, more or less continuous downslope movement of mineral, rock, and soil particles under gravitational stresses”; Bates and Jackson, 1980, p.146), slides (where stratigraphy remains intact and downslope movement occurs in coherent sheets), slumps (where the translated mass is internally deformed) and relatively fast debris flows (Posamentier and Martinsen, 2011, p.8; Moscardelli and Wood, 2008; Armandita et al., 2015). Where several MTDs are developed in a sequence then the term mass transport complex (MTC) is commonly applied (e.g. Bull et al., 2009; Ogata et al., 2012, 2014). Such repeated deposits are generally considered to represent recurrent slope failure and are typically separated from one another by intervening undeformed beds deposited during periods of stability (e.g. Kumar et al., 2021). Downslope movement of sediments may be achieved through gravity-driven fold and thrust systems (FATS) that form in the poorly lithified sediments (Alsop et al., 2017a, b; Morley et al., 2017). In such FATS, thrusting can breach the sediment surface and become emergent, or be buried under the sediment pile where intrastratal deformation is bound by upper and lower detachments that create sub-surface duplexes (e.g. Auchter et al., 2016; Alsop et al., 2021a). Auchter et al. (2016, p.13) define intrastratal deformation as “stratigraphically isolated zones of deformation bounded above and below by concordant and undeformed strata”.

Deformation within both surficial MTDs and sub-surface intrastratal FATS is considered to affect unlithified or only poorly-lithified sediments such that soft-sediment deformation (SSD) structures are produced (see Maltman 1984, 1994a, b for definitions of SSD; Shanmugam, 2017). SSD folds created during gravity-driven slumping share a close morphological similarity with folds and structures formed during tectonic deformation, potentially complicating their distinction especially in the rock record (e.g. Maltman, 1994a; Festa et al., 2016; Alsop et al., 2019). SSD can be triggered by either external deformation (allogenic/exogenic triggers), such as tectonics and earthquakes, or by processes that develop in the depositional environment (autogenic/endogenic triggers), including rapid sedimentation and floods (e.g., Chakraborty et al., 2019). These different triggers have been discussed by Moretti and Sabato (2007); Moretti and Van Loon (2014) and Van Loon (2014).

While it has previously been recognised from outcrop and seismic data that MTDs can ‘ride’ on lower or ‘basal’ detachments (e.g. Alves, 2015; Cardona et al., 2020; Kumar et al., 2021), it is generally assumed that their upper bounding surface was emergent and formed an irregular bathymetry on the seabed (Frey-Martinez et al., 2005, 2006; Ireland et al., 2011; Sobiesiak et al., 2020, p.99). This uneven surface, if buried by subsequent sedimentation, will be preserved as an unconformity in the stratigraphic record. The lower detachment may also ramp up to the sediment surface where it forms a basal shear zone as it over-rides the downslope sediments in frontally-emergent MTDs (Frey-Martinez et al., 2005, 2006; Sobiesiak et al., 2018). The implication of this model is two-fold: namely a) that all deformation in MTDs is surficial, and b) that all deformation is the same age or only slightly younger than the unlithified stratigraphy it affects. This close association between the age of sediment deposition and the timing of surficial deformation allows the dating of sediments to ‘bracket’ the age of deformation, and hence the date of earthquakes in seismogenic MTDs.

If deformation and associated structures are shown to be much younger and form in the sub-surface after sediments are buried, as in the case of some intrastratal FATS, then no clear or simple relationship can be drawn between the age of sediments and timing of deformation. In this case, Törö and Pratt (2016, p.197) have noted that such intrastratal deformation hinders analysis of seismic recurrence intervals as it “increases the degree of uncertainty in the timing” and the value of SSDs in palaeoseismic studies is thereby diminished and could even be counterproductive. Furthermore, O’Leary and Laine (1996, p.305) highlight the difficulty in distinguishing surface versus sub-surface structures and state that “Intrastratal deformation is easily confused with buried slump or slide deposits formed initially at the sea floor”. Given the significant

implications of misidentifying surface and sub-surface deformation, we therefore aim to provide and catalogue some diagnostic outcrop-based criteria that help discriminate between structures formed in the two settings.

Distinguishing erosive truncations that cut surficial MTD structures from cut-offs linked to detachments and bed-parallel slip is crucial. The importance of erosive surfaces in distinguishing SSDs formed at the surface, versus those that potentially formed at depth, has been recognised by a range of authors. Törö and Pratt (2016, p.180) note that intrastratal deformation is marked by an absence of overlying truncations created by erosive processes on the lake floor, combined with a transition into overlying and underlying beds that remain undeformed. Van Loon et al. (2016) and Belzyt et al. (2021) examined sediments deformed during post-glacial rebound and consider that deformed horizons at different stratigraphic levels are largely created by different seismic events. Conversely, Gibert et al. (2011) suggest that multiple deformed horizons may form at different stratigraphic levels during the same seismic event, while Törö and Pratt (2016, p.197) note that “it is possible a single earthquake could deform two or more closely spaced intervals separated by intact beds”. In order to link deformation to the sediment surface, it is of critical importance to identify erosive surfaces that cut underlying structures and this concept is applied to the analysis of MTDs.

While it has been suggested that some MTDs might conceal more than one seismic event, (Alsop and Marco, 2011; Alsop et al., 2016, 2020a; Jablonska et al., 2016, 2018), the role of younger deformation affecting buried sequences that contain older MTDs has so far not received the same attention. The aim of this work is therefore to provide clear descriptions and examples of structures that form at the sediment surface versus those that form in the sub-surface. The main research questions addressed are:

- Which surface and sub-surface deformation models are applicable to MTDs?
- What are the key diagnostic criteria to identify surface and sub-surface deformation?
- What controls where and when sub-surface deformation localises?
- What are the consequences of sub-surface deformation in MTDs?

Finely laminated sediments that are deposited in lacustrine settings act as an ideal template to record SSD. Such sequences are therefore increasingly used to constrain earthquake recurrence in palaeoseismic studies based on outcrops and in successions investigated via drill cores (e.g. Törö and Pratt, 2016; Hou et al., 2020; Gao et al., 2020; Lu et al., 2021a, b). We focus our attention on MTDs and horizons of SSD that are generally <1 m thick as these thinner deformed intervals can more precisely define earthquake events and have therefore been used for accurate and detailed palaeoseismic analysis in the stratigraphic record (e.g. Agnon et al., 2006; Dechen and Aiping, 2012; Hou et al., 2020; Tang et al., 2020; Belzyt et al., 2021).

2. Models of surficial versus sub-surface deformation of sediments

Deformation of poorly consolidated or only partially lithified sediments at the surface or sub-surface is known as soft-sediment deformation (SSD) (e.g. Maltman, 1984). This process has been described in terms of independent particulate flow that analyses the relationship between pore fluid pressure and cohesive strength due to grain weight (Knipe, 1986). Hydroplastic deformation develops where fluid pressure is less than grain weight and results in primary bedding being modified into structures such as folds similar to those observed in metamorphic rocks (see Alsop et al., 2020b). Conversely, liquefaction forms where fluid pressure is equal to grain weight leading to laminar flow of sediment and consequent destruction of bedding (e.g. Obermeier, 2009). Liquefaction occurs when “when grain weight is temporarily transferred

to the pore fluid, through either the collapse of a loose grain packing or an increase in pore-fluid pressure” resulting in short-lived failure (Owen and Moretti, 2011, p.141). Finally, if fluid pressure exceeds grain weight then fluidisation develops in which grains are entrained and carried in turbulent flow that destroys bedding. Fluidisation is defined by Owen and Moretti (2011, p.141) as occurring “when the upward-directed shear of fluid flowing through a porous medium counteracts the grain weight, reducing the material strength”. Fluidisation can lead to the injection of sediments into overlying sequences, indicating that the fluidised layer was buried at the time of deformation, which in some cases may be km’s below the surface (e.g. Palladino et al., 2016, 2018, 2021). Horizons of SSDs created by variable components of hydroplastic deformation, liquefaction and fluidisation can form in a range of environments including accretionary complexes (e.g. Ogawa and Mori, 2021), although we here focus on surficial MTDs or sub-surface intrastratal FATS developed in gravity-driven systems. There are effectively two end member models when interpreting multiple horizons of SSD at different stratigraphic levels within a sedimentary sequence.

2.1. Sequential failure model

In the first model, that we term the ‘*sequential failure model*’, it is considered that each successive horizon of SSDs represents a new surficial event and that deformation therefore occurred sequentially up through the sediment pile as new beds were deposited (e.g. see Sammartini et al., 2020 p.217; Kumar et al., 2021) (Fig. 1a). In our schematic summary, failure occurred in surficial sediments and created MTD 1 in time 2, while an overlying sedimentary cap was deposited out of suspension immediately afterwards in time 3 (Fig. 1a). The sedimentary cap is formed of fine-grained sediment that was thrown into suspension during slope failure and subsequently settled through the water column to create a depositional cap that drapes the underlying MTD (e.g. Alsop et al., 2021a). Overlying sediments accumulated prior to a further failure event 2 that affected surficial sediments at time 6 (Fig. 1a). Repeated surficial failures therefore sequentially created multiple MTD horizons through the succession. As deformation was contemporaneous with deposition, the number of deformed MTD horizons and associated sedimentary caps therefore represents the number of failure events.

2.2. Synchronous failure model

In the second model, that we term the ‘*synchronous failure model*’, it is considered that multiple SSDs form at different stratigraphic levels at the same time (Fig. 1b). In this scenario, some deformed horizons develop at, or close to, the contemporary surface, whereas others form deeper in the sediment pile during intrastratal deformation. Intrastratal deformation has long been recognised in sedimentary sequences with large-scale gravity-driven ‘intraformational sliding’ beneath overlying sediments being reported by Baldry (1938) and Brown (1938) (see Miller, 1922; Williams, 1960 and Maltman, 1994a, p.18 for historical perspectives). Rich (1950, p.729) suggested that unconsolidated and fluid rich layers “served as a zone of gliding along which the entire mass of overlying sediment crept down a slope and, in the process, crumpled the bedding within the siltstone”. More recently, Törő and Pratt (2015b, p.382) show several stacked intrastratal deformation horizons displaying duplex structures and separated by undeformed beds on the m scale. They also recognised MTDs in the same sequence that are marked by erosive bases that formed at the sediment surface.

In our schematic summary of the synchronous failure model, the first failure event (1) did not occur until time 6 after a significant thickness of sediment had already been deposited (Fig. 1b). This failure event occurred in surficial sediments and created MTD 1 in time 6, and also developed concurrently in the sub-surface where a detachment-bound intrastratal FATS formed in the buried sediments (Fig. 1b). This sub-surface failure in time 6 deformed sediments that were originally deposited in time 1 and are therefore significantly older (Fig. 1b). It

therefore represents an instance of younger structures forming at depth in an older sequence, with a single failure event creating synchronous surficial (MTD) and sub-surface intrastratal deformation in the sequence (Fig. 1b). As deformation was contemporaneous with a single event, but not necessarily with deposition of the deformed beds that it affects, then multiple deformed horizons can form synchronously that significantly post-date the age of sediment (Fig. 1b). Importantly, the number of deformed MTD and intrastratal FATS horizons does not therefore represent the number of failure events.

2.3. Secondary failure model

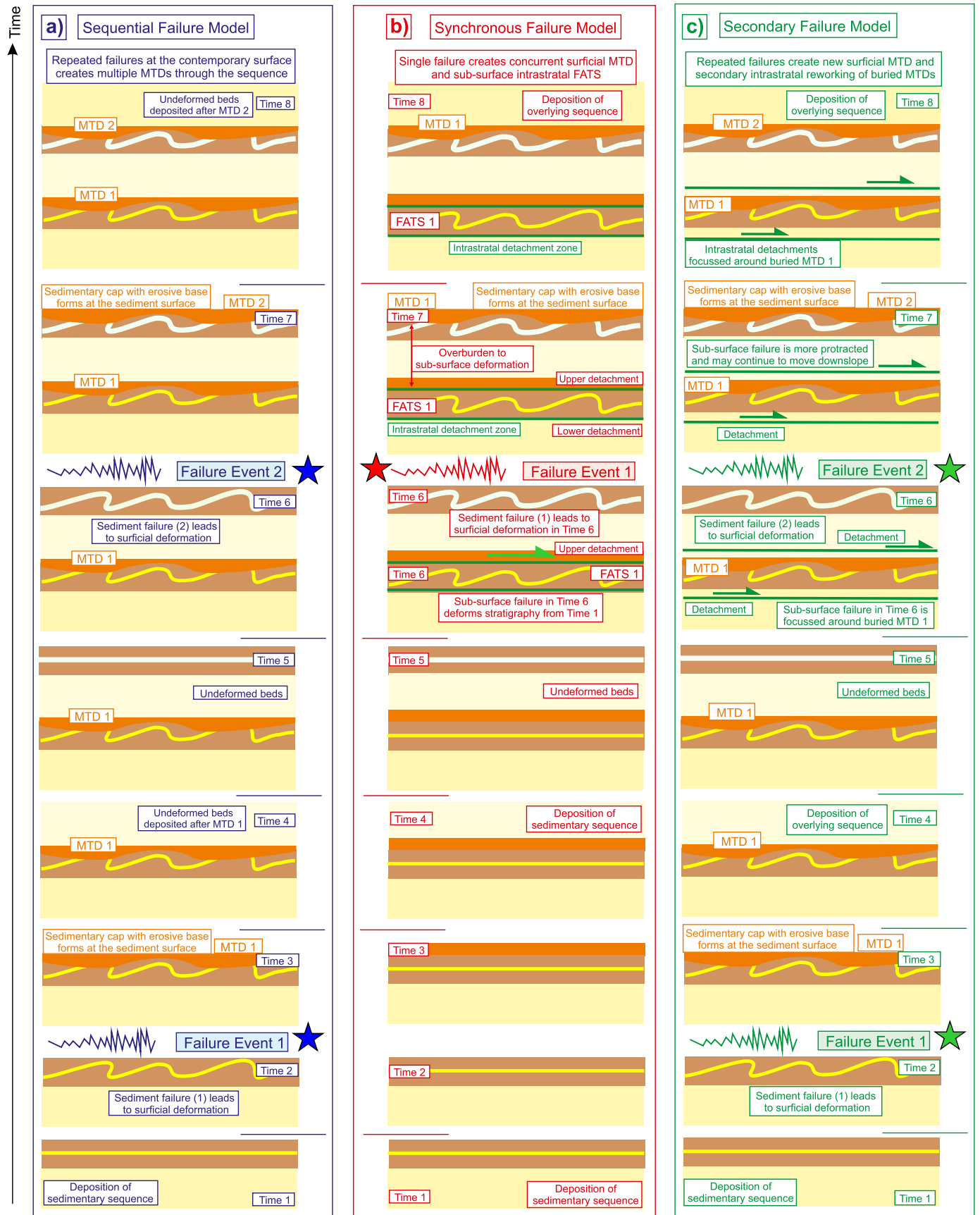
It is entirely possible that variations of the synchronous model develop and early MTDs, that later become buried in the sequence, control where secondary deformation and reworking forms in the sub-surface (Fig. 1c). This was recognised from high resolution seismics by O’Leary and Laine (1996, p.308) who state that “both mass movement and intrastratal deformation may figure in the origin of a single layer”. In our schematic summary, failure initially occurred at the surface to create MTD 1 in time 2, and this was later covered by overburden (Fig. 1c). During a second failure event during time 6, a new surficial MTD 2 was formed at the same time as secondary deformation was focussed along the boundaries of the earlier MTD 1 in the sub-surface (Fig. 1c). Reworking results in detachments and reflects the control exerted by the earlier MTD 1 on the mechanical stratigraphy. Bed-parallel detachments that developed along earlier MTDs result in slides where relatively intact stratigraphy moves downslope over a period of time. Clearly reworking of earlier MTDs by later secondary deformation could result in overprinting of surficial structures and a potential for miscounting the number of deformational events.

In our schematic summary we only show two failure events in each model (Fig. 1a, c), but the process of several horizons being deformed at the same time may be repeated up through the sequence during deposition of successive layers and repeated major events. This ultimately builds a stratigraphy containing numerous deformed horizons separated by apparently undeformed beds, as frequently observed in successions incorporating SSDs and MTDs. In order to distinguish the different end-member models, we need to carefully explore the relationships between deformation and the sediment surface as the ‘*sequential failure model*’ largely restricts deformation to the sediment-water interface marked by syn-depositional structures, whereas the ‘*synchronous failure model*’ and ‘*secondary failure model*’ permits sub-surface intrastratal deformation deeper in the sediment pile. We use the late Pleistocene lacustrine sediments of the Dead Sea Basin to test these different models and examine the effects of deformation in sedimentary sequences.

3. Geological setting

3.1. Regional geology

The Dead Sea Basin is a continental depression bound by the left-lateral eastern border fault and the western border fault zone which is characterised by a series of oblique-normal step faults (Fig. 2a and b) (e.g. Marco et al., 1996, 2003; Ken-Tor et al., 2001; Migowski et al., 2004; Begin et al., 2005). The Dead Sea Fault (DSF) system is believed to have been active from the early Miocene to Recent (Nuriel et al., 2017), including during deposition of the late Pleistocene Lisan Formation at 70–14 Ka (e.g. Haase-Schramm et al., 2004). The present study focusses on the Lisan Formation that comprises detrital-rich layers washed into Lake Lisan during flood events, while mm-scale aragonite laminae were precipitated from the hypersaline waters during the summer (Begin et al., 1974; Ben-Dor et al., 2019) (Fig. 3a). Isotopic dating, when linked with counting of the aragonite-detrital varves implies average depositional rates of ~1 mm per year for the Lisan Formation (Prasad et al., 2009). Thicker (>10 cm) detrital-rich beds were deposited more rapidly following major floods and comprise very fine (60–70 µm) sands, while



(caption on next page)

Fig. 1. Cartoons of a) sequential failure model, b) synchronous failure model, and c) secondary failure model with older events (Time 1) at the base of the diagram and younger events (Time 8) towards the top of each column. During sequential failure (a), the contemporary sediment surface fails repeatedly as new sediment is deposited leading to multiple mass transport deposits (MTDs) that in each case form at the time of sediment deposition. The surficial MTDs are cut by an overlying erosive surface and sedimentary cap (in orange) deposited from suspension after each event. During synchronous failure (b), surficial MTDs and sub-surface fold and thrust systems (FATS) form concurrently during a single failure event. Sub-surface FATS are covered by overburden and are therefore not cut by erosive surfaces and sedimentary caps. FATS are bound by upper and lower intrastratal detachments, which deform sediments in the sub-surface that are significantly older than the failure event (e.g. stratigraphy from Time 1 is deformed during Time 6). In the secondary failure model (c), MTDs created during surficial failure become buried and focus later secondary intrastratal deformation and sub-surface detachments along their margins resulting in overprinting structures. (For interpretation of the references to colour in this figure legend, the reader is referred to the Web version of this article.)

thin detrital laminae display grain sizes of $\sim 8\text{--}10\ \mu\text{m}$ (silt) (Haliva-Cohen et al., 2012). Compositionally, the detrital units consist of quartz and calcite grains with minor feldspar and clays (illite-smectite) (Haliva-Cohen et al., 2012). The Lisan Formation is considered to have been fluid saturated at the time of deformation and still contains $\sim 25\%$ fluid content (Arkin and Michaeli, 1986; Frydman et al., 2008).

3.2. Regional patterns of slope failure

The Lisan Formation extends for ~ 100 km along strike and is marked by very low $<1^\circ$ depositional dips that are directed towards the depocentre of the Dead Sea Basin. A range of gravity-driven structures associated with seismically-induced slope failure are created, including bed-parallel detachments (Alsop et al., 2020c), FATS (e.g. Alsop et al., 2021a, b), and MTDs (Alsop et al., 2020d). These structures collectively move sediment downslope towards the centre of the basin resulting in an overall radial pattern of slumping (Alsop et al., 2020a) (Fig. 2a and b). The Lisan Formation on the eastern shores of the Dead Sea in Jordan records westerly-directed movement (El-Isa and Mustafa, 1986), while the southern portion of the basin at Peratzim displays NE-directed slumping, the central portion is marked by E-directed MTDs, and the northern parts of the basin are dominated by SE-directed movements (Fig. 2b). The direction of slumping is supported by anisotropy of magnetic susceptibility (AMS) fabrics (Weinberger et al., 2017). This collective movement of sediment from the basin margins towards the centre results in the Lisan Formation being three times thicker in the depocentre where drill cores penetrate numerous MTDs (Lu et al., 2017, 2021a, b, c; Kagan et al., 2018).

3.3. Rationale for study area

Deformed horizons, breccias, slumps and MTDs within the Lisan Formation are correlated with repeated seismicity generated along the DSF (Marco et al., 1996; Agnon et al., 2006; Levi et al., 2018). In addition, gypsum horizons up to 1 m thick precipitate by overturn and mixing of the water column possibly following major earthquakes (Ichinose and Begin, 2004; Begin et al., 2005). The varve-like laminae of the Lisan Formation preserve detailed structures, making the Dead Sea Basin an ideal place to study sediment failure. The bilaminar sediments, that consist of varying proportions of aragonite and detrital input, simplify the mechanics of the resulting fold and thrust geometries (Alsop et al., 2020a, b, 2021a, b). In addition, the overall control on the kinematics of sediment movement exerted by the regional slope are well constrained, and provides a consistent framework for both surficial and sub-surface deformation. The best sections for structural analysis are preserved in the finely laminated upper ‘White Cliff’ part of the Lisan Formation dated at 31–15 ka (Torfstein et al., 2013). Previous work has shown this part of the Lisan Formation to contain:

- MTDs that are overlain by erosive surfaces and sedimentary caps associated with surficial deformation (Alsop et al., 2018; 2020a),
- shallowly-buried FATS <1 m below the sediment surface that are bound by upper detachments but may locally influence overlying sedimentation (Alsop et al., 2021a),
- intrastratal detachments marked by bed-parallel slip that create slide surfaces at depths of up to 20 m in the sub-surface which represents

the thickness of the upper ‘White Cliff’ Lisan sequence which hosts these structures (Bartov et al., 2002; Alsop et al., 2020c, p.16).

The Lisan Formation therefore contains a spectrum of deformation styles that were created at a range of depths below the sediment surface thereby providing an opportunity to examine the major influences on slope failure. The various types of gravity-driven structure are subsequently cut by clastic dykes which contain sediment that provides optically stimulated luminescence (OSL) dates of between 15 and 7 Ka (Porat et al., 2007). These dates therefore bracket the age of sub-surface deformation, which is younger than 30 Ka (depositional age of the ‘White Cliff’ section of the Lisan Formation) and older than 7 Ka (the age of the youngest cross-cutting clastic dykes).

The present study focuses on structures preserved in the Lisan Formation exposed along the western margins of the Dead Sea Basin at Miflat [N31°:21.42' E35°:22.49'], Masada [N31°:20.02' E35°:21.24'], Peratzim [N31°:04.56' E35°:21.02'], Wadi Zin [N30°:53.41' E35°:17.26'] (Fig. 2b). All of these sites are located $\sim 1\text{--}2$ km east of Cenomanian-Senonian carbonates that outcrop in the footwall of the Dead Sea western border fault zone (Fig. 2b). These marginal areas of Lake Lisan had the potential to periodically dry out, with maximum water depths of 100 m for the period between 70 and 28 Ka, and up to 200 m water depth for a short interval between 26 and 24 Ka (Bartov et al., 2002, 2003). Modern erosion associated with flash floods creates incised wadis that cut through the Lisan Formation and enable examination of vertical sections that form parallel to the movement direction of the earlier slope failures.

4. Criteria used to recognise surficial deformation

4.1. Erosive surfaces

Erosive surfaces that cut pre-existing structures are perhaps the single most important criteria to demonstrate that deformation took place at the surface (e.g. Törő and Pratt, 2016; Van Loon et al., 2016; Belzyt et al., 2021) and we therefore now document examples of these surfaces truncating different underlying structures. For consistency, East (or NE) which represents the downslope direction is towards the right on all figures, while scales on photographs are provided by a 15 mm diameter coin, 10 cm long chequered rule, 20 cm long yellow notebook and 23 cm long hammer.

4.1.1. Erosive surfaces cutting neptunian dykes

Neptunian dykes that are created by sediment infilling open fissures from above are formed at the sediment surface. Within the Lisan Formation, our investigated neptunian dykes are up to 1 m in height, typically widen upwards, and cross-cut the aragonite and detrital laminae that display no offset across the dyke (Fig. 3a and b). The infill to the dyke comprises mixed aragonite and detrital sediment that displays crude sub-horizontal stratification (Fig. 3c). Some dykes are infilled by rounded pebbles and cobbles that have been transported greater distances (Fig. 3c). The lack of associated fracturing and vertical fabrics within the infills indicate that these features are not part of the suite of late clastic dykes injected after deposition of the Lisan Formation (e.g. Levi et al., 2006a, b). We interpret them as ‘neptunian dykes’ associated with syn-depositional infilling of fissures or desiccation

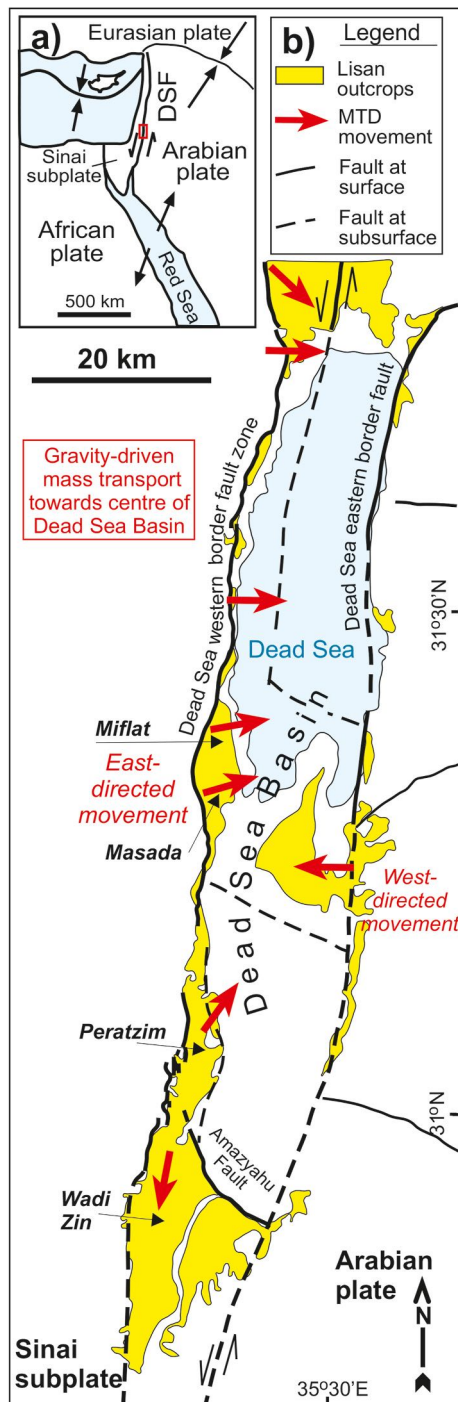


Fig. 2. a) General map showing tectonic plates in the Middle East and location of the Dead Sea Fault (DSF) which transfers opening in the Red Sea to the Taurus-Zagros collision zone. Study area marked by the red box in the Dead Sea Basin. b) Map of the Dead Sea (based on [Sneh and Weinberger, 2014](#)) showing the position of the Miflat, Masada, Peratzim and Wadi Zin localities referred to in the text. The map also highlights the limits of the Lisan Formation, together with the general movement direction of the fold and thrust systems and MTD's around the basin. (For interpretation of the references to colour in this figure legend, the reader is referred to the Web version of this article.)

cracks as Lake Lisan periodically shrank and partially dried up. The neptunian dykes are overlain by an unconformity marked by conglomerates that were deposited during a re-flooding event ([Fig. 3a and b](#)). Unconformity surfaces are irregular and typically erode more deeply into the underlying dykes ([Fig. 3d-g](#)). Neptunian dykes that are

truncated by unconformities are themselves subsequently offset by later normal faults ([Fig. 3d-g](#)). Normal faults are then cut by bed-parallel detachments that represent a subsequent stage of deformation ([Fig. 3d-g](#)). Irregular erosive surfaces potentially overlain by conglomerates and cutting underlying neptunian dykes are a key indicator of surficial processes.

4.1.2. Erosive surfaces cutting soft-sediment folds

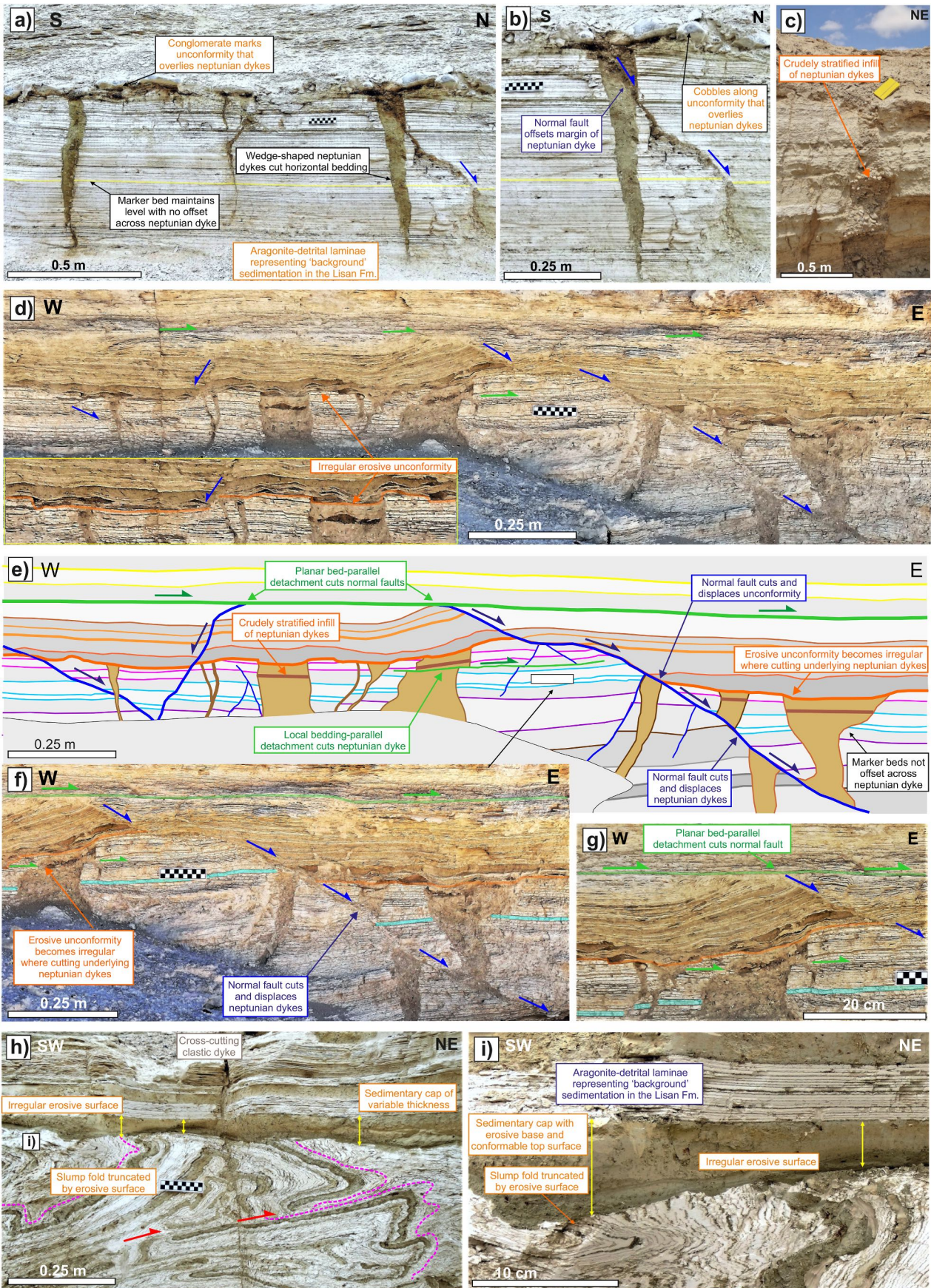
Instances of erosive surfaces cutting across slump folds in the Lisan Formation have been previously reported (e.g. [Alsop et al., 2021a](#)) and we here provide some further cases ([Fig. 3h and i](#)). Soft-sediment slump folds form within MTDs during downslope movement and develop with a range of attitudes from upright to reclined and recumbent ([Alsop et al., 2020b](#)). Irregular erosive surfaces cut directly across the limbs and hinges of both upright and recumbent folds ([Fig. 3h and i](#)). Erosion results in the potential removal of tens of cm's of folded stratigraphy, although the exact amounts are difficult to estimate (e.g. [Fig. 3h](#)). The observation that the erosive surface is irregular and locally cuts up and down the underlying earlier structures is consistent with erosion along the sediment-water interface associated with high-energy flow ([Alsop et al., 2021a](#)).

4.2. Syn-depositional fold style

Within the Lisan Formation, the initiation of folding is often associated with underlying aragonite-rich beds overlain by detrital-rich beds that form upright 'billow' folds ([Alsop and Marco, 2011](#)) ([Fig. 4a and b](#)). The aragonite beds form narrow antiforms separated by broad synforms composed of the detrital-rich units, with the wavelength of the folds being systematically spaced ([Fig. 4a and b](#)). Aragonite-cored antiforms broaden out at the crest, while the detrital-cored synforms broaden towards their troughs ([Fig. 4a and b](#)). This ultimately results in a characteristic 'fanning' arrangement of folds and associated axial planes indicating that the sediments were weak and potentially fluid-rich at the time of deformation ([Alsop et al., 2021a](#)) ([Fig. 4c-e](#)). Folds are truncated by the overlying erosive surfaces and a sedimentary cap indicating that they formed at the sediment-water interface ([Fig. 4c-e](#)). Upright billows are subsequently modified during downslope translation and carried on later thrust ramps ([Fig. 4f and g](#)). Creation of new thrusts results in the upright billow folds being 'back-rotated' away from the vertical, although new secondary vertical folds may grow off the older billows following rotation ([Fig. 4h and i](#)). While billow folds can be modified by continued MTD movement, the initial geometries associated with thickened crests and troughs is characteristic of deformation in weak surficial sediments.

4.3. Sedimentary caps

Erosive surfaces are generally overlain by a 'mixed' bed comprising mud, silt, sand and mm-scale fragments of aragonite and detrital laminae termed a 'sedimentary cap' (e.g. [Alsop et al., 2016, 2019](#)). Such caps are extremely variable in thickness but are generally <10 cm, although locally can exceed 30 cm and infill underlying irregularities along the erosive surfaces (e.g. [Fig. 3h and i](#)). The top of the cap is horizontal and is succeeded by aragonite-rich and detrital-rich couplets representing typical background sedimentation in the Lisan Formation ([Fig. 3h and i, 5a](#)). Sedimentary caps may be graded and also contain 2–3 cm long aragonite fragments that are concentrated towards the base of the bed and interpreted to be clasts 'ripped-up' from the underlying sequence ([Fig. 5a and b](#)). The mixed and graded nature of the sedimentary cap, coupled with the infilling of underlying topography, suggests that it was deposited out of suspension from the water column following the catastrophic downslope movement of surficial sediments in an MTD ([Alsop et al., 2016, 2019](#)). As such it represents syn-slumping deposition confirming that the immediately underlying folding and deformation also formed at the surface.



(caption on next page)

Fig. 3. a) Photograph and close-up (b) of infilled desiccation cracks that form neptunian dykes that are cut by an erosive unconformity marked by cobbles in the Lisan Formation (Wadi Zin). c) Neptunian dyke with the infill displaying a crude horizontal stratification of rounded pebbles (Peratzim). d) Photograph and line drawing (e) of erosive unconformity cutting crudely stratified neptunian dykes. These are then offset by a normal fault, which is subsequently truncated by a bed-parallel detachment. Inset in d) shows details of the irregular erosive unconformity. Photographs f) and g) show close-ups of the normal fault offsetting the neptunian dykes and the normal fault being cut by the detachment, respectively. h) Photograph and i) close-up of an irregular erosive surface truncating the hinge and both limbs of an underlying slump fold. The erosive surface is overlain by a sedimentary cap that infills the underlying topography and has a flat horizontal top surface (Peratzim).

4.4. Syn-depositional faulting - growth sequences across normal faults

The hangingwall of syn-sedimentary normal faults are down-faulted leading to local topography being infilled by the deposition of a greater thickness of sediment to create 'growth faults' (see Fossen, 2016, p.183). In the present case study, MTDs and adjacent beds display a thickening in the hangingwall of normal faults (Fig. 5c–h). Stratigraphy underlying the MTD is thickened on the downthrown side indicating that the normal fault was already active prior to deposition of the MTD (Fig. 5c–e). Sequences overlying the MTD are also thickened on the downthrown side, while they are thinned and 'draped' over the culmination and footwall of the fault, indicating that in this case the active faulting had ceased by the time of their deposition (Fig. 5f–h). In both examples of growth faulting, the syn-sedimentary normal faults are later cut by bed-parallel detachments which generate 'sawtooth' profiles (Alsop et al., 2020c) (Fig. 5f–h). The direct influence on sedimentation of 'growth faults' is clear evidence for MTD deformation at the sediment surface.

4.5. Syn-depositional folding – growth sequences across culminations

4.5.1. Folding at the sediment surface

Deformation at the time of deposition of the sedimentary cap results in laminated aragonite-rich beds being interfolded with the overlying detrital-rich beds and sedimentary cap (Fig. 6a), or with the cap being 'draped' over syn-slumping folds (Fig. 6b). Although the top of the cap remains horizontal and undeformed, the detrital-rich beds that grade into the overlying sedimentary cap display dramatic changes in thickness from the crests of culminations to the troughs of synforms (Fig. 6a and b). This reflects the syn-depositional growth of the folds at the sediment surface. In other cases, culminations comprise folds and thrusts that not only cause a thinning of the sedimentary cap over the crest of the culmination, but also continue to influence deposition of sediments directly above the cap (Fig. 6c–e). The overlying detrital-rich beds onlap directly onto the structural high created by the underlying fold and thrust culmination (Fig. 6c–e). The arching of the sedimentary cap and onlap of younger beds suggests that structures continued to form for some time after deposition of the cap and thereby provides clear evidence for more protracted syn-sedimentary deformation (Fig. 6c–e).

4.5.2. Folding immediately below the sediment surface

The timing of deformation relative to sedimentation is ascertained by examining the thickening or thinning of sediments that overlie culminations created by thrusting and folding. The stratigraphic position of this sedimentary thickening brackets the age of deformation (e.g. Fossen, 2016, p.184).

Thrusts and associated folds are bound by lower and upper detachments to create a duplex in laminated aragonite-rich sediments (Fig. 6f–j). Duplexing creates structural thickening that arches the upper detachment together with 3–4 cm thick panels of overlying sediment that maintain their thicknesses across the culminations, indicating that they were deposited prior to deformation (Fig. 6f–j). The uppermost layers within the arched roof panels are dark-grey detrital-rich beds that display constant 1–2 cm thickness across the underlying duplex and may have influenced mechanical stratigraphy (Fig. 6g, j). The immediately overlying detrital beds exhibit marked thickening off the crest of the culminations suggesting that they were deposited during or slightly after the duplexing that created the underlying structural high and infilled

topography on the lakebed (Fig. 6f–i). These observations, coupled with the lack of a sedimentary cap, suggest that deformation associated with duplexing formed in the shallow sub-surface at depths (<10 cm) that directly influenced deposition of the overlying sequence.

In another case of deformation immediately below the sediment surface, folds and thrusts form above a planar lower detachment and result in duplication and thickening in the fold and thrust package (Fig. 7a–c). This 'lens-shaped' pod is immediately overlain by a 7 cm thick sequence of aragonite and detrital laminae that are arched over the culmination and display little or no variation in thickness. However, a stratigraphically higher 4 cm thick detrital unit erodes into the underlying aragonite laminae and thins to just 1 cm over the crest of the culmination (Fig. 7a–c). The lack of thickness variation in the 7 cm thick arched roof sequence indicates that these sediments were deposited prior to deformation of the underlying sequence, while erosion of this arch, coupled with thinning of the detrital bed, indicates that the culmination formed immediately prior to deposition at this level. The deformation is therefore younger than the sediment it affects and cannot be viewed as synchronous with its deposition, although it is broadly coeval with the thinned detrital bed.

In a further example, fold and thrust beds form an overall lens-shaped pod that is bound by lower and upper detachments. The fold pod depresses the underlying detachment leading to footwall cut-offs of lower beds, while the upper detachment is arched upwards (Fig. 7d–h). The stratigraphic sequence overlying the fold pod maintains its thickness across the culmination and is simply arched upwards. However, beds 0.5 m above the fold pod show thinning over the crest of the culmination while the flanks are thicker, indicating that the underlying fold pod formed in the shallow (<1 m) sub-surface and influenced later sedimentation. This sedimentary signature 0.5 m stratigraphically above the deformed horizon brackets the age of deformation, which is notably younger than the age of the beds it affects.

4.5.3. Stacked erosive surfaces

Evidence for deformation in the shallow sub-surface is provided by multiple unconformity surfaces that are themselves deformed by the growth of an underlying culmination. Upright folding developed along a basal detachment was cut and displaced by a shallowly-dipping thrust (Fig. 7i and j). The overlying sequence is gently folded into a culmination that is truncated by an irregular erosive surface forming a local unconformity (1). Beds overlying this unconformity are also gently warped before being cut by a second unconformity (2) (Fig. 7i and j). The crests of culminations below each unconformity are vertically stacked above one another indicating that there has been no lateral movement across the surfaces. The progressive deformation and arching of older unconformities reflects continued growth of the underlying culmination and indicates that deformation occurred in the shallow sub-surface over a period of time i.e. deformation in the shallow sub-surface occurred at the time of deposition of the overlying 'signature' beds.

5. Criteria used to recognise deeper sub-surface deformation

5.1. Details of detachment surfaces

Bed-parallel detachments are best observed where they truncate earlier cross-cutting features such as steep faults, and can therefore be precisely located within the laminated sediments (e.g. Alsop et al., 2020c) (Fig. 8a–j). In a representative case study from Masada, early

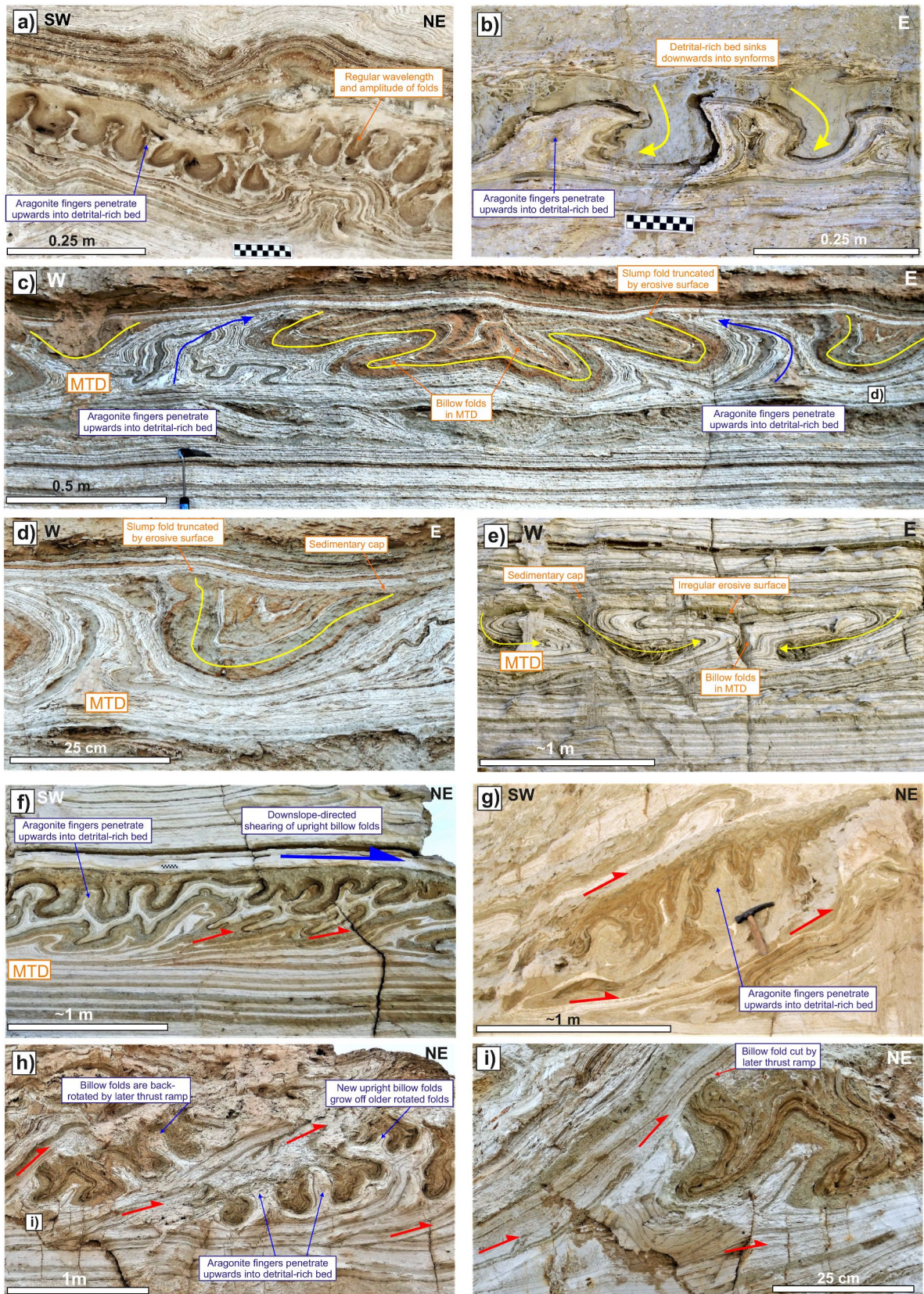


Fig. 4. Photographs of SSD folds formed during density-driven surficial deformation in MTDs. a) Periodically spaced aragonite-cored anticlines that form ‘fingers’ penetrating upwards into overlying detrital-rich sediment (Masada). b) Aragonite-cored anticlines penetrating upwards into detrital-rich sediment that ‘sinks’ downwards into synclines. c) Photograph and d) close-up of billow folds from Miflat, and e) billow folds at Peratzim, where aragonite-cored anticlines rise up into detrital-rich beds that sink downwards into intervening synclines. In each case the surficial folds are cut by an overlying erosive surface and sedimentary cap. f) Upright billow folds that are progressively sheared over during downslope-directed movement of the MTD (Peratzim). g, h, i) Photographs of upright aragonite-cored anticlines that are carried on later thrust ramps (Peratzim). The upright folds are back-rotated on later thrust ramps that cut across them (i).

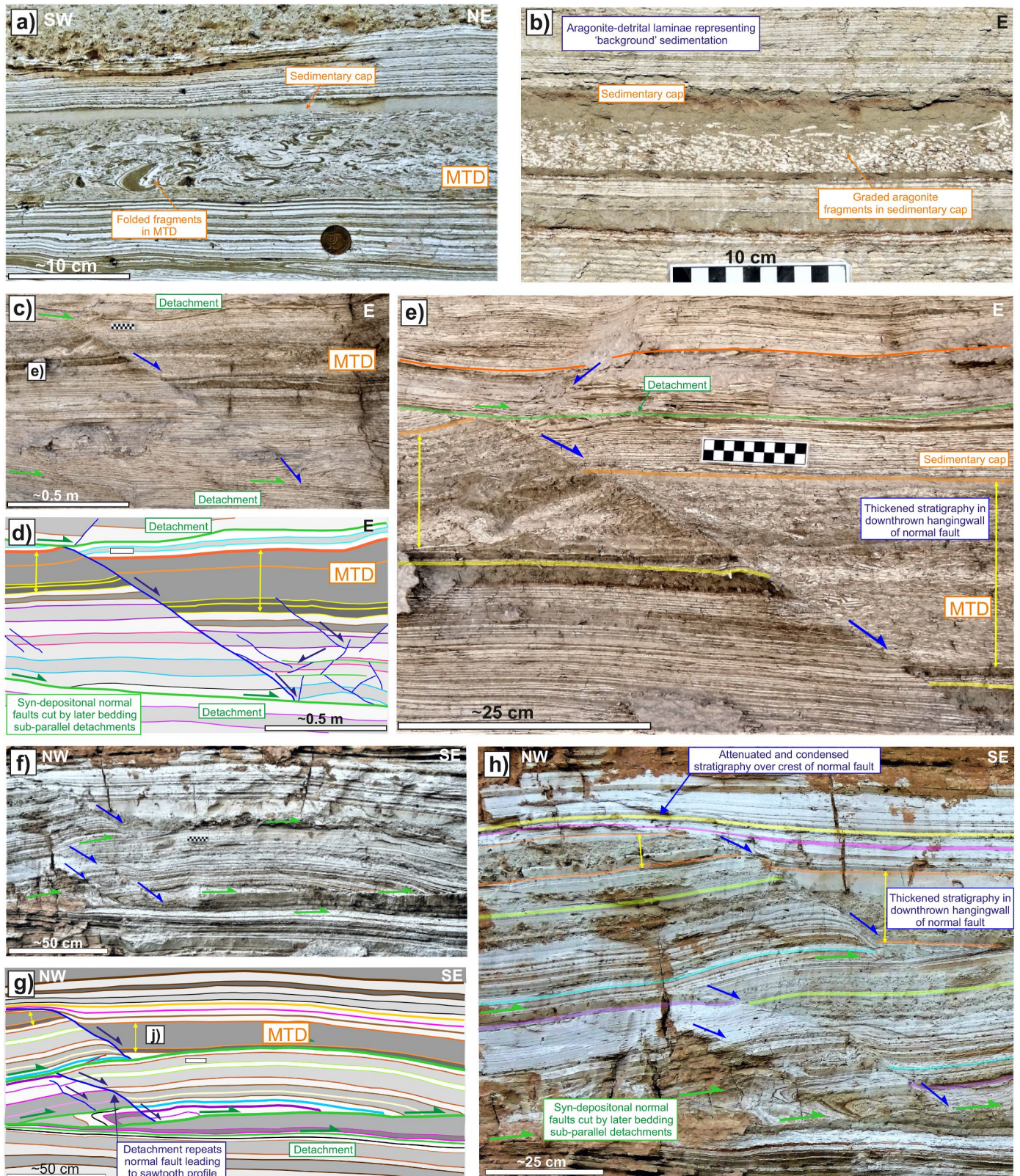
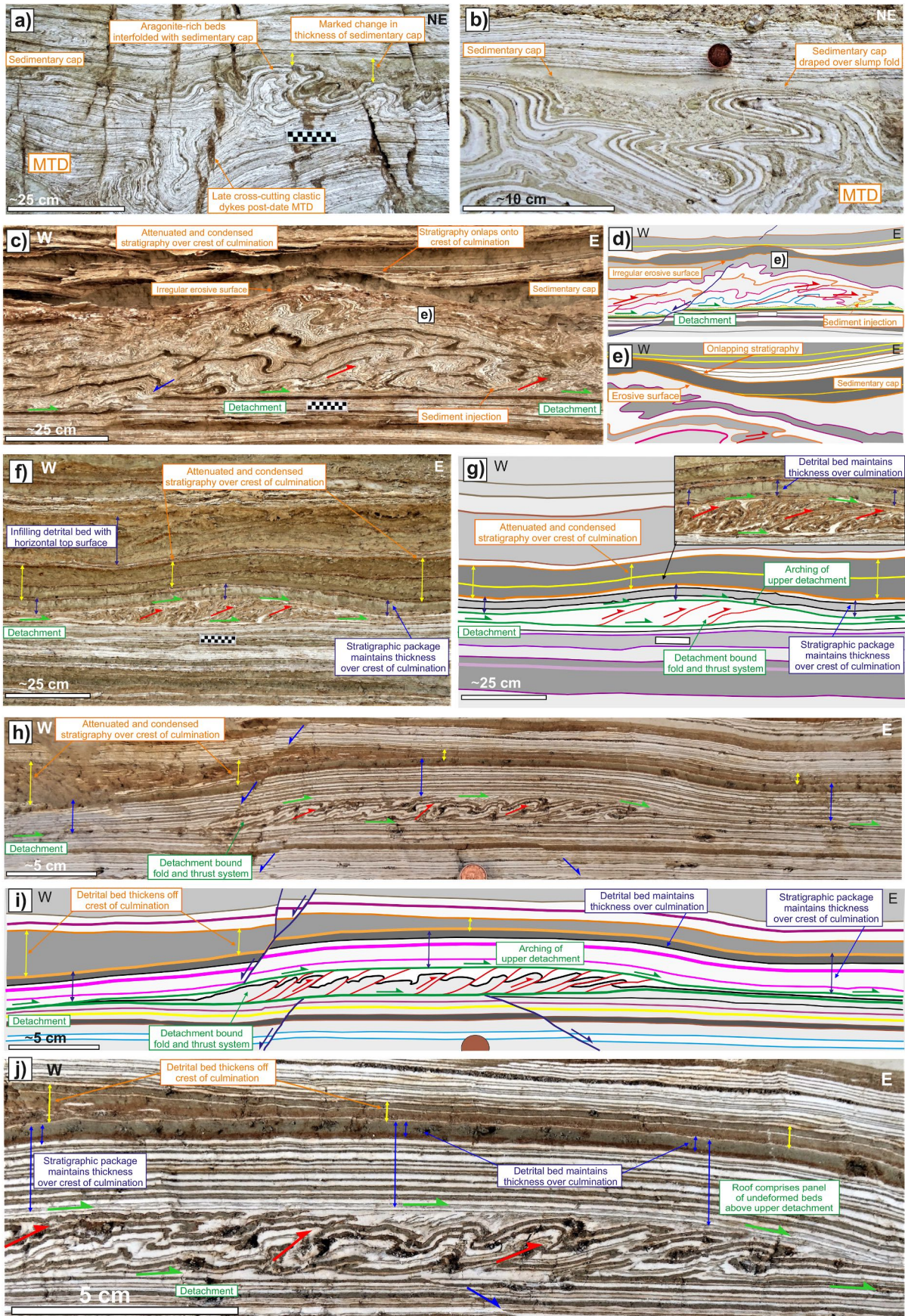


Fig. 5. Graded sedimentary caps containing a) cm-scale folded fragments (Peratzim) and b) graded aragonite fragments (Miflat). The sedimentary caps are parallel to underlying and overlying aragonite-detrital laminae representing background sedimentation. c) Photograph and d) line drawing showing depositional thickening of an MTD in the hangingwall of a growth fault (Masada). e) Close-up photograph of a normal fault and its subsequent truncation by overlying detachment. f) Photograph and g) line drawing of depositional thickening of an MTD in the hangingwall of a growth fault (Peratzim). h) Close-up photograph showing a normal fault cut by several later intrastratal detachments to create a ‘sawtooth’ profile. The normal fault is draped by overlying stratigraphy indicating that it later became inactive.



(caption on next page)

Fig. 6. a) Aragonite laminae are interfolded with a sedimentary cap that displays dramatic changes in thickness with a horizontal top indicating syn-depositional folding at the surface of a MTD (Peratzim). Later vertical fractures and sedimentary dykes cross-cut the MTD. b) Folded aragonite laminae that are draped by an overlying sedimentary cap above the MTD (Peratzim). c) Photograph and d, e) line drawings of a fold and thrust culmination formed above a detachment marked by small sediment injections (Miflat). The culmination is overlain by an erosive surface and infilling sedimentary cap indicating it formed at the surface. The overlying detrital-rich beds onlap onto the structural high created by the underlying folds, indicating that the culmination continued to grow after deposition of the cap. f) Photograph and g) line drawing of a detachment-bound fold and thrust system (FATS) that arches an overlying sequence of sediment which acted as a roof to the duplex. The sediment package overlying the roof displays thickening off the crest of the culmination, indicating that deformation occurred in the shallow sub-surface. h, j) Photographs and i) line drawing of a detachment-bound FATS that arches the overlying sequence. The overlying detrital bed displays a marked thickening off the crest of the culmination indicating that the FATS developed in the shallow sub-surface.

conjugate normal faults are cut by bed-parallel lower and upper detachments which form several individual strands that locally anastomose (Fig. 8a–j). The deformed section is positioned between overlying and underlying gypsum horizons that form prominent benches in the Lisan Formation (Fig. 8a-inset). Within the detachment zone, conjugate normal faults defining horsts and grabens are sharply truncated by the upper detachment, although upslope (west) dipping normal faults may rotate into parallelism with the detachment (Fig. 8e–j). Normal faults developed in the overlying sequence are also truncated by the upper detachment demonstrating that it developed after deposition and faulting of this overburden (Fig. 8c and d) (see section 5.3.). The detachments are sharp planar surfaces that are associated with a buff-coloured mixed detrital and aragonite gouge that has been described from faults in the Lisan Formation (Weinberger et al., 2016, 2017; Alsop et al., 2018, 2020d) (Fig. 8d, g, j). Layers of gouge are typically <5 mm thick, although can reach thicknesses of 10 mm where normal faults are truncated (Fig. 8d, g, j). While generally fine grained, gouge occasionally preserves larger (<10 mm) aragonite and detrital fragments. Gouge and associated detachments gently cut across laminae in the overlying sequence, demonstrating that the detachment formed in the sub-surface following deposition of the overburden (Fig. 8f and g).

5.2. Repetition of stratigraphy across the upper detachment surface

Interplay between early steep faults and later bed-parallel detachments can result in stratigraphic repetition (see Alsop et al., 2020c). As stratigraphic repetition is critical evidence for sub-surface deformation associated with detachments rather than erosive truncation, three separate cases of this process are provided to establish the relative timing of cross-cutting events ranked from older (1) to younger (3).

In our first example, early normal faults are cut by later detachments resulting in a repetition of stratigraphy across the detachment surface (Fig. 9a–c). An early detachment (labelled 1 in Fig. 9b) associated with thrusts and folds is subsequently downfaulted into a graben (labelled 2 in Fig. 9b). Continued movement on the detachment (3) then duplicates stratigraphy (Fig. 9c–e). The downfaulted early detachment (1) is at the same stratigraphic level below the ‘purple’ marker bed as the later detachment (3). Detachments that cut earlier faults may therefore result in a duplication of stratigraphy that is clear evidence of sub-surface repetition and cannot be created through erosion of a normal fault at the surface (Fig. 9e).

In our second case, an early bed-parallel detachment (labelled 1 in Fig. 9f–h) is downfaulted by normal faults that form conjugates (labelled 2 in Fig. 9f–h). Continued movement on non-downfaulted segments of detachments then results in duplication of stratigraphy across the upper detachment (labelled 3 in Fig. 9f–h). The downfaulted early detachment (1) is at the same stratigraphic level below the ‘purple’ marker bed as the later detachment (3). However, the stratigraphic sequence overlying the detachment is thinned compared to the same stratigraphy in the downfaulted segments, potentially reflecting attenuation of the hangingwall block as it slides downslope.

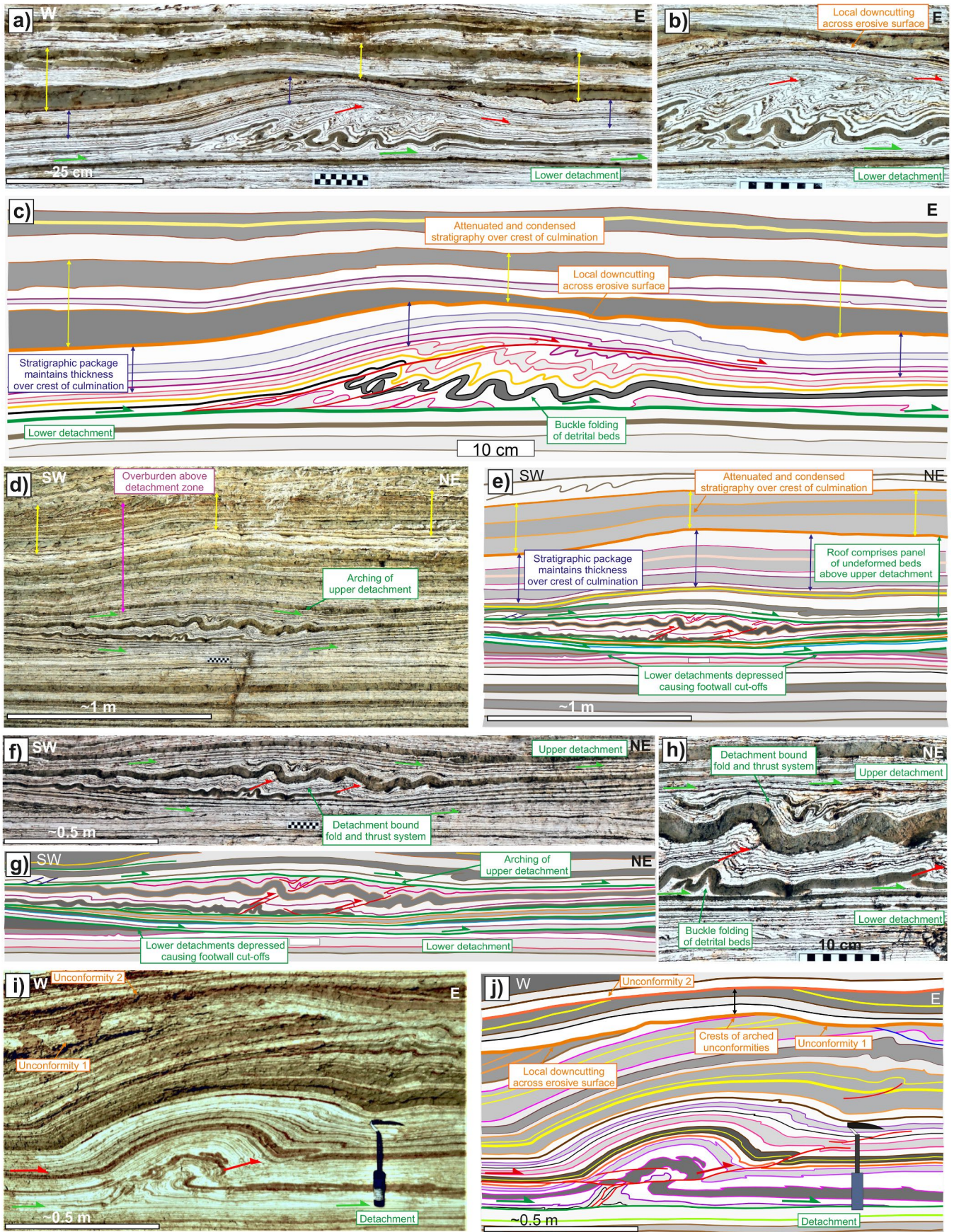
In our third example, we examine conjugate normal faults that form multiple horsts and grabens that are bound by lower and upper detachments (Fig. 10a–c). The normal faults downthrow portions of well-defined stratigraphy together with early bed-parallel detachments (labelled 1 in Fig. 10d–i). The non-downfaulted portions of the

detachment continue to move, leading to a repetition of stratigraphy across the grabens, while the crests of horsts are marked by portions of stratigraphy that are ‘missing’ across the detachment surface. The downfaulted early detachment (1) is at the same stratigraphic level as the later detachment (labelled 3 in Fig. 10d–i). This suggests that the position of detachments is at least partially controlled by mechanical stratigraphy with horizons prone to slip being re-used during different phases of downslope movement. The stratigraphic sequence overlying the detachment is thinned compared to the same stratigraphy in the downfaulted segments, and possibly reflects attenuation during downslope movement. While the normal faults defining horsts and grabens are sharply truncated by the upper detachment, they rotate towards and flatten into the lower detachment to define listric geometries and pockets of gouge where faults meet (Fig. 10a–c, k, l). There is no evidence of stratigraphic repetition across the lower detachment with normal faults rooting downwards onto this basal detachment, rather than cutting it as occurs along the upper detachment. Both the detachments, together with normal faults, are subsequently transected by regional clastic dykes that inject across the previously deformed sequence (Fig. 10 j).

5.3. Detachments cutting faults in the overlying sequence

Normal faults developed in the Lisan Formation must clearly be younger than the stratigraphy they offset. Such normal faults are subsequently cut by underlying bed-parallel detachments, which are therefore younger than the normal faults and the age of sediment offset by that normal fault (e.g. Alsop et al., 2020c). Where normal faults extend for several metres above the detachment they provide an estimate of the minimum depth at which the intratratral detachment operated in the sub-surface (e.g. Pratt and Rule, 2021, p.21).

In the first case we describe a normal fault that is cut by a lower detachment zone and which is traced upwards for 1.5 m before being cut by an upper detachment that develops directly beneath a gypsum horizon (Fig. 11a–c). We use a displacement-distance (D-D) plot to compare the amount of displacement of marker beds across the normal fault with the hangingwall distance of that marker from a fixed reference point (‘R’) (Fig. 11a, d) (e.g. Muraoka and Kamata, 1983; Hughes and Shaw, 2014). As displacement across faults is usually considered to be time dependent then the older parts of faults accumulate the largest offsets, with the point(s) of maximum displacement on D-D plots corresponding to the site(s) of fault nucleation (e.g. Ellis and Dunlap, 1988; Ferrill et al., 2016). Here, the greatest displacement is recorded across the orange and pink detrital beds, suggesting that the normal fault nucleated in these competent marker beds immediately above where the detachment zone subsequently formed (Fig. 11a–d). The normal fault forms a high angle cut-off (>70°) with the lower detachment zone that abruptly truncates it (Fig. 11c, e, f). Where the normal fault is cut by several strands of the detachment zone, it forms a series of segments each displaced by < 30 cm downslope to create a ‘staircase’ geometry (see Alsop et al., 2020c) (Fig. 11c, e, f). The detachment zone is up to 30 cm thick and is bound by sharp curvi-planar upper and lower detachment surfaces that are linked by downslope-verging thrust faults and associated FATS, which form where the detachment zone ramps upwards through stratigraphy (Fig. 11e and f). Stratigraphy within the intratratral detachment zone is laterally traceable for several metres and



(caption on next page)

Fig. 7. a, b) Photographs and c) line drawing of a fold and thrust culmination formed above a detachment (Miflat). The culmination is overlain by a stratigraphic package that maintains its thickness over the crest, and which is then cut across by an erosive surface and infilling detrital sequence indicating it formed in the shallow sub-surface. Arching of the erosive surface, coupled with thickening of the overlying detrital beds off the crest of the culmination, indicates that the culmination continued to grow after deposition of the overlying sediments. d, f, h) Photographs and e, g) line drawings of a detachment-bound fold and thrust duplex that locally depresses the lower detachment and arches the upper detachment (Miflat). Immediately overlying stratigraphic packages maintain thickness over the culmination, while upper parts of the overburden are thinned over the crest of the culmination indicating that the FATS developed in the shallow sub-surface. i) Photograph and j) line drawing of FATS that creates an arching of two overlying erosive unconformity surfaces. (Miflat). Arching of stacked unconformities indicates that the culmination continued to grow in the shallow sub-surface over a period of time.

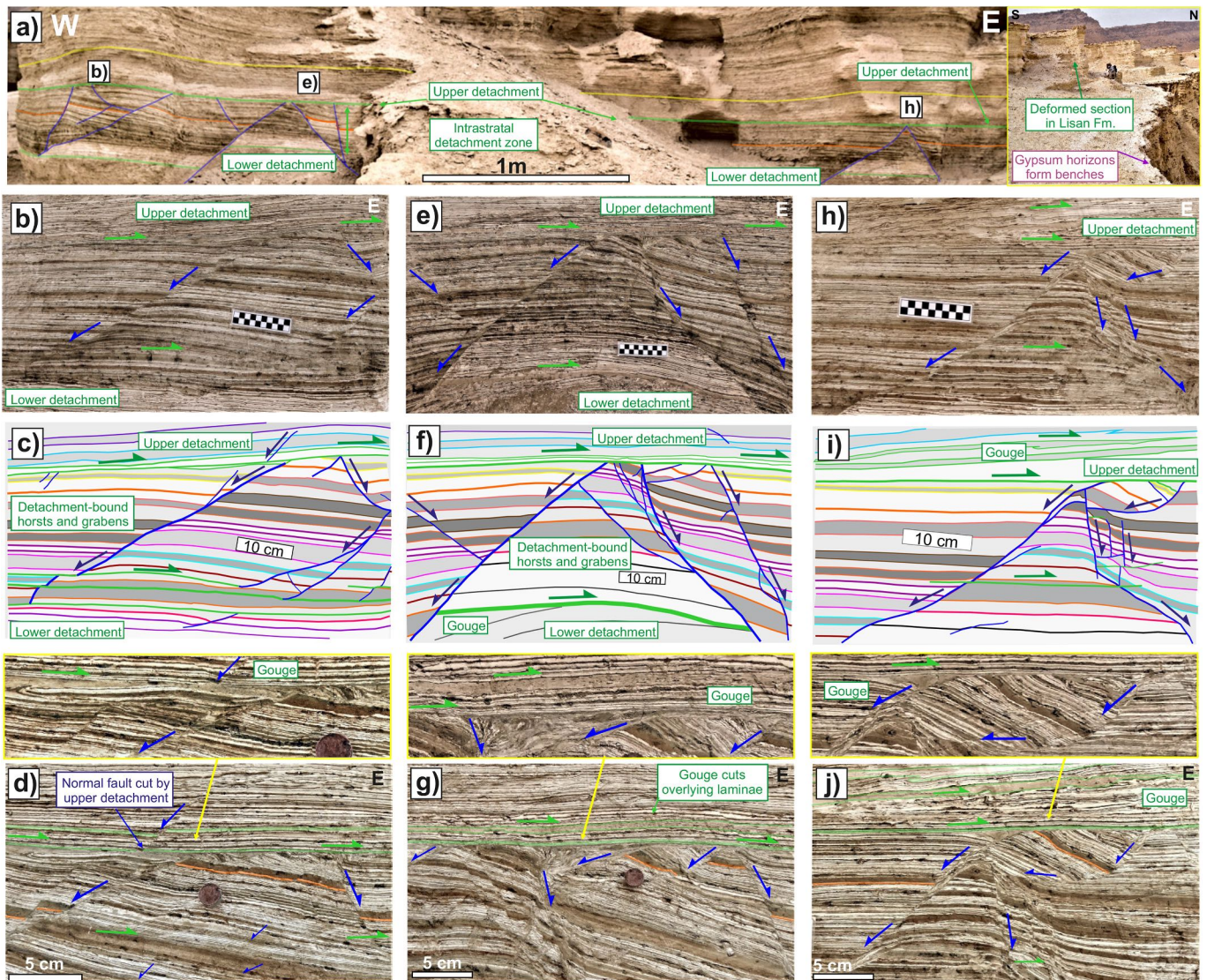


Fig. 8. a) Overview photograph and b, e, h) detailed photographs with line drawing (c, f, i) of detachment-bound conjugate normal faults (Masada). Close-up photographs (d, g, j) show details of gouge and cut-offs developed across the upper detachment surface. Truncation of overlying faults (c, d) indicates that deformation occurred in the sub-surface.

is correlated with the adjacent sequence developed above and below the detachment.

In our second example, conjugate normal faults are traced for 1.5 m above a lower detachment that markedly cross-cuts and truncates them (Fig. 12a and b). The normal faults displace thin MTD horizons before being cut by the underlying intrastratal detachment zone (Fig. 12a and b). This zone, which is bound by upper and lower detachments approximately 15 cm apart, contains beds that correlate with the overlying sequence, indicating stratigraphic repetition across the upper detachment (Fig. 12c and d). Within the detachment zone extensional faults form upslope of downslope verging folds (FATS) that are created

where the detachment zone locally ramps downwards into the underlying sequence (Fig. 12c and d). The location of the detachment zone directly beneath a pre-existing MTD horizon suggests that the buried MTD could have influenced mechanical stratigraphy and the position of subsequent intrastratal deformation (see section 5.5.).

In our third case, conjugate normal faults are bound between upper and lower detachments that are themselves overlain by a gypsum horizon (Fig. 12e–g). The lower detachment is associated with multiple strands that are marked by downslope-verging folds and thrusts that are best developed directly below the normal faults (Fig. 12g–i). Antithetic normal faults that dip towards the west and up the regional slope are

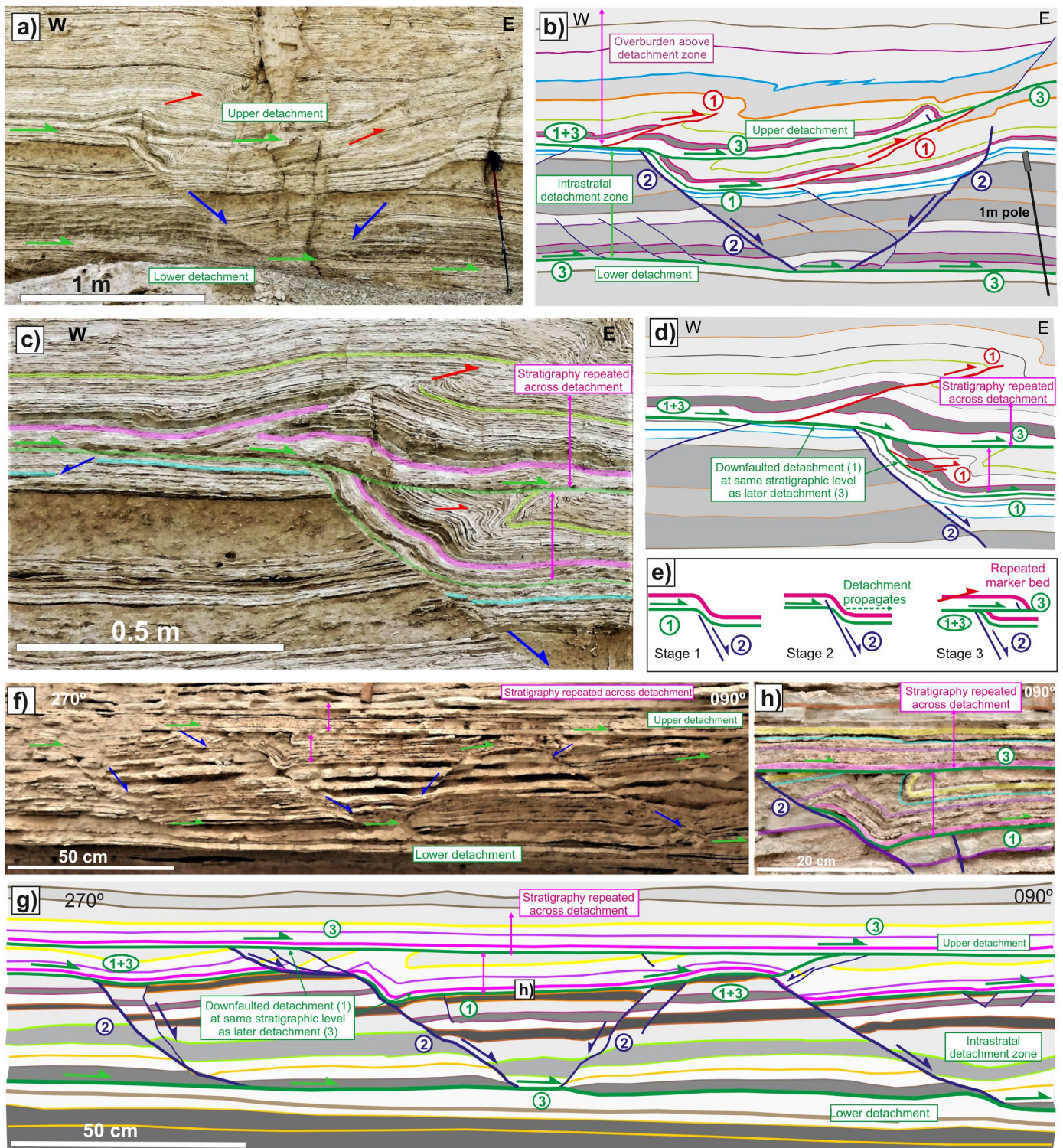


Fig. 9. a, c) Photographs and b, d) line drawings of conjugate normal faults that are cut by an upper detachment leading to repetition of stratigraphy across the underlying graben (Miflat). An early detachment (1) is downfaulted in the graben and is at the same stratigraphic level as the later detachment (3). e) Schematic summary with circled numbers referring to the relative timing of faulting and detachments based on cross-cutting relationships. Repetition of overburden stratigraphy can only be achieved through sub-surface intrastratal detachments rather than erosive truncation. f, h) Photographs and g, h) line drawings of conjugate normal faults that are cut by an upper detachment leading to repetition of stratigraphy across the underlying graben (Peratzim). Details of repeated stratigraphy are shown in h) with circled numbers referring to the relative timing of faulting and detachments.

also associated with downslope-verging folds in the underlying detachment zone. This suggests that the footwalls to these normal faults have moved downslope thereby allowing the hangingwalls to drop down, resulting in excision of stratigraphy along the underlying

detachment (Fig. 12g–i).

Finally, we examine normal faults that are truncated by detachments that develop directly beneath a gypsum horizon, but also root downwards onto detachments that form part of a deeper intrastratal

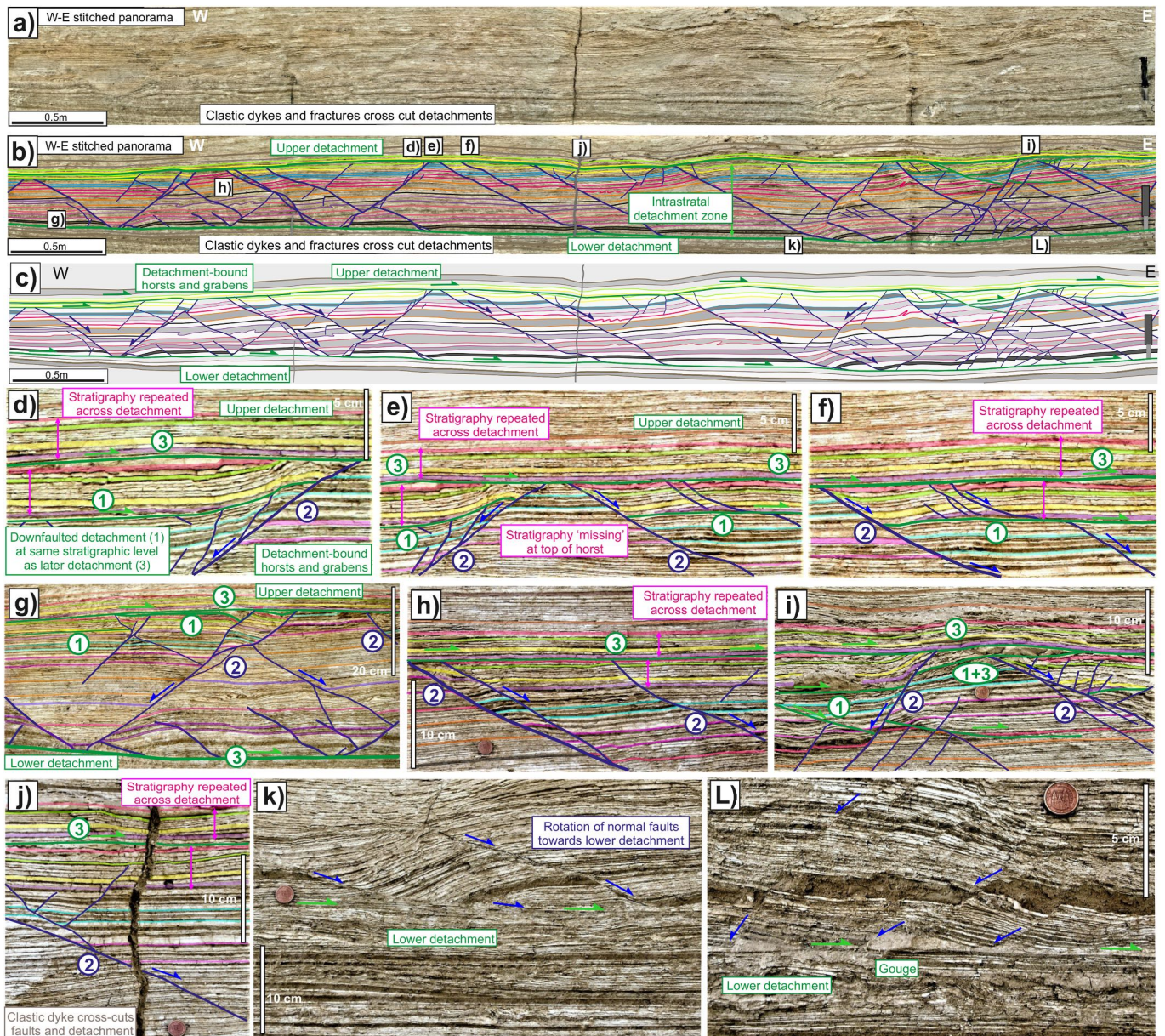


Fig. 10. a) Overview photograph, b) interpreted photograph and, c) line drawing of detachment-bound conjugate normal faults (Masada). Close-up photographs (d–j) show details of cut-offs and highlight stratigraphic repetition or ‘missing’ stratigraphy across the upper detachment surface. k, l) Normal faults becoming listric and rotating into the lower detachment, which is marked by pockets of gouge. Circled numbers refer to the relative timing of faulting and detachments. Repetition of overburden stratigraphy can only be achieved through sub-surface intrastratal detachments rather than erosive truncation.

detachment zone or system that develops up to 4 m below the gypsum (Fig. 13a–c). Normal faults become listric and sole into the underlying detachment zone (Fig. 13d and e), or alternatively are cut by the lower detachments indicating a coeval development (Fig. 13f and g). The lower detachment zone bounds folds and thrusts that develop down-slope of where major listric normal faults sole into the detachment system, while the same unit upslope remains relatively unfolded (Fig. 13a–c). The observation that normal faults may offset folds and thrusts within the detachment zone, but are themselves truncated by the upper and lower detachments bounding this zone, demonstrates that the detachments continued to operate after both the thrusting and normal faulting and could have had a protracted history of down-slope movement (Fig. 13f and g). These observations indicate that extension and down-slope movement along listric normal faults was transferred to the deeper detachment zone and created local folds and thrusts bound by the detachments (Fig. 13f and g).

5.4. Faults affecting overlying gypsum horizons

Gypsum horizons form prominent benches within the Lisan Formation (Fig. 13a and b). Faults and detachment folds which cut the gypsum, and by inference the detachments that offset these faults, must therefore post-date the creation of gypsum and are therefore potentially much younger than the sediments they affect.

5.4.1. Thrust faults

Deeply-rooted thrust faults may ramp upwards and deform overlying gypsum horizons (Fig. 14a and b). Thrusts develop early (labelled 1 in Fig. 14b) and are then cut by detachments (labelled 2 in Fig. 14b) that displace the thrust ramps down-slope towards the east. Detailed analysis reveals several strands of anastomosing detachments that are concentrated beneath the competent gypsum horizon, suggesting that the presence of gypsum has influenced the position of later intrastratal

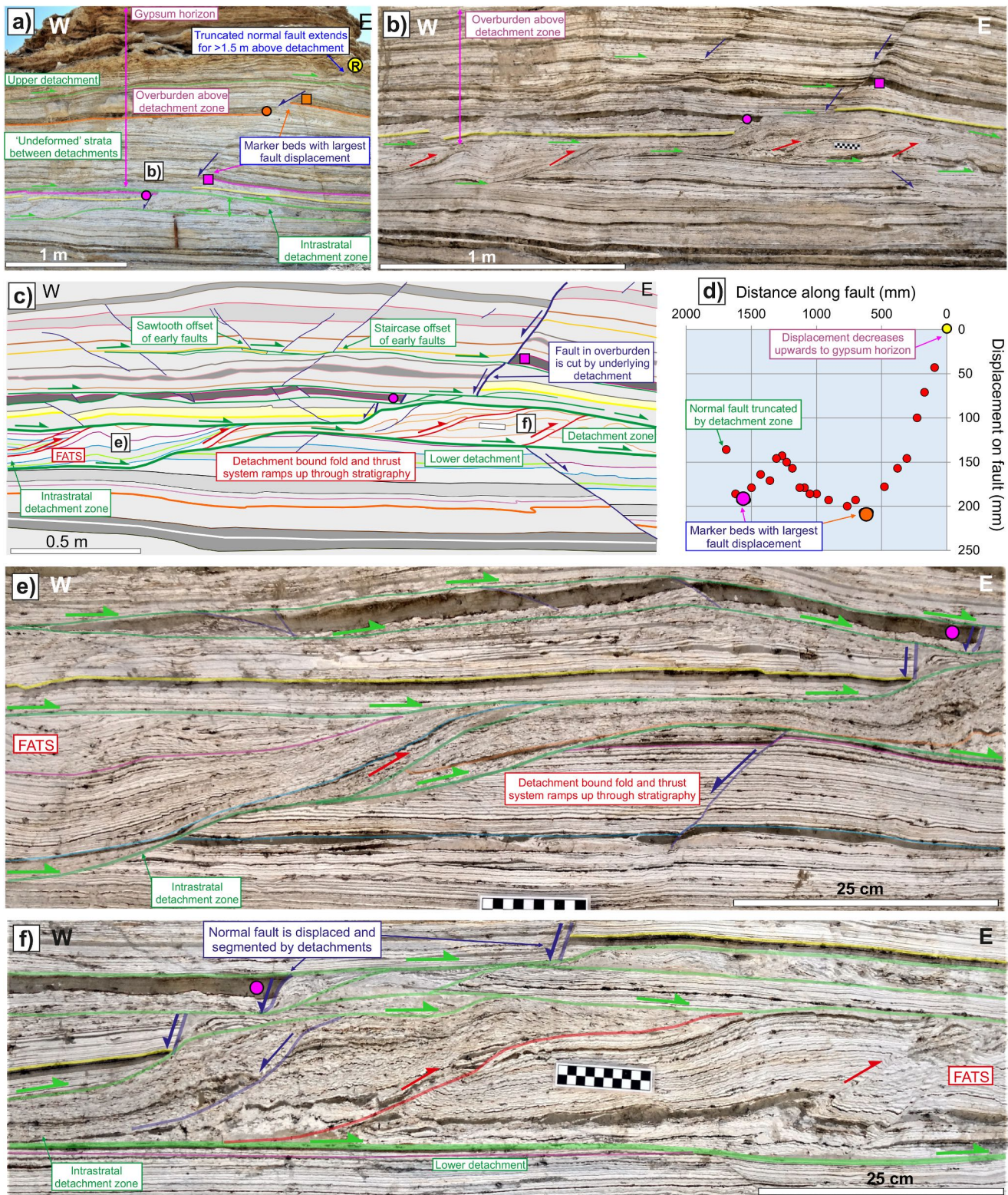


Fig. 11. a) Overview photograph, b) detailed photograph, and c) line drawing of detachment zone cutting a normal fault that is traced through 1.5 m of overburden (Miflat). The normal fault is cut by an upper detachment beneath an overlying gypsum horizon. In the photographs (a–c), matching coloured pink and orange squares (footwall) and circles (hangingwall) mark offset horizons across the normal fault, with displacement generally decreasing towards the upper reference point ('R' in yellow circle). d) Displacement-distance (D–D) graph plotted for the normal fault with hangingwall cut-off markers (coloured circles) defining a displacement profile drawn from the yellow reference point (R) at the right-hand origin. e, f) Photographs showing details of the detachment-bounded fold and thrust system (FATS) that displaces and segments the overlying normal fault. The intrastratal detachment zone is therefore younger than the most recent sediment offset by the normal fault and formed in the sub-surface beneath >1.5 m of overburden. (For interpretation of the references to colour in this figure legend, the reader is referred to the Web version of this article.)

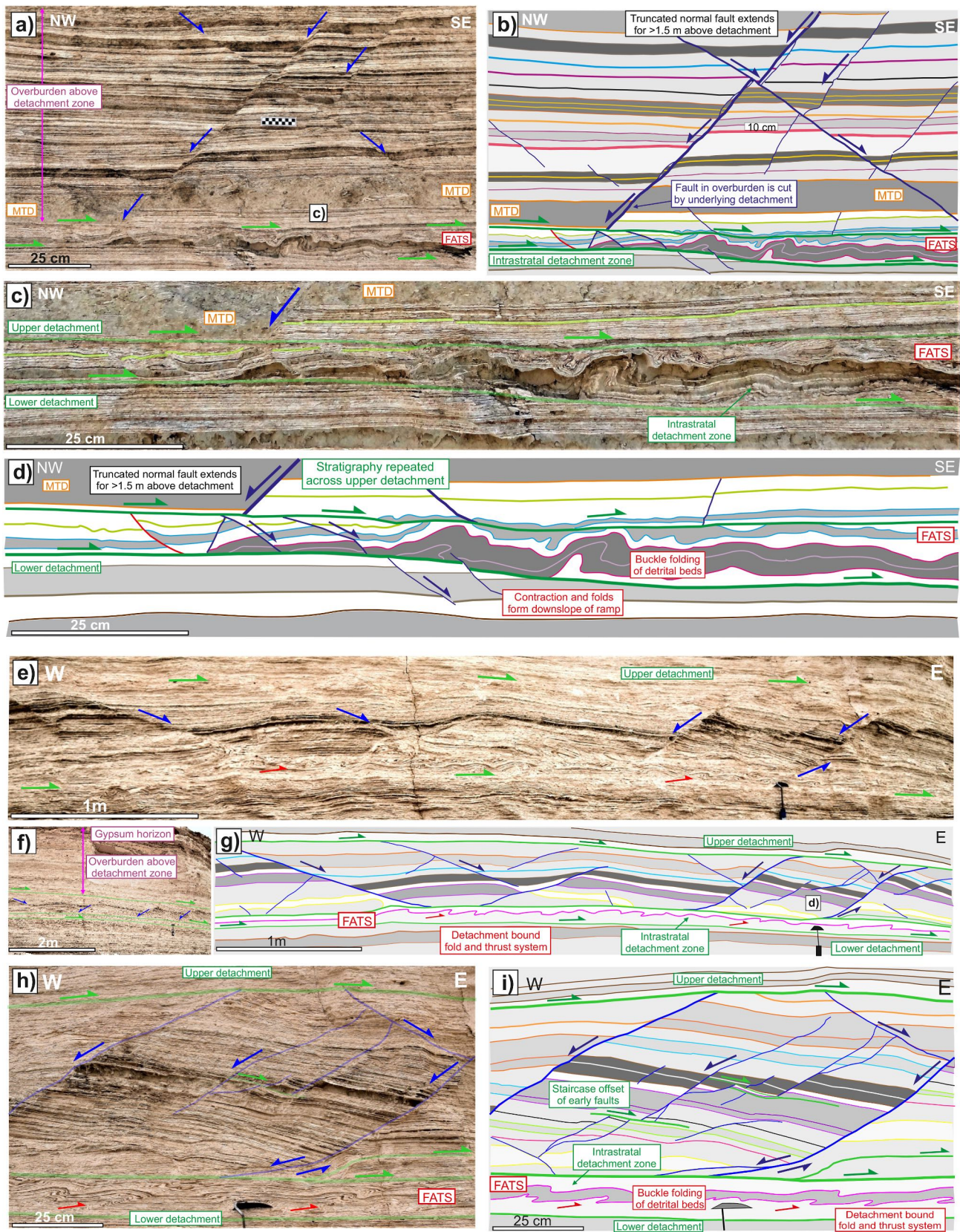


Fig. 12. a, c) Photographs and b, d) line drawings of an intrastratal detachment zone cutting a normal fault that is traced through 1.5 m of overburden (Miflat). The detachment zone comprises extensional and contractional folds and thrusts that form downslope of where detachments ramp through the stratigraphy. Repetition of stratigraphy, coupled with truncation of the overlying normal fault, indicates that the detachment FATS formed in the sub-surface. e) Photograph, f) overview photograph and, g) line drawing of an intrastratal detachment zone and associated FATS formed beneath ~2 m of overburden and a gypsum horizon. h) Close-up photograph and, i) line drawing of downslope verging FATS formed directly beneath upslope-dipping normal faults.

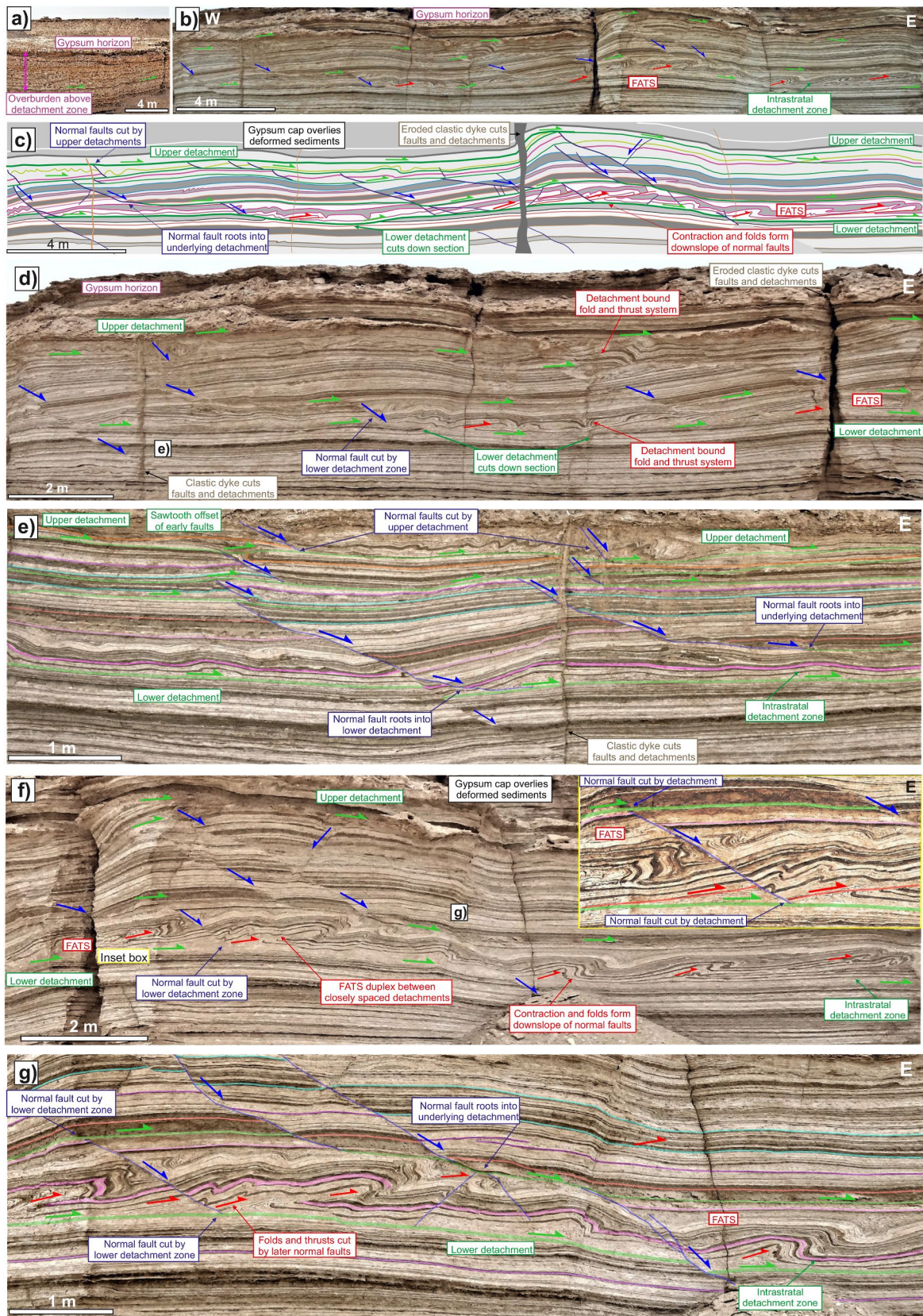
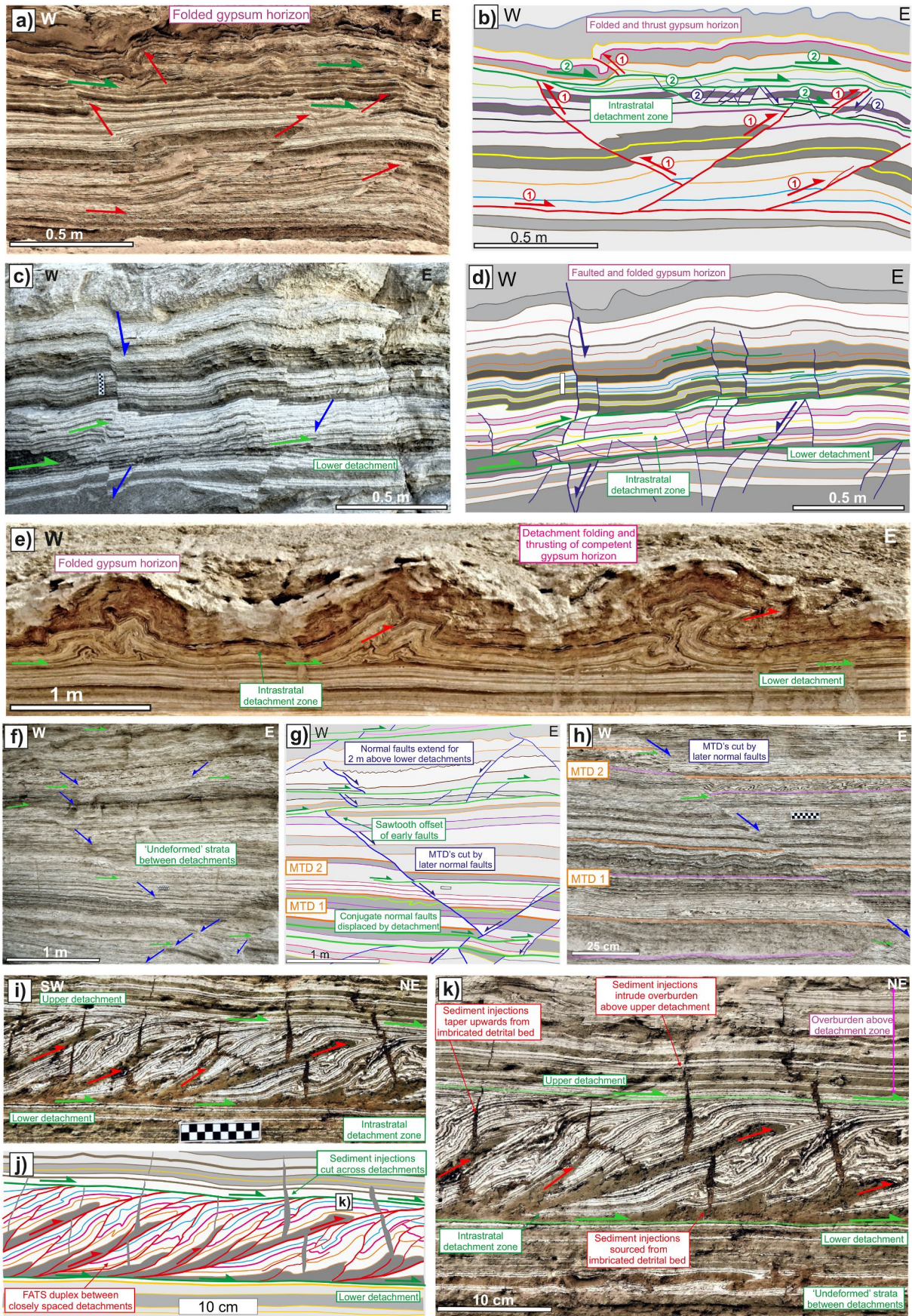


Fig. 13. a) Overview photograph, b) photograph, and c) line drawing of detachment zone and associated FATS that forms beneath ~4 m of overburden and overlying gypsum horizon (Miflat). Detailed photographs are provided of the western (d, e) and eastern (f, g) parts of the section. Normal faults in the overburden are cut by detachments beneath the gypsum horizon, and become listric and root downwards into the underlying intrastratal detachment zone. The FATS is developed downslope of where normal faults in the overburden sole into the detachment zone and formed in the sub-surface.



(caption on next page)

Fig. 14. a) Photograph and b) line drawing of thrusts causing folding in an overlying gypsum horizon. The thrusts are then cut by a intrastratal detachment zone that later forms beneath the gypsum (Miflat). c) Photograph and d) line drawing of normal faults causing folding in an overlying gypsum horizon. The normal faults are then cut by a later intrastratal detachment zone (Sedom). e) Detachment folds that form in a competent gypsum horizon that is carried on an underlying detachment. f) Photograph, g) line drawing and, h) close-up photograph of multiple MTD horizons that are offset by later normal faults (Miflat). Normal faults are truncated by intrastratal detachments that are traced for 2 m into the overburden, indicating that detachments formed in the sub-surface. i) Photograph, j) line drawing and, k) close-up photograph of sediment injections that intrude overburden above an intrastratal FATS. Sediment injections taper upwards and cut the upper detachment indicating that they formed shortly after movement on the FATS had ceased.

detachments (Fig. 14a and b).

5.4.2. Normal faults

Normal faults cut stratigraphy as well as overlying gypsum horizons where they create local folds (Fig. 14c and d). Normal faults are later displaced by bed-parallel detachments with the upper block moving downslope towards the east (Fig. 14c and d). Several anastomosing detachment strands form ~1 m below the gypsum horizon suggesting that their position is influenced by this horizon.

5.4.3. Detachment folds

Detachment folds generally form classic buckle fold geometries and are created where a sequence has moved directly above an underlying detachment (e.g. Butler et al., 2020). Detachment folds can be cut by subsequent thrust ramps (break-thrust folds) or simply be carried on the underlying detachment. In our example, detrital-rich beds form class 1B (parallel) folds while the aragonite-rich beds form Class 1C or Class 2 (similar) folds with thickened hinges indicating that the detrital-rich beds are more competent at the time of folding (Alsop et al., 2020b, 2021a, b) (Fig. 14e). The buckle folds lack the ‘billow’ shape noted for surficial folds and are commonly asymmetric with vergence directed downslope towards the east. Detachment folds deform overlying gypsum beds that form competent horizons, and such deformation must have operated after the gypsum horizon had precipitated (Fig. 14e) (Alsop et al., 2020c, p.6). In summary, the deformation of gypsum horizons by underlying structures indicates that deformation not only post-dates the gypsum and is therefore sub-surface, but that intrastratal detachments are concentrated beneath the competent gypsum reflecting its role in the mechanical stratigraphy.

5.5. MTDs displaced by later faults

Where MTDs and adjacent stratigraphy are cut by later faults that extend for several metres through the overlying sequence, the later faulting significantly post-dates the MTD after it has become buried in the sub-surface. In our example, MTDs form thin (<1 m) horizons that develop at the sediment surface and are subsequently blanketed by a sedimentary cap that is deposited out of suspension (see section 4.3.). Following further deposition and burial by overlying sediments, the whole sequence is subsequently cut by later normal faults that transect several metres of stratigraphy above the MTD (e.g. Fig. 12a–d). This indicates that the normal faults are unrelated to the original MTD as they offset both it and its associated sedimentary cap, with the MTD itself having been sub-surface at the time of faulting.

In a further instance, multiple thin MTDs are offset by normal faults that are traced for 2 m above detachments that form below the MTDs (Fig. 14f–h). The MTDs contain downslope verging folds and are overlain by sedimentary caps which are displaced by the normal faults (Fig. 14f–h). This indicates that normal faults entirely post-date the MTDs and their sedimentary caps, and that the lower detachment was developed at least 2 m below the surface. These relationships collectively indicate that MTDs formed at the sediment surface while later normal faults and detachments developed in the sub-surface after the sequence was buried.

6. Sediment injections into overlying sequences

Where sediment becomes over-pressured and fluidised, it can

mobilise and intrude into adjacent sequences to create sediment injections (e.g. Baldry, 1938, p.352; Brown, 1938, p.396; Smith, 2000; Törő and Pratt, 2016, p.191) (Fig. 14i–k). Sediment injections may taper upwards indicating intrastratal injection up into overlying beds and intrusions are therefore younger than the stratigraphy they cross-cut (e.g. Törő et al., 2015, p.222; Törő and Pratt 2016, p.191) (Fig. 14i–k). In some cases, sediment injections are rooted directly into and develop off underlying detachments (e.g. Baldry, 1938, p.352; Brown, 1938, p.396; O’Leary and Laine, 1996, p.309), indicating that these detachments that generate the injections are also younger than the overlying sequence and therefore formed in the sub-surface (Fig. 14i–k). Sediment injections cut directly across the upper detachment suggesting that they formed shortly after movement on the FATS had ceased (Fig. 14i–k).

6.1. Injections above a thrust duplex

Gravity-driven FATS that are bound above and below by intrastratal detachments in the otherwise largely undeformed sequence may be associated with sedimentary injections (Fig. 15a–e). The sediment injections are formed of a fine-grained mixed aragonite and detrital matrix that contains larger (<10 mm) clasts of aragonite and detrital fragments, presumably sourced from the adjacent Lisan Formation (Fig. 15a–e). The injections take the form of rounded ‘blobs’ with no discernible deformation or offset of adjacent laminae in the host sediment. The gravity-driven FATS comprises folds and imbricate thrust ramps which join into the upper and lower detachments to create a duplex with a minimum of 0.5 m of overburden (Fig. 15a–c) (see Alsop et al., 2021a). The lower detachment locally cuts down section in the direction of transport and may also repeat stratigraphy from the footwall sequence (Fig. 15a–d). The upper detachment comprises an anastomosing system of braided strands that truncate and repeat stratigraphy, as well as truncating underlying folded layering (Fig. 15d and e). The injections form directly along the upper detachment, with traces of injected sediment preserved along the detachment surface, indicating that the injections were sourced from sediment that was mobilised along the detachment (Fig. 15a–e).

In a second example, sedimentary injections that form minor (cm-wide) dykes are displaced by thrust imbricates within FATS and also by bed-parallel detachments (Fig. 16a–c). Sedimentary dykes do not offset adjacent laminae, which they sharply cross-cut, although local downwarping of laminae and the underlying detachment suggests that the dykes were relatively competent at the time of deformation (Fig. 16d and e). Note that these sedimentary dykes appear to be sourced from adjacent to lower detachments in the FATS and should not be confused with the larger and extensive regional set of clastic dykes that cut across MTDs and FATS in the Lisan Formation (Levi et al., 2006a, b). The dykes act as displacement markers and suggest offsets of up to 40 cm across detachments, although an inability to correlate dykes across detachments suggests displacement could be larger (Fig. 16b and c). Sedimentary dykes that develop above upper detachments and cut overlying stratigraphy are significant as they demonstrate that the overlying sequence was already deposited at the time of the FATS deformation that created injections (i.e. the deformation must be sub-surface).

6.2. Injections along upper detachments

In this example the gravity-driven FATS is bound above and below by

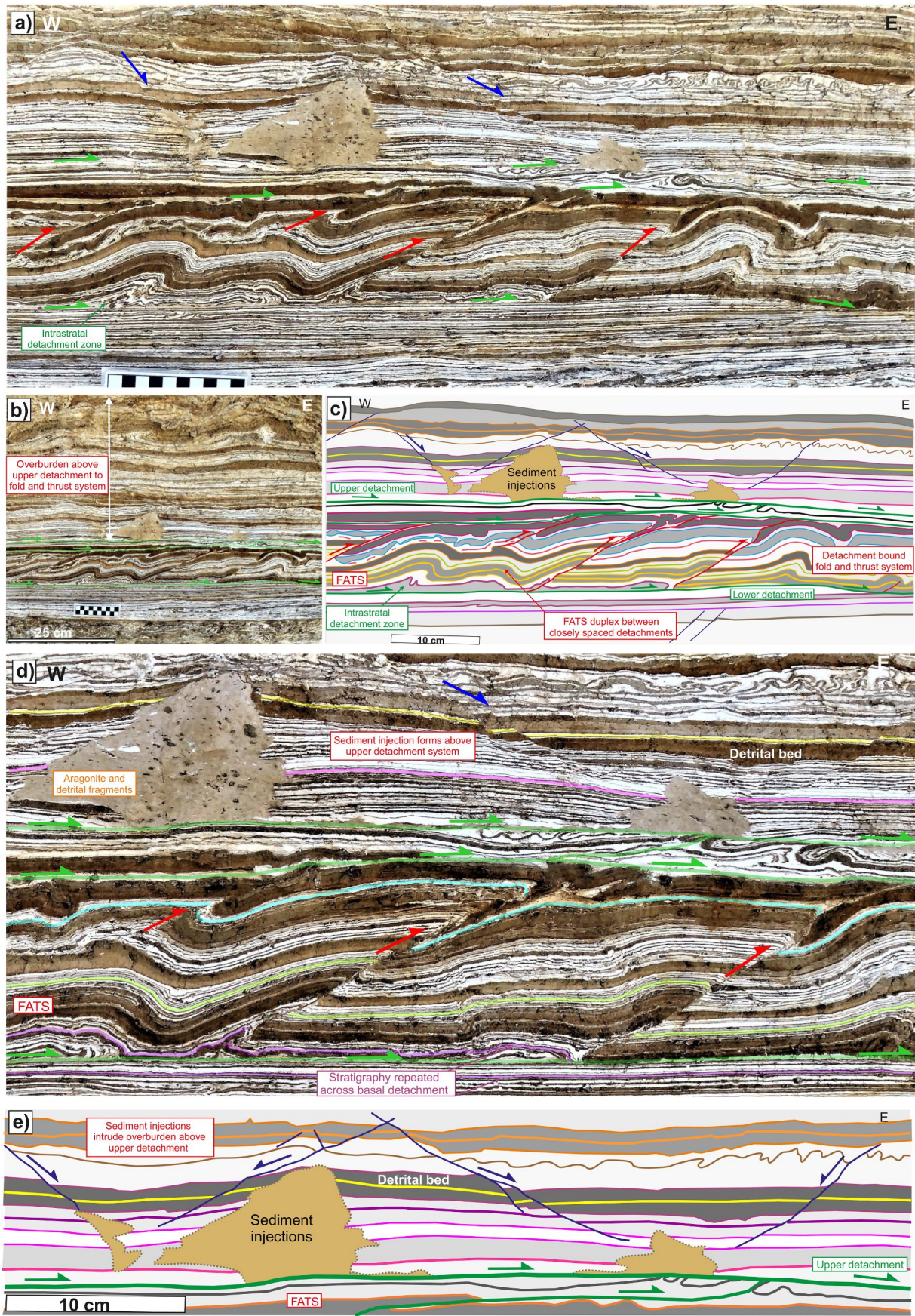


Fig. 15. a) Photograph, b) overview photograph, and c) line drawing of sediment injections that form above a detachment-bound FATS (Miflat). d) Detailed photograph and e) line drawing of a duplex in the FATS and the braided upper detachment system from which sediment injections are sourced.

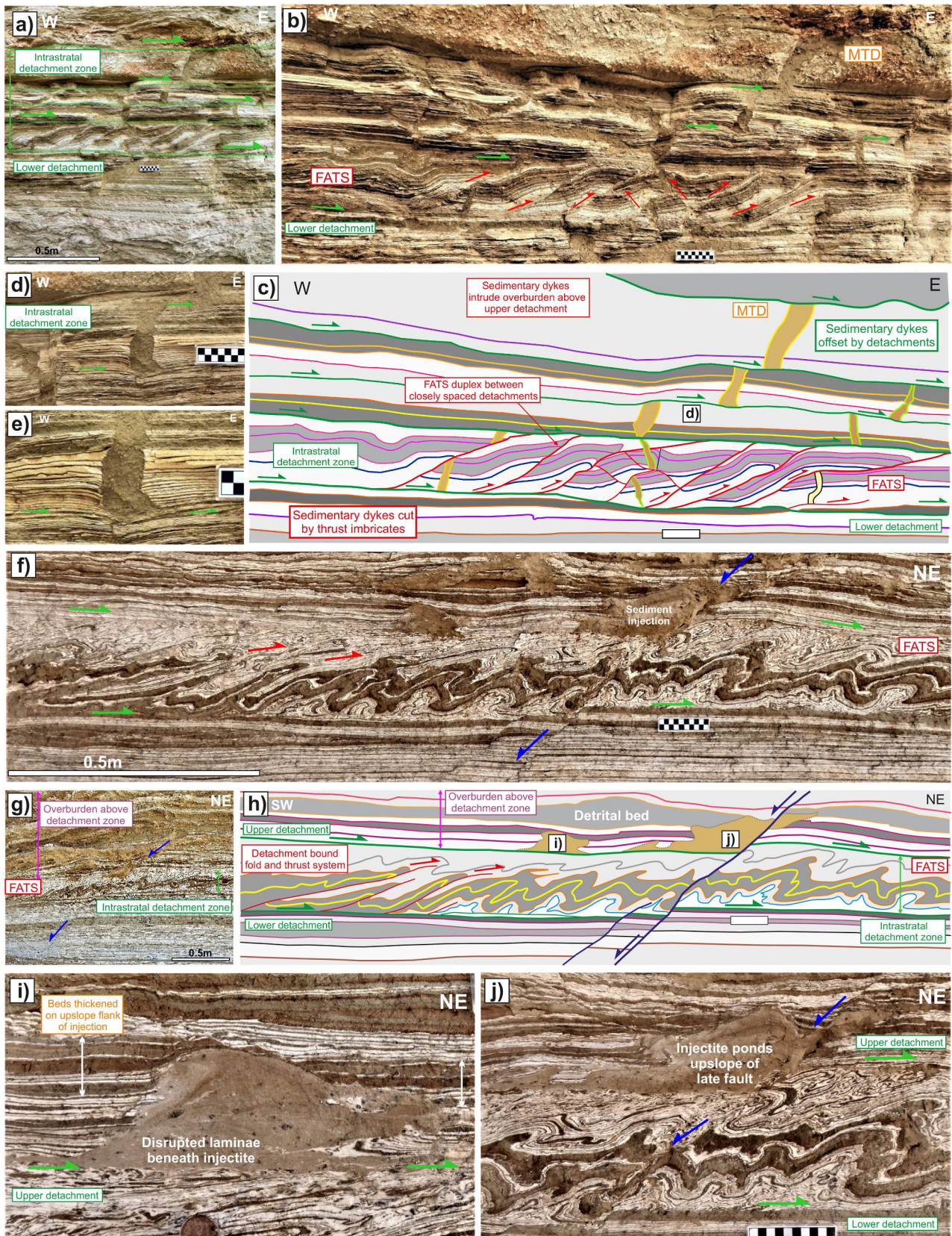


Fig. 16. a) Overview photograph, b) photograph, and c) line drawing of sedimentary dykes and injections intruding overburden above an intrastratal FATS (Miflat). Sedimentary dykes are cut by thrusts in the FATS, as well as overlying detachments. d, e) Detailed photographs of sedimentary dykes being cut and displaced by detachments. f) Overview photograph, g) photograph, and h) line drawing of sedimentary injections forming along an upper detachment above an intrastratal FATS (Miflat). i, j) Details of sedimentary injections which locally ‘pond’ on the upslope margin of a normal fault that cuts the detachments and injections.

bed-parallel detachments that are subsequently cut and displaced by a normal fault that extends into the underlying and overlying sequence for >0.5 m (Fig. 16f–h). No sedimentary cap is developed above the folds and thrusts within the FATS, and the upper contact is marked by a detachment that forms a sharp planar boundary above which the sedimentary injections develop (Fig. 16h–j). The upper detachment is marked by sediment injections that ‘pond’ upslope in the hangingwall of the normal fault (Fig. 16h, j). The normal fault locally cuts the injection, suggesting that injections formed during movement along the upper detachment and shortly before the later normal fault that cross cuts both the detachment and injection. The injection does not offset the laminae in the host sediment, although it is notable that some detrital layers are thicker on the upslope flank of the injection (Fig. 16i). This suggests that there may have been a component of later layer-parallel compaction and thickening on the upslope margin of the injection that acted as a local buttress and barrier to continued downslope movement.

In summary, sedimentary injections that develop from upper detachments and cut overlying stratigraphy are significant as they demonstrate that the overlying sequence already formed an overburden at the time of the deformation that created the injections (e.g. Törö et al., 2015, p.222). As such, they provide critical evidence that the FATS and associated deformation must be sub-surface.

7. Reactivation of surficial MTD horizons by later MTDs

7.1. Folding of earlier MTD horizons

Where MTDs and their associated caps are folded or thrustled then it is clear that at least two episodes of surficial deformation, and potential seismicity, are recorded by the MTDs. In this example, both an older MTD (1) and younger MTD (2) are folded and repeated around a later recumbent fold that is oblique to the section (Fig. 17a–d). MTD 1 contains a 5 cm thick panel of undeformed aragonite-rich laminae that locally divides this MTD into two sub-units (Fig. 17 a-d). MTD 2 is marked by a sedimentary cap with a pronounced erosive base that is repeated around the later fold closure, while the top of the sedimentary cap remains unfolded (Fig. 17a–d). This indicates that the folding formed and continued during deposition of the sedimentary cap and is therefore a later stage feature of MTD 2 (Fig. 17a–d). This highlights the complications that can develop where locally undeformed beds divide MTDs into two sub-units (MTD 1a and b), or where sedimentary caps are repeated around fold closures (MTD 2). In both cases the duplication of MTDs and caps is a consequence of processes operating during MTD development and should not be viewed as a later process (Fig. 17a–d).

7.2. Thrusting of earlier MTD horizons

In this example, an older MTD 1 and its overlying sedimentary cap are cut across by younger thrusts associated with MTD 2 (Fig. 17e–h). The thrusts displace the sedimentary cap of MTD 1 and tip out into asymmetric folds in MTD 2 that are overlain by an undeformed sedimentary cap (2) (Fig. 17e–h). This deformed sequence that conceals two separate MTDs is itself overlain by a detachment system that contains a FATS duplex (3) (Fig. 17g–j). The roof to the duplex is arched over the culmination where the 50 cm thick overburden is locally truncated by an erosive surface, indicating that the duplex formed in the shallow sub-surface. The modification of MTD 1 by the overlying MTD 2 demonstrates that MTDs may conceal more than one episode of deformation that in many cases can only be distinguished by examination of the sedimentary cap that overlies the older MTD.

8. Reworking of surficial MTD horizons by secondary sub-surface deformation

MTD horizons represent major heterogeneities within a sedimentary sequence due to the mixed and irregular shape of the unit, internal

faulting, folding and thrusting that disrupts original layers, and expulsion of fluids from within deforming sediments (e.g. Alsop et al., 2021a). Such mechanical heterogeneities caused by MTDs are particularly pronounced in otherwise well-bedded or laminated lacustrine sediments such as developed in the Lisan Formation. The mechanical heterogeneity introduced into an otherwise relatively uniform sequence by MTDs during surficial deformation may be utilised by later sub-surface deformation that focuses secondary intrastratal detachments and associated structures next to MTDs (Fig. 1c). Faults that cut the overburden above MTDs and extend downwards into detachments next to the MTD demonstrate that the detachments formed in the sub-surface after the MTD had become buried.

8.1. Secondary detachments above earlier MTDs

As noted above, secondary deformation becoming localised along the tops of pre-existing MTDs can result in duplexes being created that arch the overlying roof panel (Fig. 17h–j). In a further case that involves reworking and reactivation of earlier normal faults, upper and lower detachments bound a FATS that creates duplexes developed directly above detrital-rich MTDs (Fig. 18a and b). Stratigraphy is repeated both above the lower detachment and beneath the upper detachment, indicating that these truncating structures are detachments rather than erosive surfaces (Fig. 18a and b). Early normal faults that offset the MTD are locally reactivated by thrusting, while later normal faults cut across the entire detachment zone (Fig. 18a and b).

Normal faults can also form conjugate systems between detachments that develop above pre-existing MTDs (Fig. 18c–f). In some instances, upper and lower intrastratal detachments appear to be ‘sandwiched’ between underlying MTDs and thick overlying detrital-rich beds (Fig. 18c–f). The MTD contains billow folds with ‘fanning’ axial planes that are truncated by an irregular erosive surface at the base of the overlying sedimentary cap (Fig. 18f). The lower detachment forms a sharp contact a few cm above the sedimentary cap of the underlying MTD, while the upper detachment is developed within aragonite-rich beds and abruptly truncate normal faults that form a conjugate system between the two detachments (Fig. 18c–f). It is important to note that the upper detachment is within aragonite-rich units and is not therefore an erosive surface at the base of the overlying detrital-rich beds, while the lower detachment is also unrelated and separated from erosive processes along the sedimentary cap (Fig. 18f). In summary, the upper and lower detachments bound a zone of conjugate normal faulting that developed after deposition of the MTD, and also the overlying detrital beds that formed an overburden to the sub-surface intrastratal deformation.

8.2. Secondary detachments below earlier MTDs

Detailed examination is required to distinguish truncation of pre-existing structures by erosive surfaces that form along the base of MTDs, from intrastratal detachments that may subsequently localise along the base of MTDs and also cut across earlier faults. In our first example, a detachment forms beneath a MTD that contains large (>20 cm) clasts of aragonite, and which is itself overlain by a thick sequence of detrital beds (Fig. 19a–c). Normal faults are abruptly cut by the detachment that forms an extremely sharp truncation (Fig. 19a–c). The detachment is a planar bed-parallel surface that is associated with a thin (<1 cm) mixed gouge unit that is especially well developed where the detachment intersects detrital-rich beds in the footwall of normal faults (Fig. 19d and e). A critical observation is that a thin (2 cm) panel of aragonite-rich laminae is preserved above the detachment and below the base of the MTD (Fig. 19d and e). This panel of undeformed laminae proves that the truncation of the underlying normal faults has been created by the intrastratal detachment, rather than erosion along the base of the MTD which does not actually intersect the faults (Fig. 19d and e).

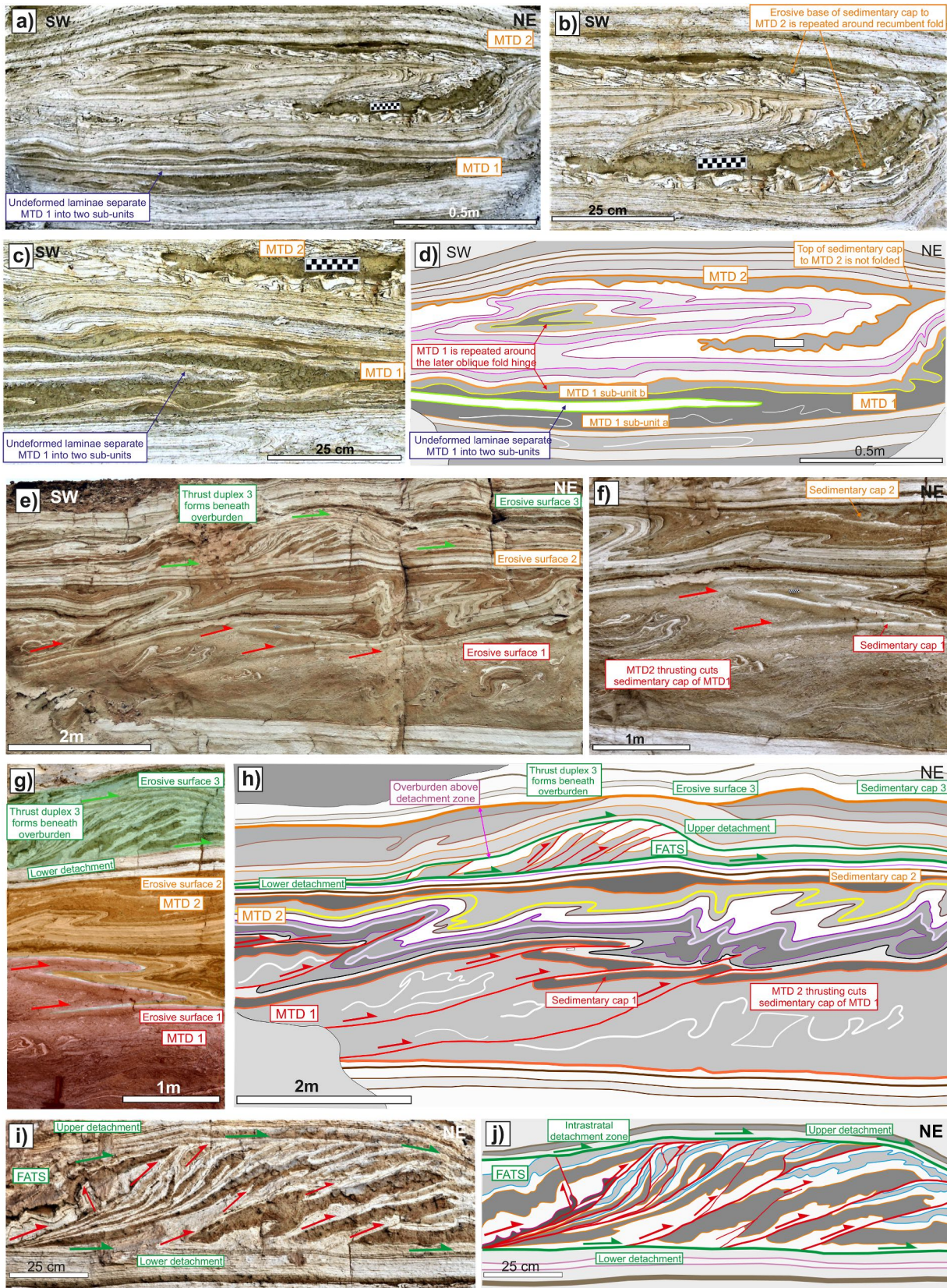


Fig. 17. a) Overview photograph, b) photograph, c) detailed photograph, and d) line drawing of an older MTD 1 and its sedimentary cap being repeated around a later recumbent fold that is part of a younger MTD 2 (Miflat). MTD 1 is locally separated into two sub-units by an undeformed package of aragonite laminae. e) Overview photograph, f) photograph, g) detailed colour-coded photograph, and h) line drawing of an older MTD 1 and its sedimentary cap being cut by thrusts associated with MTD 2 (Peratzim). The sedimentary cap to MTD 2 remains undeformed and is overlain by FATS that creates a duplex. i, j) Details of duplex that arches up an overlying panel of sediment indicating that the intrastratal FATS formed in the sub-surface. (For interpretation of the references to colour in this figure legend, the reader is referred to the Web version of this article.)

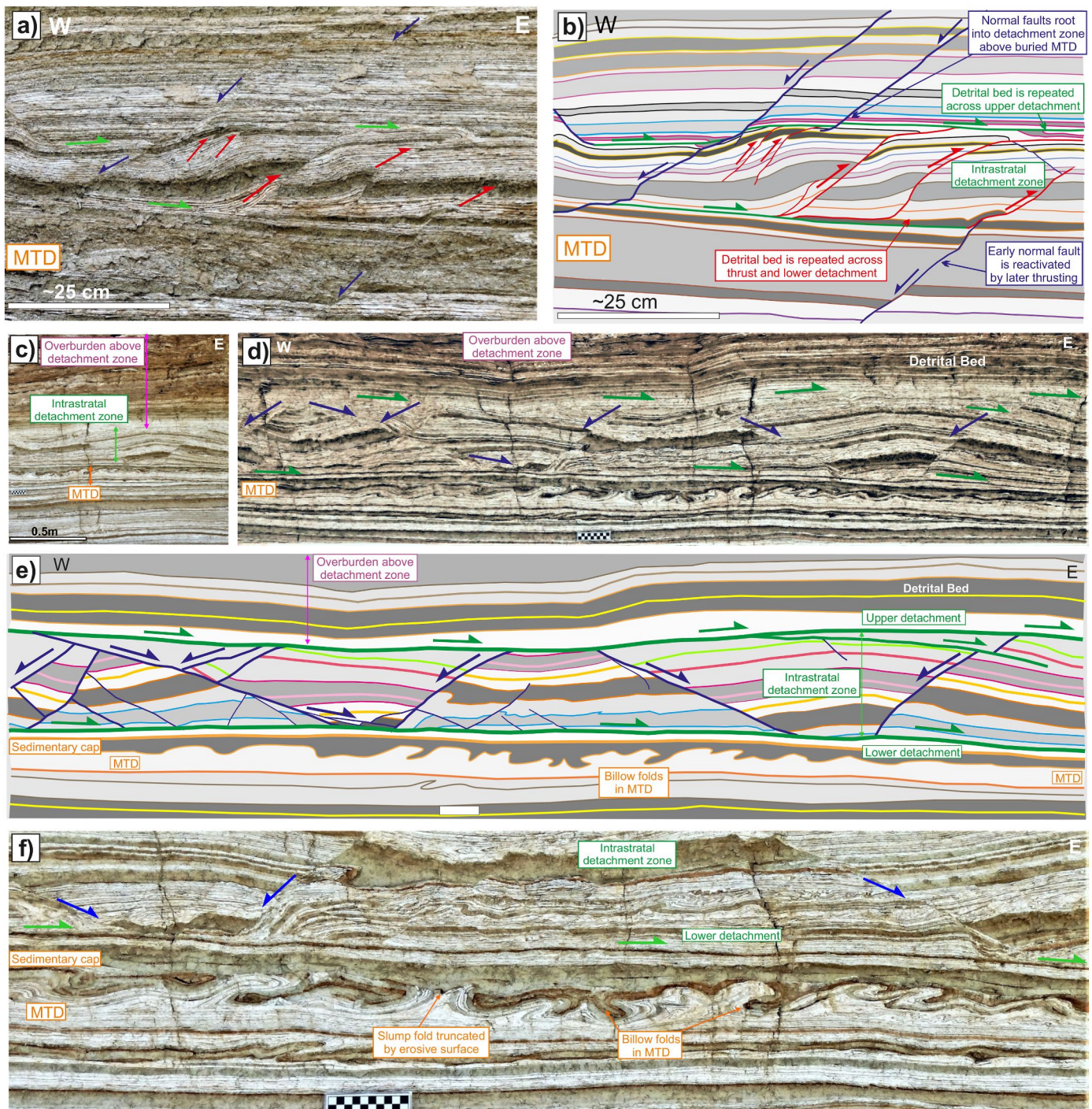


Fig. 18. a) Photograph, and b) line drawing of a FATS that forms above an MTD (Miflat). Early normal faults that offset the MTD are locally reactivated as thrusts. c) Overview photograph, d) photograph, and e) line drawing of an intrastratal detachment zone with conjugate normal faults forming above an older MTD (Miflat). Details of billow folds within the MTD that are cut by an overlying erosive surface and sedimentary cap are shown in f).

In the second case, a series of thin MTDs are developed that are offset by a listric normal fault and later detachment surface (Fig. 19f–h). The listric normal fault offsets MTD 1 and MTD 2 and is cut by an overlying bed-parallel detachment (Fig. 19f–h). A thin (3 cm) panel of aragonite-rich laminae is preserved above the detachment and below the base of the overlying thicker (25 cm) MTD 3 (Fig. 19i and j). In detail, thin mm-scale aragonite laminae that overlie the detachment are locally cut out, indicating that it is a later tectonic excision rather than an erosive unconformity (Fig. 19i and j). The thin panel of undeformed sediment that separate the detachment surface from the base of MTD 3 prove that the

MTD has not created the truncation of faults. In summary, MTDs represent heterogeneity below which later sub-surface detachments may nucleate. It is critical to recognise thin panels of undeformed strata that demonstrate it is the intrastratal detachment that cuts the earlier faults rather than the erosive base of an MTD.

9. Discussion

The criteria described above to distinguish surface versus sub-surface deformation in gravity-driven MTDs and FATS developed around the

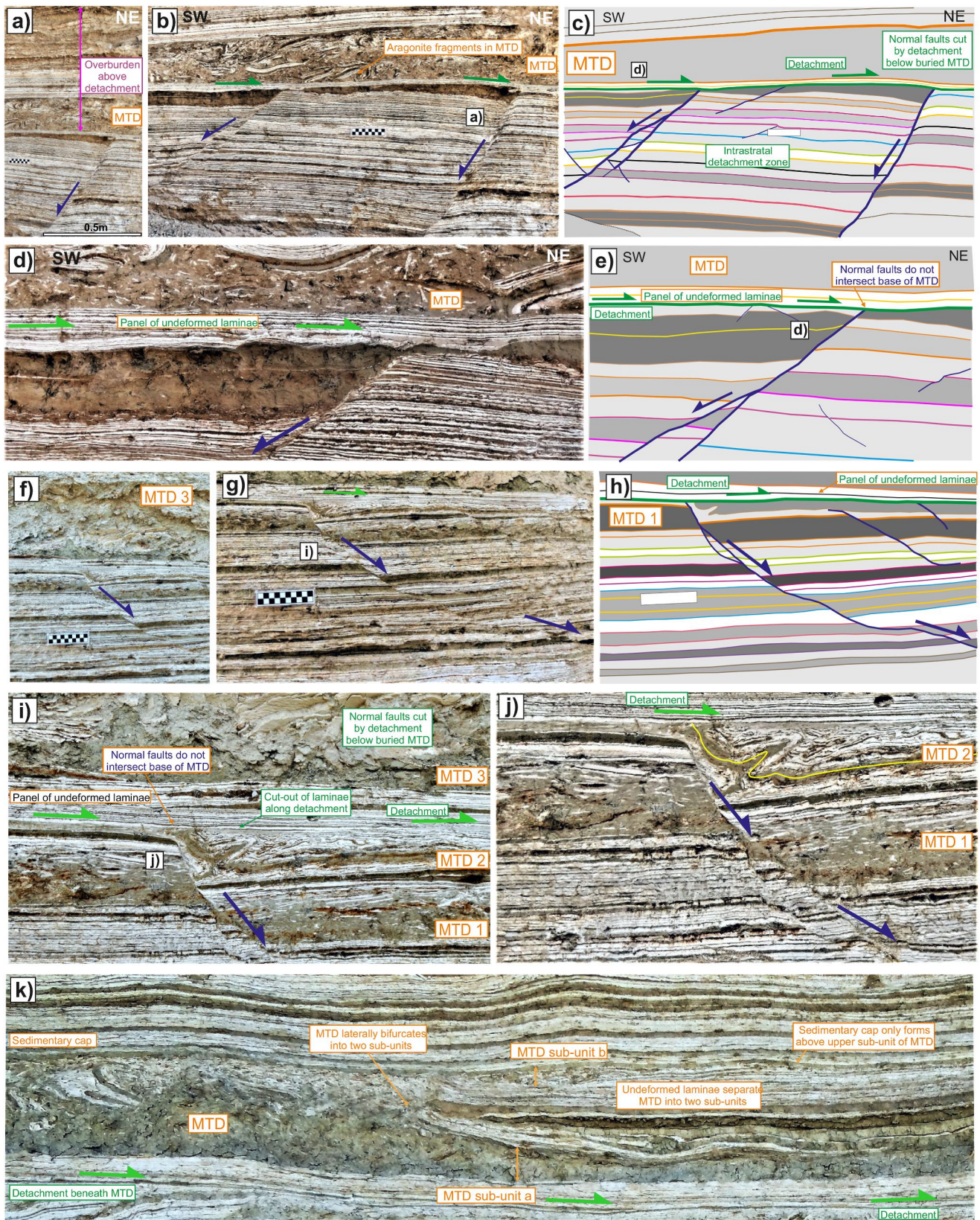


Fig. 19. a) Overview photograph, b) photograph, and c) line drawing of a detachment that forms beneath an MTD (Miflat). d) Photograph and e) line drawing of early normal faults being cut by the detachment that is separated from the overlying MTD by a thin panel of undeformed sediment. The normal faults are truncated by the intrastratal detachment rather than the erosive base of the MTD. f) Overview photograph, g) photograph and h) line drawing of MTDs being cut by normal faults that are truncated by a detachment. i, j) Photographs of MTD 1 and MTD 2 being cut by the normal fault, while MTD 3 overlies the intrastratal detachment. k) Photograph of a detachment formed beneath an MTD that is locally separated into two sub-units by an undeformed package of laminae. Only one sedimentary cap is developed above the upper sub-unit.

Dead Sea are largely based on classical stratigraphic principles (cross-cutting relationships etc.) as well as fundamental observations linked to structural geology. As such, they may be equally applicable to deformation of sediments in other basinal settings, including accretionary complexes where the distinction between tectonic features and gravity-driven structures formed within soft-sediments may become more problematic (see [Ogawa and Mori, 2021](#) for details).

9.1. Which surface and sub-surface deformation models are applicable to MTDs?

Sequential failure models have been typically applied to MTDs, whereby each MTD represents a separate failure event at the contemporary sediment surface that sequentially build up with deposition of new overlying sediment ([Figs. 1a and 20a, b](#)). Each deformed horizon therefore represents a new failure event that broadly corresponds to the age of the affected sediment (e.g. [Basilone et al., 2014](#); [Van Loon et al., 2016](#)). Where pre-existing buried MTDs act as competent horizons in the sedimentary sequence, they can localise later intrastratal detachments and focus secondary failure along the margins of the MTD ([Figs. 1c and 20a, c](#)). Conversely synchronous failure models, where single failure events concurrently generate multiple deformed horizons at the surface and sub-surface, have so far largely been applied to sequences that lack downslope movement (e.g. [Gibert et al., 2011](#)) ([Figs. 1b and 20a, d](#)). Several deformed horizons may be generated during a single failure event and affect sediments that are significantly older than the age of the event ([Figs. 1b and 20a, d](#)).

9.1.1. Evidence for surficial deformation and the sequential failure model

The surficial failure model summarised in [Fig. 1a](#) is usually applied to both gravity-driven downslope deformation of unlithified sediments to create slumps and MTDs, and also where there is a lack of downslope movement and deformation is driven by contrasts in density of adjacent beds (e.g. [Owen, 2003](#) for a review; [Van Loon et al., 2016](#)). Deformation is considered to be contemporaneous with deposition of each layer at the surface (e.g. [Rossetti and Goes, 2000](#); [Basilone et al., 2016](#), p.320; [Kumar et al., 2021](#)), with erosion above slump folds indicating that folding took place at the surface prior to deposition, and ‘blanketing’ by overlying beds ([Ortner and Kilian, 2016](#), p.357). Surficial deformation and remobilisation of sediment occurred at depths of up to 20 cm from the sediment surface in Chilean lakes, with this depth increasing with greater slope angles and larger magnitude earthquakes ([Molenaar et al., 2021](#)). The stratigraphic record preserved by seismo-turbidites in basinal sediments is crucial to recognise earthquake-induced surficial deformation of sediments in slope settings ([Molenaar et al., 2021](#)).

The significance of turbidites that directly overlie units of SSDs in the sedimentary record from the Dead Sea has been recognised and analysed by [Lu et al. \(2021b, c\)](#). The link between deformation and the sedimentary record demonstrates that SSDs in these cases formed at the sediment surface in the depocentre of Lake Lisan. Within the case study area, six individual MTDs up to 2 m thick were analysed by [Alsop et al. \(2016\)](#). Each of these MTDs is separated from the others by undeformed beds, and each is overlain by a sedimentary cap with a locally erosive base that was deposited out of suspension after the failure event. These observations are summarised in [Fig. 20a](#) and [b](#) and collectively indicate that each individual MTD sequentially formed at the sediment surface during recurrent failure of the gentle slope.

9.1.2. Surficial deformation horizons that laterally bifurcate

In some instances, a single deformed horizon may bifurcate laterally into two or more deformed units at different stratigraphic levels and separated by intervening undeformed beds (e.g. [Gibert et al., 2011](#); [Morsilli et al., 2020](#)). The upper deformed sub-unit may remain at the sediment surface, while the lower bifurcated unit will develop in the shallow sub-surface. This has been interpreted as a result of liquefaction at different levels in a multi-layered system during a single earthquake

([Gibert et al., 2011](#)). [Morsilli et al. \(2020\)](#) further suggest that the intervening undeformed sediments affected porosity and acted as a barrier to fluid flow and thereby facilitated liquefaction in adjacent sediments. Both of these cases focus on SSDs and seismites in sections which are marked by fluidisation and liquefaction structures associated with density-driven deformation. They appear to lack significant preferred orientation and development of asymmetrical folds and faults that characterise downslope mass transport of sediments ([Morsilli et al., 2020](#), p.12).

Within the Lisan Formation, examples of bifurcating deformed horizons are developed on the metre-scale where 5 cm thick panels of undeformed aragonite laminae locally separate MTDs into upper and lower sub-units ([Fig. 17a–d, 19k, 20a, b](#)). Only a single sedimentary cap is developed (above the upper unit) and this provides a reference for the position of the surface at the time of deformation. Despite the extensive exposures around the Dead Sea Basin, we find no evidence for larger scale bifurcating of MTD systems where individual slumps and MTDs are traced downslope for 500 m and consistently maintain distinct stratigraphic levels with each deformed horizon overlain by an individual sedimentary cap ([Alsop et al., 2016](#)). This may reflect the largely ‘layer-cake’ stratigraphy within the varved lake sediments, together with the simple bilaminar nature of sediments that comprises only aragonite- and detrital-rich beds. Clearly, even if deformed horizons were to bifurcate laterally into several individual horizons at different stratigraphic levels, there is still only one interface between sediment and the water column, and hence only a single sedimentary cap will form.

9.1.3. Evidence for sub-surface intrastratal deformation of buried MTDs and the secondary failure model

Pre-existing MTDs that formed at the surface can subsequently affect the mechanical stratigraphy of a sedimentary sequence and control where later secondary intrastratal deformation is focussed in the sub-surface ([Figs. 1c and 20a, c](#)). In a highly perceptive paper, [Brown \(1938\)](#) noted that sediment that had previously undergone folding nearer the surface could, after further burial, be overprinted by discrete, downslope-directed slide surfaces. [Brown \(1938, p.36\)](#) declared that “These large-scale slides will be superimposed on beds which have already suffered from sealing-wax flow (folding) and rupture on a small scale, mostly along bedding-planes”. More recently, [Sammartini et al. \(2021\)](#) have shown from silt-dominated lacustrine sediments that when surficial MTDs are buried to depths >1.5 m, they have greater shear strengths than undeformed sediment of equivalent depth. It is considered that increasing deformation and lateral compaction in the central part of MTDs may have resulted in reduction in porosity and expulsion of water leading to increased absolute shear strength in the MTDs ([Sammartini et al., 2021](#), p14). Similar relationships are recorded by [Daxer et al. \(2020, p.251\)](#) who note that slope failures in lacustrine sediments generally occur at <1 m depth below the sediment-water interface, with the top of older MTDs controlling where the basal slip surface of younger failure events develops. Sub-seismic scale MTDs may clearly play a role in acting as baffles and barriers to hydraulic flow across a range of scales in the sub-surface (e.g. [Steventon et al., 2021](#)).

Within the Lisan Formation, shallow sub-surface FATS can create duplexes where water is considered to be expelled from folds and thrusts and migrates upwards to weaken the overlying sequence and thereby help drive the upper detachment to the system ([Alsop et al., 2021a](#)). The consequence of this is that such deformed horizons become over-compacted and then act as baffles to later fluid flow. Overlying MTDs may themselves also act as barriers to fluid flow and influence where younger sub-surface intrastratal deformation focuses. MTDs and sub-surface FATS exert significant controls on subsequent fluid flow, and hence the localisation of secondary deformation, which is focussed adjacent to older deformed levels ([Figs. 17–19](#)).

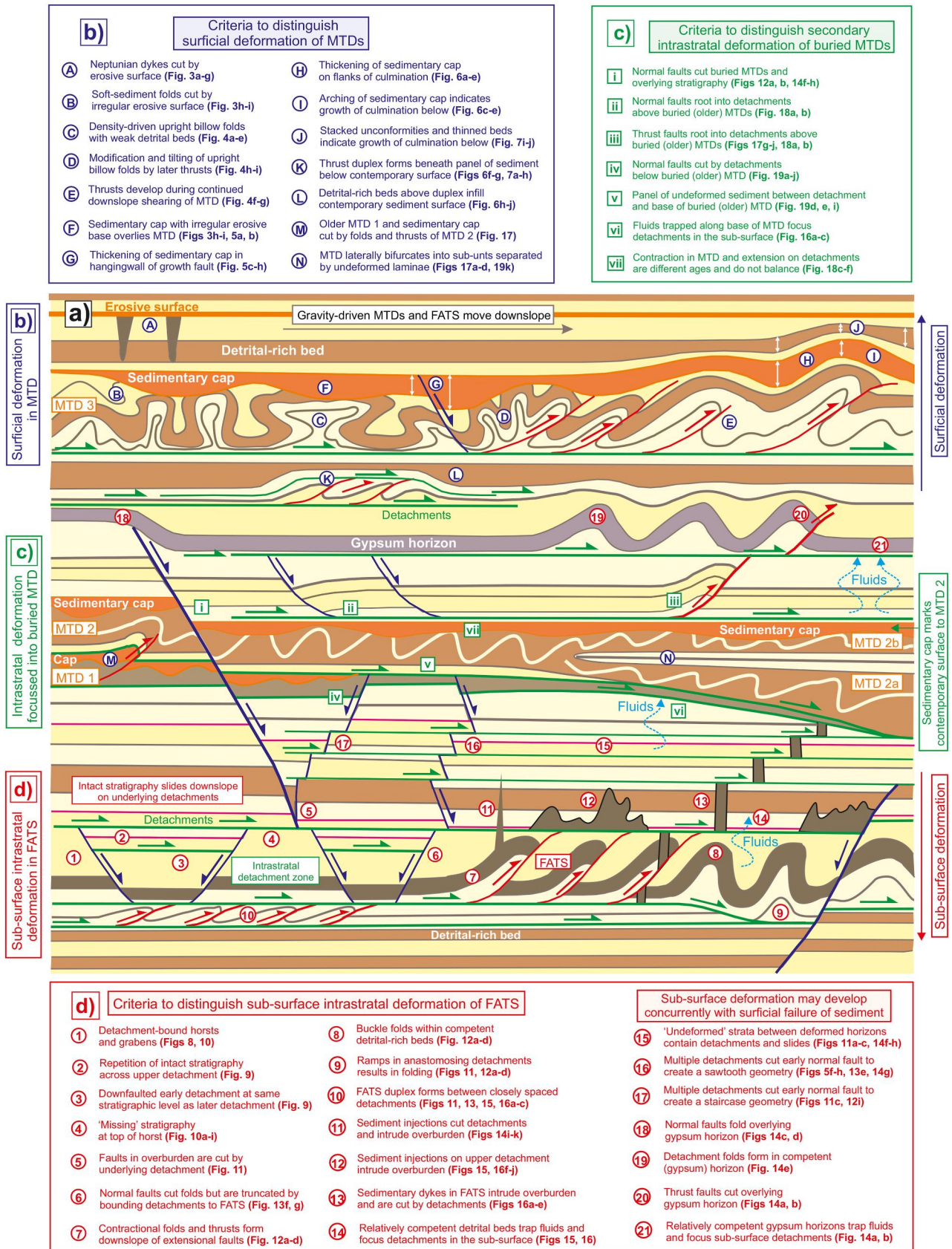


Fig. 20. a) Cartoon summarising structures used to distinguish deformation created at the surface (MTD) versus sub-surface (FATS) and also during secondary reworking of MTDs. Criteria are based on observations from the present study (denoted by figure numbers) and are separated into b) surficial deformation of MTDs (circled blue letters A-N), c) intrastratal secondary reworking of buried MTDs (boxed green roman numerals i-vii), and d) sub-surface intrastratal deformations in FATS (circled red numbers 1–21). Sub-surface reworking and FATS develop concurrently with deformation of surficial sediments during single events. (For interpretation of the references to colour in this figure legend, the reader is referred to the Web version of this article.)

9.1.4. Evidence for sub-surface intrastratal deformation and the synchronous failure model

The synchronous failure model involves deformation in both the surface and sub-surface during a single event (Fig. 1b) and therefore necessitates the identification of deeper-seated structures (Fig. 20a, d). Evidence for the sub-surface deformation of un lithified sediments has been provided in a number of previous studies including Budillon et al. (2014) who describe relatively deep gravity-driven slope failures which are associated with recurrent sediment failures along the seabed, and which also create internal slip planes within the MTD. Evidence for sub-surface deformation has also been presented by Moretti and Van Loon (2014, p.167) who suggest that deformation in marginal lake areas can take place at depths of up to 9 m in some environments. In this setting, deeper water-saturated sediments are prone to liquefaction and deformation, especially where overlain by less permeable sediments (e.g. Moretti and Van Loon, 2014, p.167). Sub-surface deformation of un lithified sediments has also been reported from Lake Superior where high resolution seismic and sonar data from fine grained glacio-lacustrine sediments has revealed polygonal systems of normal faults that penetrate un lithified sediments (Wattrus et al., 2003). The faults terminate at a lower bed-parallel intrastratal surface where sediment has mobilised and flowed laterally at depths of 10 m below the sediment-water interface, presumably in response to movement on the overlying faults (Wattrus et al., 2003).

In a further example of the synchronous failure model, Auchter et al. (2016) suggest that the rapid emplacement of a thick MTD creates intrastratal deformation and thrust duplexing in the underlying sequence. Three intrastratal deformation zones are considered to have developed synchronously during this single event, with positions partially controlled by the morphology of depositional sand lobes within the sequence. Stratigraphic thicknesses suggest that these sub-surface intrastratal failures formed concurrently at depths of ~60–70 m, ~30–40 m, and ~10 m below the contemporary sediment surface (Auchter et al., 2016, p.20).

Seismicity linked to post-glacial rebound in late Pleistocene lacustrine deposits results in liquefaction occurring at depths of up to 0.6 m (Belzyt et al., 2021, p.12). Deformation that creates ball and pillow structures, load casts, and broken laminae, is considered to develop within decimetres of the sediment surface, with each SSD horizon generally forming during separate events. However, Belzyt et al. (2021, p.20) note that sediment injections intrude from underlying SSDs into the overlying sequence and cross-cut the younger SSD horizons, leading them to suggest that some deformed horizons that lack overlying erosional truncations could have developed concurrently during a single failure event. The lack of erosive surfaces truncating underlying structures meant that Belzyt et al. (2021) were unable to determine the maximum number of seismic triggering events for SSDs, although the number of erosive surfaces provides a minimum estimate.

Although many MTDs recorded in the Lisan Formation preserve sedimentary caps with erosive bases that formed at the sediment surface, there are also cases of deformed horizons where no cap or erosive surface is present (e.g. Figs. 2, 8–130a, d). In these cases the deformed horizon is bound by upper and lower bed-parallel detachments that form during sub-surface intrastratal deformation and the age relationship with surficial sediments is therefore lost.

9.2. What are the key diagnostic criteria to identify surface and sub-surface deformation?

Distinguishing gravity-driven surficial deformation and gravity-driven sub-surface structures might not be straightforward as both are governed by the same slope that creates similar kinematics and comparable orientations of downslope-verging structures. For instance, folds created above sub-surface detachments share the same orientation as folds formed in earlier MTDs (Alsop et al., 2020c). These movement directions have also been corroborated by magnetic fabrics in AMS

studies of MTDs (Weinberger et al., 2017) confirming that movement is directed downslope around the basin. The orientation of folds and thrusts in MTDs or FATS is therefore of little value in distinguishing their mode of origin and further criteria need to be established.

9.2.1. Recognising erosive truncation versus bed-parallel detachments

It is crucial to distinguish surficial processes that create erosive surfaces from deeper-seated structures, such as intrastratal detachments that also cut across pre-existing structures but could be much younger than the overlying stratigraphy (Figs. 1b and 20a, b, d). Törö et al. (2015) record seismically generated intrastratal deformation in lacustrine deposits that lack erosive truncations, leading to an interpretation of intrastratal deformation rather than processes operating directly on the lake floor. Van Loon et al. (2016) and Belzyt et al. (2021) have also recognised the importance of identifying erosive surfaces in establishing surficial SSD in liquified horizons. If a detachment surface is established, then the associated deformation could have formed at depth in the sediment pile and the link to the surface (and precise age of deformation) is then broken. While some erosive surfaces are planar, others display significant relief on the scale of metres, and are also irregular on the cm-scale (e.g. Fig. 3h and i). Such rugosity severely hinders displacement along a detachment surface and is therefore a characteristic feature that supports an erosive surficial origin.

Issues around establishing the true nature of a bed-parallel surface are more likely to arise when dealing with planiform erosive surfaces that display similar geometries to detachments. In some cases, bed-parallel slip is associated with stratabound horizons of microfractures that help identify intrastratal deformation that formed at depth below the sediment surface (e.g. Grimm and Orange, 1997). The difficulty in recognising bed-parallel slip that creates glide planes at the base of sediment packages has also been highlighted by Ortner (2007, p.112). Ortner (2007) recognised local ramps that enable identification of bed-parallel glide planes that operated at depths of 6–7 m below the sediment surface during tilting associated with regional tectonics. Basilone et al. (2014, p.320) described translational slides in deepwater carbonates where sediment moved downslope above a detachment with the slide block maintaining its coherency. The detachment zones contain units of relatively undeformed strata that are bound by lower and upper detachments (e.g. Basilone et al. (2014, p.313, their Fig. 3). Regional uplift and overall tilting of the sea floor is, in this case, considered to drive the downslope movement along relatively discrete detachments (Basilone, 2017).

Within the Lisan Formation, no regional tilting has developed and the bed-parallel detachments translate overlying sediments down gentle (<1°) slopes towards the depocentre of the basin (Alsop et al., 2020c). Detachments are generally planar but are recognised by their offset of older faults (Fig. 20a, d). They are considered to operate within the upper 20 m of the Lisan Formation, with direct measurement of 10 m thick overburden above a detachment being deformed (e.g. Alsop et al., 2021a, p.3. their Fig. 1c and d).

9.2.2. Recognising sedimentary caps versus fluidisation that creates erosion in the sub-surface

It has been suggested from experimental work that unconformable surfaces that truncate underlying structures may potentially develop within buried sedimentary sequences (Moretti et al., 1999, p.376). In this scenario, silty sand is considered to undergo selective fluidisation and be transported upwards through overlying medium-coarse grained sand to create an upper layer of fine-grained sediment. This fine-grained horizon will be discordant and can truncate structures in the underlying coarser sand layer, while the top of the layer is horizontal and parallel to the overlying beds (Moretti et al., 1999, p.376). These experimental observations suggest that unconformable and erosive relationships could potentially develop in the sub-surface and are therefore not necessarily diagnostic of surficial processes. The creation of unconformable surfaces in the sub-surface by diffuse fluidisation and

elutriation of fine sediment does not leave clear evidence of focussed upward movement of fluids and could therefore be problematic to recognise in the sedimentary sequence.

Within the Lisan Formation, the sedimentary caps that overlie erosive surfaces contain larger cm-scale fragments of folded aragonite laminae, graded aragonite grains, evidence of currents resulting in cross laminations, and overall scouring resulting in irregular wave-like erosive surfaces along the base of the cap (e.g. [Alsop and Marco, 2011](#); [Alsop et al., 2016, 2021a](#)). In addition, laminae, although folded and faulted, are generally preserved in the underlying deformed horizon, while caps thicken in the hangingwall of sedimentary faults to create 'growth' sequences ([Fig. 3h and i, 6a-e](#)). These observations collectively indicate that sedimentary caps and underlying erosive surfaces in the Lisan Formation were created at the surface prior to deposition of the overlying sedimentary sequence that subsequently buried the unconformities.

9.2.3. Recognising sedimentary caps versus gouge along detachments

Given the importance of sedimentary caps in recognising surficial deformation, it is critical that they are clearly distinguished from gouge or breccia that forms during slip events (e.g. [Weinberger et al., 2016](#); [Alsop et al., 2020c](#)). Examination of horizons of carbonate breccia led [Van Loon et al. \(2013\)](#) to suggest that breccia layers with vertical clasts may have formed in the sub-surface after deposition of overlying beds that acted as a seal. They propose that although original brecciation developed on the sediment surface, the subsequent rotation of clasts to vertical attitudes reflects high pore fluid pressures leading to rapid fluid escape ([Van Loon et al., 2013](#)). Vertical clasts are atypical of sedimentary deposition and developed in the shallow sub-surface after the deformed horizon was buried by overlying sediments.

Within the Lisan Formation, gouge that is developed along steep-moderate dipping normal faults or thrusts is readily identified due to the cross-cutting nature of the fault plane (e.g. [Alsop et al., 2018](#)). However, gouge that forms along discrete bed-parallel detachments can be more problematic as it remains largely parallel to the adjacent sedimentary layers ([Fig. 8a-j](#)). Gouge along detachments typically has a buff colour that reflects the mixing of aragonite and detrital layers, and is especially well developed where the detachment transects adjacent laminae. In addition, sediment injections may develop from the gouge layers and intrude overlying beds ([Figs. 15 and 16](#)), demonstrating that the gouge is created during high fluid pressures that develops along the detachment and is inconsistent with deposition of a sedimentary cap at the surface.

9.2.4. Recognising depositional infilling versus hydroplastic thickening of beds

Over the past century it has been increasingly recognised that depositional infilling of underlying structures is a key piece of evidence in support of surficial deformation with [Miller \(1922, p.602\)](#) noting that surficial deformation is marked by "the distinct evidence of the filling of the depressions on the upper surface of the corrugated zone before the general layers of overlying materials were laid down". Although it is commonly observed that sediments will locally thicken and thin as they 'drape' over and fill irregular bathymetry at the sediment-water interface (e.g. [Basilone, 2017](#)), beds may also display changes in thickness where they undergo folding and thrusting associated with hydroplastic deformation in the sub-surface. In the Lisan Formation, sedimentary caps frequently infill underlying erosive scours resulting in pronounced changes in thickness to the cap ([Fig. 3h and i](#)). MTDs can also display growth and thickening in the hangingwall of normal faults, indicating that the faults were active at the time of deposition ([Fig. 5c-h](#)). In other cases, the sedimentary packages immediately above FATS maintain thickness across underlying culminations, and it is detrital units higher in the stratigraphy that record changes in depositional thicknesses. The age of the sediment package that displays changes in syn-tectonic thickness provides a bracket on the timing of the deformation. It is

normally detrital beds that record thickness changes as these units are deposited more rapidly during flood events and in general form thicker units. Continued deformation may fold these growth geometries ([Fig. 7](#)), that locally display onlapping relationships onto culminations indicating the surficial nature of the deformation ([Fig. 6c-e](#)). Alternatively, aragonite layers can display marked thickness variations around folds that were created in the sub-surface. In this case, the attenuation and thinning of units is achieved through hydroplastic deformation that operates in the sub-surface ([Fig. 13f and g, 16f-h](#)). In summary, depositional infilling is normally accommodated by detrital-rich beds that are rapidly deposited from flood events, whereas hydroplastic folding leads to thickening and attenuation concentrated in aragonite beds ([Alsop et al., 2020b](#)).

9.2.5. Recognising surficial MTD folding versus sub-surface detachment folds

Although there has been considerable effort to distinguish folds formed during SSD from those created during hard rock tectonism in lithified sequences (e.g. [Elliot and Williams, 1988](#); [Waldron and Gagnon, 2011](#); [Alsop et al., 2019, 2020](#)), there has been rather less work on discriminating between soft-sediment folds formed directly at the sediment surface versus those created during intrastratal deformation in the sub-surface. While much of the folding associated with SSD is frequently assumed to develop at the sediment surface, folding in the sub-surface is also described by [Ortner and Kilian \(2016, p.350\)](#) noting that "Sub-surface sediment mobilization may also create soft-sediment folds that reflect either the downslope direction or fluid movement after break of the seal ([Ortner, 2007](#)).". Distinguishing surficial and sub-surface intrastratal folding can be relatively straight forward where folds are truncated by overlying erosive surfaces and sedimentary caps that form at the surface ([Fig. 20a and b](#)), but is perhaps more problematic where such features do not exist and fold styles and geometries become more important.

The upright billow folds that form in surficial MTDs of the Lisan Formation ([Fig. 4a-g](#)) are interpreted to be a consequence of horizontal shortening associated with coaxial dominated deformation at the initial stage of slumping ([Alsop and Marco, 2011, p.449](#)). The upright folding could also reflect density-driven fold initiation where variations in density of aragonite-rich and detrital-rich beds lead to vertical movement driven by Rayleigh-Taylor (inverse density gradient) or Kelvin Helmholtz (normal-density gradient) instabilities (e.g. [Heifetz et al., 2005](#); [Wetzler et al., 2010](#); [Lu et al., 2017, p.15](#); [Lu et al., 2021c, p.6](#)). The observation that underlying aragonite-rich beds penetrate upwards as narrow antiformal 'fingers' into the overlying detrital-rich beds suggests that the aragonite beds are less dense than the detrital-rich beds. We speculate that this partially reflects the 'stellate' form of needle-like aragonite crystals that may trap significant volumes of interstitial water, thereby reducing the overall density of aragonite-rich beds (see also section 9.3.3.). In other cases, the detrital-rich beds display buckle folds (Class 1B parallel folds, [Ramsay, 1967](#)) suggesting that the detrital-rich beds were more competent and formed via horizontal compression above a basal detachment in the sub-surface ([Fig. 7a-h, 12c-d](#)) (see [Alsop et al., 2020b](#)). The initiation of folding in MTDs will therefore take a variety of forms depending on the arrangement of beds of differing densities, and the amount of dewatering that may already have occurred in beds prior to downslope movement.

9.2.6. Recognising truncation of overlying structures

Structures such as faults or folds may be truncated by either overlying erosive surfaces or by overlying detachments, and as such, truncation from above is non-diagnostic. However, where faults are cut across by underlying structures then this becomes a key observation as erosive surfaces clearly cannot truncate features in the overlying sequence that was not deposited at the time of erosion (e.g. [O'Leary and Laine, 1996, p.311](#)). Rotational slumps studied by [Basilone et al. \(2016\)](#) comprise folded and faulted beds that are draped by overlying

undeformed beds indicating surficial deformation during creation of MTDs. Conversely, [Basilone et al. \(2016, p.319 their table1\)](#) also recognise a second type of 'gravity-slide' packages comprising relatively undeformed beds that are shown to have an upper surface that truncates folds in the overlying sequence. This relationship suggests that the overlying sediments were already deposited at the time of deformation, which was therefore sub-surface. In addition, [Pratt and Rule \(2021, p.22\)](#) have used the length of faults developed in overburden to suggest that intrastratal sliding occurred under 'tens of centimetres' of burial.

Within the Lisan Formation, normal faults that offset stratigraphy are themselves truncated by underlying detachments ([Fig. 11a–f, 12a–d, 14f–h, 20a, d](#)). Similarly, aragonite-detriral laminae can also be transected by underlying detachments, although the low-angle nature of the cut-offs makes such relationships more difficult to identify (e.g. [Fig. 8g](#)). Normal faults therefore act as steep markers that allow underlying bed-parallel intrastratal detachments to be identified ([Alsop et al., 2020c](#)). Where normal faults extend for several metres above detachments then the detachment must be younger than the sediments affected by the normal fault. This provides a minimum estimate for the depth at which the detachment operated. In the case of the Lisan Formation this depth is typically 5 m before exposure is lost ([Alsop et al., 2020c](#)), although deformation may potentially be up to 20 m below the surface ([Alsop et al., 2020c](#)). One of the important keys to identifying and understanding bed-parallel detachments that operate in the sub-surface is the truncation of *overlying* faults that extend upwards through stratigraphy towards the surface ([Fig. 20a, d](#)).

9.3. What controls where and when sub-surface deformation localises?

9.3.1. Control on sub-surface deformation by de-watering and 'seismic strengthening'

The focussing of sub-surface deformation into particular horizons reflects the overall strength of the sequence, which is highly dependent on dewatering and build-up of fluid-pressures in the sedimentary pile (e.g. [Owen, 2003; Locat et al., 2014](#)). [Ortner and Kilian \(2016, p.350\)](#) note that "Incomplete dewatering near the sediment surface can lead to sub-surface sediment mobilization at a later stage, after some burial". This subsequent deeper mobilization may result in sediment injections but can also weaken the entire sequence as overpressured layers act as 'easy slip' horizons along which later deformation localises. Such weak horizons may include volcano-clastic beds that contain large amounts of fluid and influence the position of subsequent failure surfaces (e.g. [Kuhlmann et al., 2016](#)).

[Molenaar et al. \(2021\)](#) also recognised that, although much of the deformation observed in sediment cores from lakes in Chile is linked to surficial deformation associated with megathrust earthquakes, other SSDs are created deeper in the sediment pile by seismic-induced dewatering of intercalated volcanic deposits, which would consequently weaken overlying sediment and facilitate sub-surface deformation ([Moernaut et al., 2019](#)). Tephra layers dewater during seismic shaking leading to an increase in density of these layers and a weakening of the overlying lake sediment, which then fails and translates downslope ([Moernaut et al., 2019, p.100](#)). Such tephra layers are typically 0.3–0.5 m below the sediment-water interface at the time of seismic shaking, while deeper buried tephra layers suffer repeated seismicity resulting in denser grain packing and 'seismic strengthening' over time ([Moernaut et al., 2019](#)). This seismic strengthening process involves the creation of excess pore-pressure during earthquakes, and subsequent dissipation and gentle escape of fluids during interseismic intervals, thereby leading to over-consolidated sequences ([Moernaut et al., 2019; Lenz and Sawyer, 2021](#)). However, it is possible for more deeply buried tephra layers to fail if the overburden reaches a critical thickness of >6 m sporadically resulting in larger scale translational sliding of the sequence ([Moernaut et al., 2019, p.101](#)). [Molenaar et al. \(2019, p.6021\)](#) examined sediments in the NE Japan trench and report increases in shear strength in sediments buried to 9 cm depth below the sediment-water interface,

which they attribute to a reduction in voids associated with seismic strengthening. Sediments at 9–15 cm depth have shear strengths that are comparable to 3–7 m depth of burial in normally consolidated sequences, suggesting that repeated seismicity has increased the shear strength of shallowly-buried sediment.

Numerous earthquakes are reported along the DSF that cause repeated slope failures and creation of MTDs within the Lisan Formation. As noted above, recurrent seismicity may also lead to sediment repacking, dewatering and seismic strengthening that results in buried MTDs forming relatively competent horizons that focus later deformation in the stratigraphic sequence (see section 9.1.3.). Concentration of sub-surface detachments adjacent to MTDs in the secondary failure model creates the potential for overprinting of surficial structures created during original MTD emplacement by later intrastratal detachments formed during continued downslope movement in the sub-surface ([Fig. 20a, c](#)).

9.3.2. Control on sub-surface deformation by detrital-rich beds

The control exerted by original sedimentary layering on subsequent sub-surface deformation is an important factor with [Brown \(1938, p.360\)](#) originally noting that "sliding in more finely stratified beds is like that of a pack of cards". However, where significant variations in the depositional architecture is formed, such as thicker sandstone lobes, then these sedimentary geometries may control where later intrastratal deformation develops in the sub-surface ([Auchter et al., 2016](#)).

Within the Lisan Formation, it has been recognised that detrital beds focus detachments when they are deformed close (<1 m) to the surface ([Alsop et al., 2016, their Fig. 8c and d](#)) suggesting they are relatively weak fluid-rich horizons. However, detailed analysis of thrust-related folding at potentially deeper levels in the sediment pile shows that detrital layers form more competent horizons, resulting in parallel (Class 1B) fold styles compared to similar (Class 2) folds in aragonite-rich beds ([Alsop et al., 2020b; 2021a](#)). We speculate that the differing relative competence of detrital and aragonite beds that varies with depth could reflect greater dewatering of detrital beds as they become buried. This is possibly related to more rounded detrital grains undergoing greater re-sorting and denser packing after repeated seismic events compared to the acicular aragonite crystals that form interlocked clusters that trap fluids. Competent detrital beds act as baffles or seals that trap fluids beneath them causing potential increases in pore fluid pressure and localising later sub-surface detachments ([Alsop et al., 2018](#)). The build-up in fluid pressure may ultimately cause fluidised sediment from along detachments to rupture and break through the overlying competent bed ([Alsop et al., 2018](#)).

9.3.3. Control on sub-surface deformation by early precipitation of cements

Mechanically distinctive horizons formed by early precipitation of cements may create heterogeneity within a sequence and control where subsequent sub-surface deformation develops. Intrastratal deformation in the shallow sub-surface can be created during downslope sliding of poorly-lithified carbonates which have undergone incipient cementation ([Ettensohn et al., 2011; Pratt and Rule, 2021, p.21](#)). In mixed clastic and carbonate sequences, clastic sediments undergo surficial deformation cut by erosive surfaces, while carbonate sediments experience early cementation and are marked by intrastratal deformation below the sediment surface ([Chen and Lee, 2013](#)). Some carbonates display folding in the upper part of the bed while the lower part remains undeformed, suggesting that the upper bed is weaker reflecting a vertical variation in cementation ([Dechen and Aiping, 2012, p.81](#)). The timing of precipitation of cements in carbonates can therefore play an important role in localising sub-surface deformation, with a number of recent studies highlighting intrastratal deformation in mixed siliclastic-carbonate sequences (e.g. [Hou et al., 2020; Walker et al., 2021](#)).

Within the Lisan Formation, gypsum horizons are considered to precipitate when the usually stratified water column of Lake Lisan was mixed and overturned, possibly following major earthquakes ([Ichinose](#)

and Begin, 2004; Begin et al., 2005). The competent gypsum horizons subsequently act as baffles that hinder the upward migration of trapped fluids through the sedimentary pile. This can result in potential increases in fluid pressure and concomitant reductions in shear strength of sediments directly beneath the gypsum (e.g. Alsop et al., 2020c). The focussing of sub-surface deformation and detachments beneath gypsum could therefore be a consequence of increased fluid pressures at these particular levels. The control exerted by MTDs, overlying detrital beds, or gypsum horizons on later secondary deformation demonstrates that deformation developed after the overlying barrier to flow had already formed, thereby indicating sub-surface intrastratal deformation.

9.4. What are the consequences of sub-surface deformation in MTDs?

The critical importance of recognising intrastratal deformation has been highlighted by O'Leary and Laine (1996, p.305) who state "An accurate understanding of basin development and marine mass movement requires correct discrimination of intrastratal deformation from buried surficial slide deposits, as the origins and geological implications of these two kinds of stratiform features are significantly different". The realisation that sub-surface deformation, as well as surficial MTDs, develop during gravity-driven downslope movement of sediments has a number of important consequences.

9.4.1. Consequences for balancing of deformation

It is widely considered that extension developed in the upslope 'head' of gravity-driven MTDs should broadly balance and be equivalent to the amount of shortening preserved in the downslope 'toe' region (e.g. Farrell, 1984). However, several authors including Butler and Paton (2010), de Vera et al. (2010), Morley and Naghadeh (2018) and Steventon et al. (2019) have noted that extension and contraction do not balance in MTDs. A failure to recognise younger sub-surface deformation developed adjacent to older MTDs that are buried in the stratigraphic sequence has important implications for the balancing of shortening and extension in such systems. For instance, extensional conjugates associated with sub-surface deformation are developed adjacent to older contractional folds in MTDs (Fig. 18c–f). A confusion between structures formed during older surficial MTD movement and younger sub-surface intrastratal deformation will result in such systems failing to 'balance' as deformation is of two different ages.

9.4.2. Consequences for rates of deformation

Deformation associated with surficial MTDs is considered to be rapid as structures form before creation of the overlying erosive surface and sedimentary cap that is deposited out of suspension. Estimates of time required to deposit sediments out of suspension in lacustrine environments following an earthquake suggest settling of 1 μm particles from a 1 m thick suspension cloud would take ~2 weeks, while slightly coarser 4 μm particles could be deposited in a matter of hours or days (Wils et al., 2021). This is similar to previous estimates in the Lisan Formation where sedimentary caps are thought to be deposited out of suspension "in a matter of just hours or days" (Alsop et al., 2016, p.80). These short-lived timescales linked to deposition therefore provide rigorous constraints on the rates of deformation within the surficial MTDs. However, once the direct 'link' to sediment deposition is broken during sub-surface deformation, then there are fewer controls and deformation could potentially be slower and relate to downslope creep of the sedimentary pile. Indeed, Ortner and Kilian (2016, p.361) have suggested that some slumps form by continuous creep down submarine slopes prior to complete lithification of the (carbonate) sediments. Similarly, Basilone (2017) also suggests that intact and coherent stratigraphic packages moved downslope on bed-parallel detachments via a process of sediment creep in deepwater carbonates.

Field evidence for slumping associated with creep processes within Holocene sediments around the Dead Sea Basin has been provided by Alsop and Weinberger (2020, p.13). Several observations collectively

support downslope creep of sediments including: i) growth of evaporite concretions affecting developing fold geometries within slumps, ii) topography created above slumps infilled by sediment with several overlying beds thickening and 'ponding' in synformal depressions suggesting ongoing fold development, iii) continued and protracted thrusting affecting unconformities that form above slumps, and, iv) the lack of overlying sedimentary caps suggesting slumping was not rapid enough to throw sediment into suspension in the water column. Although these Holocene slumps are considered to be slow moving on slopes of 4–6°, they are still thought to develop at the sediment surface due to the presence of unconformities and erosive surfaces.

In the present study focussing on structures created in the sub-surface of the Lisan Formation, rates of movement are difficult to determine as the direct link to sedimentation is broken. However, the observation that the sedimentary cap itself is arched over underlying culminations (e.g. Fig. 6c–e), or that a number of overlying detrital beds are thinned over structural highs created by FATS (e.g. Fig. 7a–h), suggests that intrastratal deformation was more protracted than observed at the surface. Sequences of stacked unconformities that are deformed above growing culminations (e.g. Fig. 7i and j) also supports more prolonged deformation related to downslope creep of sediments immediately below the surface. In some cases, normal faults that develop in the overburden cut folds and thrusts in the detachment zone but are themselves truncated by the upper and lower detachments (Fig. 13f and g). This indicates that detachments continued to operate after FATS had formed in the sub-surface and suggests protracted downslope creep of the sediment pile can lead to reworking of structures that typifies deformation in the sub-surface.

9.4.3. Consequences for age of deformation

The potential role of seismicity during intrastratal deformation has been recognised over the past century with Miller (1922, p.600) noting intrastratal deformation in Quaternary sands and clays where "under the action of gravity or gravity aided by earthquake shocks, overlying beds have moved differentially over lower-level beds in the general direction of the dip". O'Leary and Laine (1996, p.305) studied high-resolution seismics from the continental slope and stated that "Intrastratal deformation that occurs within a few hundred metres below the sea floor may indicate rapid, non-disintegrative failure due to seismic shock", amongst other things. It has therefore been increasingly appreciated that the simple counting of the number of deformed horizons in the sedimentary record cannot be used to accurately determine the number and age of seismic events. Törő and Pratt (2016, p.196) summarise this dilemma by noting that "In the simplest sense, each deformed interval records a single earthquake, although it is clear that some [structures] do record a second or even a third event".

There are a range of factors that will affect the accuracy of using deformed horizons in palaeoseismic studies. In some cases, deformed horizons are created by processes entirely unrelated to seismicity, such as unequal loading or wave and tidal action (see Owen, 2003; Owen and Moretti, 2011; for a summary). In deformed horizons that are created by seismicity, multiple earthquakes can affect the same deformed horizon (e.g. Wils et al., 2021). In such cases, structures with different deformation styles can be superimposed on one another indicating that the deformed horizon was affected by more than one event (e.g. Berra and Felletti, 2011; Törő and Pratt, 2016). These overprinting relationships suggest that the sediments were at different stages of consolidation at the time of each deformation episode (Berra and Felletti, 2011), and that the change from plastic to brittle structures records increasing sediment 'stiffness' with time (Törő and Pratt, 2016). In other cases, sediments may undergo liquefaction at the contemporary surface marked by erosional features, followed by later re-liquefaction of the same horizon after being buried in the sub-surface during repeated seismicity (Woźniak et al., 2021). Individual horizons can therefore conceal more than one earthquake event, while in other cases there may be a lack of suitable fluid-rich sediments that can easily deform and therefore they

do not record any earthquake event (e.g. see Morsilli et al., 2020). Multiple generations of sedimentary dykes that overprint one another in deformed intrastratal horizons indicate several closely spaced injection events occurred in the sub-surface (e.g. Törö and Pratt, 2015b), potentially reflecting multiple seismic events affecting the same horizon.

The recognition in this and other studies that deformed horizons can bifurcate laterally into two or more separate horizons also has clear implications for the counting and use of such layers to estimate the recurrence times of palaeoseismic events (e.g. Gibert et al., 2011; Morsilli et al., 2020). Belzyt et al. (2021) were unable to identify sedimentary caps above each of their deformed horizons leading them to suggest that some horizons could have deformed concurrently at the surface and sub-surface during a single seismic event.

Within this case study both surficial and sub-surface intrastratal deformation has been recognised and is schematically summarised in Fig. 20a–d. Following previous workers who studied SSD intervals that lack downslope movement (e.g. Van Loon et al., 2016; Belzyt et al., 2021), we have stressed the importance of recognising erosive surfaces and sedimentary caps that link MTDs with the surface. Sub-surface deformation of the sedimentary sequence clearly leads to issues with simple age-depth correlations where the timing of seismic events is estimated from the level (depth) of sediment that they affect and bracketed by dated horizons (see Moernaut, 2020 and Kempf and Moernaut, 2021 for reviews). The consequences of sub-surface intrastratal deformation is that the link with the age of the sediment is removed and it therefore cannot be assumed that deformation affecting stratigraphically lower beds is older and triggered by older earthquakes. The identification of sub-surface intrastratal deformation, coupled with the synchronous failure model, therefore raise fundamental issues for the use of SSD in palaeoseismic studies necessitating careful observations and application of the detailed criteria outlined in this study.

10. Conclusions

In this study we have used the Lisan Formation deposited around the Dead Sea to document features and stratigraphic relationships that form at the sediment surface during creation of MTDs and compared these with intrastratal structures that are created in the sub-surface during downslope movement of gravity-driven FATS. In such studies, the orientation and vergence of structures may be of little value in distinguishing surface versus sub-surface deformation as both are controlled by the same downslope movement and will therefore have similar trends. Key points arising from this study are highlighted below.

- 1) Gravity-driven deformation of sediments associated with slope failure is divided into two end-member models: i) sequential failure model where repeated slope failures at the sediment surface systematically build-up multiple MTDs in the stratigraphic record, and ii) synchronous failure model where a single event creates concurrent surficial and sub-surface intrastratal deformed horizons at different stratigraphic levels.
- 2) An intermediate secondary failure model, where buried MTDs subsequently focus later sub-surface deformation, is also developed. This reflects the fact that MTDs frequently form significant heterogeneities within the otherwise layer-cake stratigraphy of the lacustrine sediments due to earlier dewatering and seismic strengthening. Other markers, such as thick detrital beds and precipitated gypsum horizons, also localise later sub-surface intrastratal deformation beneath them.
- 3) Irregular erosive surfaces and overlying sedimentary caps deposited out of suspension are key features in recognising surficial deformations of MTDs. Sub-surface deformation associated with FATS are marked by upper detachments that display thin horizons of gouge, repetitions of stratigraphy across the detachment, and truncation of faults in the overlying sequence. Additionally, injection of

fluidised sediment that forms along detachment surfaces can intrude into the overlying sequence that buried the detachment.

- 4) Sub-surface deformation cuts through entire stratigraphic sequences containing several separate MTDs and therefore affects and locally repeats what are considered to be the ‘undeformed’ beds between individual MTDs. Sub-surface deformation tends to be focussed along discrete intrastratal detachments with the overlying sequence carried downslope as relatively intact ‘slides’.
- 5) The recognition of both surficial MTDs and sub-surface intrastratal deformation within a sequence means that care must be taken to clearly differentiate structures of different ages and depths of deformation, as misidentification may lead to contractional-extensional systems failing to balance.
- 6) As sub-surface deformation is not directly correlated with the rapid deposition of sedimentary caps above MTDs, the rates of gravity-driven movement along deeper detachments are unconstrained and could be associated with slower downslope creep of the sediment pile.
- 7) As sub-surface intrastratal deformation is not directly correlated with the depositional age of the beds it affects, it cannot be assumed that deformation is older in stratigraphically lower beds. This weakens the age-depth correlations frequently used to estimate the timing of earthquake recurrence in palaeoseismic studies.

Declaration of competing interest

The authors declare that they have no known competing financial interests or personal relationships that could have appeared to influence the work reported in this paper.

Acknowledgements

SM acknowledges the Israel Science Foundation (ISG Grant No. 1645/19) and the Ministry of National Infrastructures, Energy and Water Resources (grant #214-17-027). TL acknowledges the Israeli government GSI DS project 40706. We thank Fabrizio Agosta for efficient editorial handling and two reviewers for constructive comments that helped improve the manuscript.

References

- Agnon, A., Migowski, C., Marco, S., 2006. Intraclast breccia layers in laminated sequences: recorders of paleo-earthquakes. In: Enzel, Y., Agnon, A., Stein, M. (Eds.), *New Frontiers in Dead Sea Paleoenvironmental Research*. Geological Society of America Special Publication, pp. 195–214.
- Alsop, G.I., Marco, S., 2011. Soft-sediment deformation within seismogenic slumps of the Dead Sea basin. *J. Struct. Geol.* 33, 433–457.
- Alsop, G.I., Weinberger, R., 2020. Are slump folds reliable indicators of downslope flow in recent mass transport deposits? *J. Struct. Geol.* 135, 104037. <https://doi.org/10.1016/j.jsg.2020.104037>.
- Alsop, G.I., Marco, S., Weinberger, R., Levi, T., 2016. Sedimentary and structural controls on seismogenic slumping within mass transport deposits from the Dead Sea basin. *Sediment. Geol.* 344, 71–90.
- Alsop, G.I., Marco, S., Levi, T., Weinberger, R., 2017a. Fold and thrust systems in mass transport deposits. *J. Struct. Geol.* 94, 98–115.
- Alsop, G.I., Marco, S., Weinberger, R., Levi, T., 2017b. Upslope-verging back thrusts developed during downslope-directed slumping of mass transport deposits. *J. Struct. Geol.* 100, 45–61.
- Alsop, G.I., Weinberger, R., Marco, S., 2018. Distinguishing thrust sequences in gravity-driven fold and thrust belts. *J. Struct. Geol.* 109, 99–119.
- Alsop, G.I., Weinberger, R., Marco, S., Levi, T., 2019. Identifying soft-sediment deformation in rocks. *J. Struct. Geol.* 125, 248–255. <https://doi.org/10.1016/j.jsg.2017.09.001>.
- Alsop, G.I., Weinberger, R., Marco, S., Levi, T., 2020a. Fold and thrust systems in mass transport deposits around the Dead Sea Basin. In: Ogata, K., Festa, A., Pini, G.A. (Eds.), *Submarine Landslides: Subaqueous Mass Transport Deposits from Outcrops to Seismic Profiles*. American Geophysical Union Monograph Series, vol. 246. John Wiley & Sons Inc. ISBN 978-1-119-50058-2, pp. 139–154, 384.
- Alsop, G.I., Weinberger, R., Marco, S., Levi, T., 2020b. Folding during soft-sediment deformation. Geological society special publication. In: Bond, C.E., Lebit, H.D. (Eds.), *Folding and Fracturing of Rocks: 50 Years since the Seminal Text Book of J.G. Ramsay*, vol. 487, pp. 81–104. <https://doi.org/10.1144/SP487.1>.

- Alsop, G.I., Weinberger, R., Marco, S., Levi, T., 2020c. Bed-parallel slip: identifying missing displacement in mass transport deposits. *J. Struct. Geol.* 131, 103952.
- Alsop, G.I., Weinberger, R., Marco, S., Levi, T., 2020d. Distinguishing coeval patterns of contraction and collapse around flow lobes in mass transport deposits. *J. Struct. Geol.* 134, 104013.
- Alsop, G.I., Weinberger, R., Marco, S., Levi, T., 2021a. Detachment fold duplexes within gravity-driven fold and thrust systems. *J. Struct. Geol.* 142, 104207. <https://doi.org/10.1016/j.jsg.2020.104207>.
- Alsop, G.I., Weinberger, R., Marco, S., Levi, T., 2021b. Criteria to discriminate between different models of thrust ramping in gravity-driven fold and thrust systems. *J. Struct. Geol.* 150, 104396. <https://doi.org/10.1016/j.jsg.2021.104396>.
- Alves, T.M., 2015. Submarine slide blocks and associated soft-sediment deformation in deep-water basins: a review. *Mar. Petrol. Geol.* 67, 262–285.
- Arkin, Y., Michaëli, L., 1986. The significance of shear strength in the deformation of laminated sediments in the Dead Sea area. *Isr. J. Earth Sci.* 35, 61–72.
- Armandita, C., Morley, C.K., Rowell, P., 2015. Origin, structural geometry, and the development of a giant slide: the South Makassar Strait mass transport complex. *Geosphere* 11, 376–403.
- Auchter, N.C., Romans, B.W., Hubbard, S.M., 2016. Influence of deposit architecture on intrastratal deformation, slope deposits of the Tres Pasos Formation, Chile. *Sediment. Geol.* 341, 13–26.
- Baldry, R.A., 1938. Slip-planes and breccia zones in the Tertiary rocks of Peru. *Quarterly Journal of the Geological Society* 94, 347–358.
- Bartov, Y., Stein, M., Enzel, Y., Agnon, A., Reches, Z., 2002. Lake levels and sequence stratigraphy of Lake Lisan, the late Pleistocene precursor of the Dead Sea. *Quat. Res.* 57, 9–21.
- Bartov, Y., Goldstein, S.L., Stein, M., Enzel, Y., 2003. Catastrophic arid episodes in the eastern mediterranean linked with the north atlantic Heinrich events. *Geology* 31, 439–442.
- Basilone, L., 2017. Seismogenic rotational slumps and translational glides in pelagic deep-water carbonates. Upper Tithonian-Berriasian of Southern Tethyan margin (W Sicily, Italy). *Sediment. Geol.* 356, 1–14.
- Basilone, L., Lena, G., Gasparo-Morticelli, M., 2014. Synsedimentary tectonic, soft sediment deformation and volcanism in the rifted Tethyan margin from the Upper Triassic-Middle Jurassic deep-water carbonates in Central Sicily. *Sediment. Geol.* 308, 63–79. <https://doi.org/10.1016/j.sedgeo.2014.05.002>.
- Basilone, L., Sulli, A., Gasparo Morticelli, M., 2016. The relationships between soft-sediment deformation structures and synsedimentary extensional tectonics in Upper Triassic deep-water carbonate succession (Southern Tethyan rifted continental margin — central Sicily). *Sediment. Geol.* 344, 310–322.
- Bates, R.L., Jackson, J.A., 1980. *Glossary of Geology*, second ed. American Geological Institute, Falls Church, Virginia, USA, p. 751.
- Begin, Z.B., Ehrlich, A., Nathan, Y., 1974. Lake Lisan, the Pleistocene precursor of the Dead Sea. *Geol. Surv. Isr. Bull.* 63, 30.
- Begin, B.Z., Steinberg, D.M., Ichinose, G.A., Marco, S., 2005. A 40,000 years unchanging of the seismic regime in the Dead Sea rift. *Geology* 33, 257–260.
- Belzyt, S., Pisanska-Jamroz, M., Bitinas, A., Woronko, B., Phillips, E.R., Piotrowski, J.A., Juszczyk, A., 2021. Repetitive Late Pleistocene soft-sediment deformation by seismicity-induced liquefaction in north-western Lithuania. *Sedimentology*. <https://doi.org/10.1111/sed.12883>.
- Ben-Dor, Y., Neugebauer, I., Enzel, Y., Schwab, M.J., Tjallingii, R., Erel, Y., Brauer, A., 2019. Varves of the Dead Sea sedimentary record. *Quat. Sci. Rev.* 215, 173–184.
- Berra, F., Felletti, F., 2011. Syndepositional tectonics recorded by soft-sediment deformation and liquefaction structures (continental Lower Permian sediments, Southern Alps, Northern Italy): stratigraphic significance. *Sediment. Geol.* 235, 249–263.
- Brown, C.B., 1938. On a theory of gravitational sliding applied to the Tertiary of Ancon, Ecuador. *Quarterly Journal of the Geological Society* 94, 359–368.
- Budillon, F., Cesarano, M., Conforti, A., Pappone, G., Di Martino, G., Pelosi, N., 2014. Recurrent superficial sediment failure and deep gravitational deformation in a Pleistocene slope marine succession: the Poseidonia Slide (Salerno Bay, Tyrrhenian Sea). In: Krastel, S., Behrmann, J.-H., Volker, D., Stipp, M., Berndt, C., Urgeles, R., Chaytor, J., Huhn, K., Strasser, M., Harbitz, C.B. (Eds.), *Submarine Mass Movements and Their Consequences, Advances in Natural and Technological Hazards Research*, vol. 37. © Springer International Publishing Switzerland, pp. 273–284. <https://doi.org/10.1007/978-3-319-00972-8-24>, 2014.
- Bull, S., Cartwright, J., Huuse, M., 2009. A review of kinematic indicators from mass-transport complexes using 3D seismic data. *Mar. Petrol. Geol.* 26, 1132–1151.
- Butler, R.W.H., Paton, D.A., 2010. Evaluating lateral compaction in deepwater fold and thrust belts: How much are we missing from “nature’s sandbox”. *GSA Today (Geol. Soc. Am.)* 20, 4–10.
- Butler, R.W.H., Bond, C.E., Cooper, M.A., Watkins, H., 2020. Fold-thrust structures – where have all the buckles gone? *Geological Society Special Publication*. In: Bond, C. E., Lebit, H.D. (Eds.), *Folding and Fracturing of Rocks: 50 Years since the Seminal Text Book of J.G. Ramsay*, vol. 487, pp. 21–44.
- Cardona, S., Wood, L.J., Dugan, B., Jobe, Z., Strachan, L.J., 2020. Characterization of the Rapanui mass-transport deposit and the basal shear zone: mount messenger formation, Taranaki basin, New Zealand. *Sedimentology* 67, 2111–2148. <https://doi.org/10.1111/sed.12697>.
- Chakraborty, P.P., Sharma, R., Kumar, P., 2019. Earthquake-induced soft sediment deformation (SSD) structures from the Bilara limestone formation, Marwar basin, India. *Journal of Earth System Science* 128. <https://doi.org/10.1007/s12040-019-1182-x>, 162, 16.
- Chen, J., Lee, H.S., 2013. Soft-sediment deformation structures in Cambrian siliciclastic and carbonate storm deposits (Shandong Province, China): differential liquefaction and fluidization triggered by storm-wave loading. *Sediment. Geol.* 288, 81–94.
- Daxer, C., Sammartini, M., Molenaar, A., Piechl, T., Strasser, M., Moernaut, J., Georgiopoulou, A., Amy, L.A., Benetti, S., Chaytor, J.D., Clare, M.A., Gamboa, D., Houghton, P.D.W., Moernaut, J., 2020. Morphology and spatio-temporal distribution of lacustrine mass-transport deposits in Wörthersee, Eastern Alps, Austria. In: Mountjoy, J.J. (Ed.), *Subaqueous Mass Movements and Their Consequences: Advances in Process, Understanding, Monitoring and Hazard Assessments*, vol. 500. Geological Society, London, Special Publications, pp. 235–254.
- de Vera, J., Granado, P., McClay, K., 2010. Structural evolution of the Orange Basin gravity-driven system, offshore Namibia. *Mar. Petrol. Geol.* 27, 223–237.
- Dechen, S., Aiping, S., 2012. Typical earthquake-induced soft-sediment deformation structures in the mesoproterozoic Wumishan formation, Yongding river valley, Beijing, China and interpreted earthquake frequency. *J. Palaeogeogr.* 1, 71–89. <https://doi.org/10.3724/SP.J.1261.2012.00007>.
- El-Isa, Z.H., Mustafa, H., 1986. Earthquake deformations in the Lisan deposits and seismotectonic implications. *Geophys. J. Roy. Astron. Soc.* 86, 413–424.
- Elliot, C.G., Williams, P.F., 1988. Sediment slump structures: a review of diagnostic criteria and application to an example from Newfoundland. *J. Struct. Geol.* 10, 171–182.
- Ellis, M.A., Dunlap, W.J., 1988. Displacement variation along thrust faults: implications for the development of large faults. *J. Struct. Geol.* 10, 183–192.
- Ettensohn, F.R., Zhang, C., Gao, L., Lierman, R.T., 2011. Soft-sediment deformation in epicontinental carbonates as evidence of paleoseismicity with evidence for a possible new seismogenic indicator: accordion fold. *Sediment. Geol.* 235, 222–233.
- Farrell, S.G., 1984. A dislocation model applied to slump structures, Ainsa Basin, South Central Pyrenees. *J. Struct. Geol.* 6, 727–736.
- Ferrill, D.A., Morris, A.P., Wigginton, S.S., Smart, K.J., McGinnis, R.N., Lehmann, D., 2016. Deciphering thrust fault nucleation and propagation and the importance of footwall synclines. *J. Struct. Geol.* 85, 1–11.
- Festa, A., Ogata, K., Pini, G.A., Dilek, Y., Alonso, J.L., 2016. Origin and significance of olistostromes in the evolution of orogenic belts: a global synthesis. *Gondwana Res.* 29, 180–203.
- Fossen, H., 2016. *Structural Geology*, second ed. Cambridge University Press, Cambridge, UK, p. 510.
- Frey Martinez, J., Cartwright, J., Hall, B., 2005. 3D seismic interpretation of slump complexes: examples from the continental margin of Israel. *Basin Res.* 17, 83–108.
- Frey-Martinez, J., Cartwright, J., James, D., 2006. Frontally confined versus frontally emergent submarine landslides: a 3D seismic characterisation. *Mar. Petrol. Geol.* 585–604.
- Frydman, S., Charrach, J., Goretzky, I., 2008. Geotechnical properties of evaporite soils of the Dead Sea area. *Eng. Geol.* 236–244.
- Gao, Y., Jiang, Z., Best, J.L., Zhang, J., 2020. Soft-sediment deformation structures as indicators of tectono-volcanic activity during evolution of a lacustrine basin: a case study from the Upper Triassic Ordos Basin, China. *Mar. Petrol. Geol.* 115, 104250.
- Garcia-Tortosa, F.J., Alfaro, P., Gibert, L., Scott, G., 2011. Seismically induced slump on an extremely gentle slope (<1°) of the Pleistocene Tecopa paleolake (California). *Geology* 39, 1055–1058.
- Georgiopoulou, A., Amy, L.A., Benetti, S., Chaytor, J.D., Clare, M.A., Gamboa, D., Houghton, P.D.W., Moernaut, J., Mountjoy, J.J., 2020. Subaqueous mass movements and their consequences: advances in process understanding, monitoring and Hazard assessments. *Geological Society, London, Special Publications* 500, 634. <https://doi.org/10.1144/SP500>.
- Gibert, L., Sanz de Galdeano, C., Alfaro, P., Scott, G., Lopez Garrido, A.C., 2005. Seismic-induced slump in early Pleistocene deltaic deposits of the Baza basin (SE Spain). *Sediment. Geol.* 179, 279–294.
- Gibert, L., Alfaro, P., Garcia-Tortosa, F.J., Scott, G., 2011. Superposed deformed beds produced by single earthquakes (Tecopa Basin, California): insights into paleoseismology. *Sediment. Geol.* 235, 148–159.
- Grimm, K.A., Orange, D.L., 1997. Synsedimentary fracturing, fluid migration, and subaqueous mass wasting: intrastratal microfractured zones in laminated diatomaceous sediments, Miocene Monterey Formation, California, USA. *J. Sediment. Res.* 67, 601–613.
- Haase-Schramm, A., Goldstein, S.L., Stein, M., 2004. U-Th dating of Lake Lisan aragonite (late Pleistocene Dead Sea) and implications for glacial East Mediterranean climate change. *Geochem. Cosmochim. Acta* 68, 985–1005.
- Haliva-Cohen, A., Stein, M., Goldstein, S.L., Sandler, A., Starinsky, A., 2012. Sources and transport routes of fine detritus material to the late quaternary Dead Sea basin. *Quat. Sci. Rev.* 50, 55–70.
- Heifetz, E., Agnon, A., Marco, S., 2005. Soft sediment deformation by Kelvin Helmholtz instability: a case from Dead Sea earthquakes. *Earth Planet Sci. Lett.* 236, 497–504. <https://doi.org/10.1016/j.epsl.2005.04.019>.
- Hou, Z., Chen, S., Zhang, S., Yang, H., 2020. Sedimentary deformation features as evidence for paleoseismic events in the middle Eocene in the Dongying Depression of the southern Bohai Bay Basin, eastern China. *Can. J. Earth Sci.* 57, 954–970. <https://doi.org/10.1139/cjes-2019-0160>.
- Hughes, A.N., Shaw, J.H., 2014. Fault displacement-distance relationships as indicators of contractional fault-related folding style. *AAPG (Am. Assoc. Pet. Geol.) Bull.* 98, 227–251.
- Huhn, K., Arroyo, M., Cattaneo, A., Clare, M.A., Gràcia, E., Harbitz, C.B., Krastel, S., Kopf, A., Løvholt, F., Rovere, M., Strasser, M., Talling, P.J., Urgeles, R., 2020. Modern submarine landslide complexes: a short review. In: Ogata, K., Festa, A., Pini, G.A. (Eds.), *Submarine Landslides: Subaqueous Mass Transport Deposits from Outcrops to Seismic Profiles*. American Geophysical Union Monograph Series, vol. 246. John Wiley & Sons Inc. 384pp, ISBN 978-1-119-50058-2, pp. 183–200.
- Ichinose, G.A., Begin, Z.B., 2004. Simulation of Tsunamis and Lake Seiches for the Late Pleistocene Lake Lisan and the Dead Sea. *Geological Survey of Israel Report GSI/77/04*, p. 50.

- Ireland, M.T., Davies, R.J., Gouly, N.R., Moy, D.J., 2011. Thick slides dominated by regular-wavelength folds and thrusts in biosiliceous sediments on the Vema Dome offshore of Norway. *Mar. Geol.* 289, 34–45.
- Jablonska, D., Di Celma, C., Korneva, I., Tondi, E., Alsop, I., 2016. Mass-transport deposits within basinal carbonates from southern Italy. *Italian Journal of Geosciences* 135, 30–40.
- Jablonska, D., Di Celma, C., Tondi, E., Alsop, G.I., 2018. Internal architecture of mass-transport deposits in basinal carbonates: a case study from southern Italy. *Sedimentology* 65, 1246–1276. <https://doi.org/10.1111/sed.12420>.
- Jolly, B.A., Lonergan, L., Whittaker, A.C., 2016. Growth history of fault-related folds and interaction with seabed channels in the toe-thrust region of the deep-water Niger delta. *Mar. Petrol. Geol.* 70, 58–76.
- Kagan, E.J., Stein, M., Marco, S., 2018. Integrated palaeoseismic chronology of the last glacial Lake Lisan: from lake margin seismites to deep-lake mass transport deposits. *J. Geophys. Res.: Solid Earth* 123 (4), 2806–2824.
- Kempf, P., Moernaut, J., 2021. Age uncertainty in recurrence analysis of paleoseismic records. *Journal of Geophysical research, Solid Earth*. <https://doi.org/10.1029/2021JB021996>.
- Ken-Tor, R., Agnon, A., Enzel, Y., Marco, S., Negendank, J.F.W., Stein, M., 2001. High-resolution geological record of historic earthquakes in the Dead Sea basin. *J. Geophys. Res.* 106, 2221–2234.
- Knappe, R.J., 1986. Deformation Mechanism Path Diagrams for Sediments Undergoing Lithification, vol. 166. *Memoir of the Geological Society of America*, pp. 151–160.
- Korneva, I., Tondi, E., Jablonska, D., Di Celma, C., Alsop, I., Agosta, F., 2016. Distinguishing tectonically- and gravity-driven synsedimentary deformation structures along the Apulian platform margin (Gargano Promontory, southern Italy). *Mar. Petrol. Geol.* 73, 479–491.
- Krastel, S., Behrmann, J.-H., Völker, D., Stipp, M., Berndt, C., Urgeles, R., Chaytor, J., Huhn, K., Strasser, M., Harbitz, C.B., 2014. Submarine mass movements and their consequences. *Advances in Natural and Technological Hazards Research* 37, 683. <https://doi.org/10.1007/978-3-319-00972-8> (© Springer International Publishing Switzerland).
- Kuhlmann, J., Huhn, K., Ikari, M.J., 2016. Do embedded volcanoclastic layers serve as potential glide planes?: an integrated analysis from the Gela Basin offshore southern Sicily. In: Lamarche, G., Mountjoy, J., Bull, S., Hubble, T., Krastel, S., Lane, E., Micallef, A., Moscardelli, L., Mueller, C., Pecher, I., Woelz, S. (Eds.), *Submarine Mass Movements and Their Consequences, Advances in Natural and Technological Hazards Research*, vol. 41, pp. 273–280. https://doi.org/10.1007/978-3-319-20979-1_27.
- Kumar, P.C., Omosanya, K.O., Eruteya, O.E., Sain, K., 2021. Geomorphological characterization of basal flow markers during recurrent mass movement: a case study from the Taranaki Basin, offshore New Zealand. *Basin Res.* 33, 2358–2382. <https://doi.org/10.1111/bre.12560>.
- Lamarche, G., Mountjoy, J., Bull, S., Hubble, T., Krastel, S., Lane, E., Micallef, A., Moscardelli, L., Mueller, C., Pecher, I., Woelz, S., 2016. Submarine mass movements and their consequences: progress and challenges. In: Lamarche, G., Mountjoy, J., Bull, S., Hubble, T., Krastel, S., Lane, E., Micallef, A., Moscardelli, L., Mueller, C., Pecher, I., Woelz, S. (Eds.), *Submarine Mass Movements and Their Consequences, Advances in Natural and Technological Hazards Research*, vol. 41, pp. 1–14. https://doi.org/10.1007/978-3-319-20979-1_1.
- Lenz, B.L., Sawyer, D.E., 2021. Mass transport deposits in reflection seismic data offshore Oregon, USA. *Basin Res.* <https://doi.org/10.1111/BRE.12611>.
- Levi, T., Weinberger, R., Aifa, T., Eyal, Y., Marco, S., 2006a. Injection mechanism of clay-rich sediments into dikes during earthquakes. *G-cubed* 7 (12), Q12009.
- Levi, T., Weinberger, R., Aifa, T., Eyal, Y., Marco, S., 2006b. Earthquake-induced clastic dikes detected by anisotropy of magnetic susceptibility. *Geology* 34 (2), 69–72.
- Levi, T., Weinberger, R., Alsop, G.I., Marco, S., 2018. Characterizing seismites with anisotropy of magnetic susceptibility. *Geology* 46 (9), 827–830.
- Liang, L., Qiao, X., Dai, F., Zhong, N., Jiang, H., 2021. Seismically triggered soft-sediment deformation structures in Tashkorgan lacustrine sediments, northeastern Pamir, China. *Quat. Int.* <https://doi.org/10.1016/j.quaint.2021.06.021>.
- Locat, J., Leroueil, S., Locat, A., Lee, H., 2014. Weak layers: their definition and classification from a geotechnical perspective. In: Krastel, S., Behrmann, J.-H., Völker, D., Stipp, M., Berndt, C., Urgeles, R., Chaytor, J., Huhn, K., Strasser, M., Harbitz, C.B. (Eds.), *Submarine Mass Movements and Their Consequences, Advances in Natural and Technological Hazards Research*, vol. 37. © Springer International Publishing Switzerland, pp. 3–12. <https://doi.org/10.1007/978-3-319-00972-8-1>.
- Lu, Y., Waldmann, N., Alsop, G.I., Marco, S., 2017. Interpreting soft sediment deformation and mass transport deposits as seismites in the Dead Sea depocenter. *J. Geophys. Res.: Solid Earth* 122, 8305–8325.
- Lu, Y., Marco, S., Wetzler, N., Fang, X., Alsop, G.I., Hubert-Ferrari, A., 2021a. A paleoseismic record spanning 2-Myr reveals episodic late Pliocene deformation in the western Qaidam Basin, NE Tibet. *Geophys. Res. Lett.* 48, e2020GL090530 <https://doi.org/10.1029/2020GL090530>.
- Lu, Y., Moernaut, J., Waldmann, N., Bookman, R., Alsop, G.I., Hubert-Ferrari, A., Strasser, M., Wetzler, N., Agnon, A., Marco, S., 2021b. Orbital- and millennial-scale changes in lake levels facilitate earthquake-triggered mass failures in the Dead Sea Basin. *Geophys. Res. Lett.* 48 (14), e2021GL093391 <https://doi.org/10.1029/2021GL093391>.
- Lu, Y., Moernaut, J., Bookman, R., Waldmann, N., Wetzler, N., Agnon, A., Marco, S., Alsop, G.I., Strasser, M., Hubert-Ferrari, A., 2021c. A new approach to constrain the seismic origin for prehistoric turbidites as applied to the Dead Sea Basin. *Geophys. Res. Lett.* 48, e2020GL090947 <https://doi.org/10.1029/2020GL090947>.
- Maltman, A., 1984. On the term soft-sediment deformation. *J. Struct. Geol.* 6, 589–592.
- Maltman, A., 1994a. Introduction and overview. In: Maltman, A. (Ed.), *The Geological Deformation of Sediments*. Chapman & Hall, London, pp. 1–35.
- Maltman, A., 1994b. Deformation structures preserved in rocks. In: Maltman, A. (Ed.), *The Geological Deformation of Sediments*. Chapman & Hall, London, pp. 261–307.
- Marco, S., Stein, M., Agnon, A., Ron, H., 1996. Long term earthquake clustering: a 50,000 year paleoseismic record in the Dead Sea Graben. *J. Geophys. Res.* 101, 6179–6192.
- Marco, S., Hartal, M., Hazan, N., Lev, L., Stein, M., 2003. Archaeology, history, and geology of the A.D. 749 earthquake, Dead Sea transform. *Geology* 31, 665–668.
- Migowski, C., Agnon, A., Bookman, R., Negendank, J.F.W., Stein, M., 2004. Recurrence pattern of Holocene earthquakes along the Dead Sea transform revealed by varve-counting and radiocarbon dating of lacustrine sediments. *Earth Planet Sci. Lett.* 222, 301–314.
- Miller, W.J., 1922. Intraformational corrugated rocks. *J. Geol.* 30, 587–610.
- Moernaut, J., 2020. Time-dependent recurrence of strong earthquake shaking near plate boundaries: a lake sediment perspective. *Earth Sci. Rev.* 210, 103344.
- Moernaut, J., Van Daele, M., Heirman, K., Wiemer, G., Molenaar, A., Vandorpe, T., Melnick, D., Hajdas, I., Pino, M., Urrutia, M.P., De Batist, M., 2019. The subaqueous landslide cycle in south-central Chilean lakes: the role of tephra, slope gradient and repeated seismic shaking. *Sediment. Geol.* 381, 84–105.
- Molenaar, A., Moernaut, J., Wiemer, G., Dubois, N., Strasser, M., 2019. Earthquake impact on active margins: Tracing surficial remobilization and seismic strengthening in a slope sedimentary sequence. *Geophys. Res. Lett.* 46, 6015–6023. <https://doi.org/10.1029/2019GL082350>.
- Molenaar, A., Van Daele, M., Vandorpe, T., Degenhart, G., De Batist, M., Urrutia, M.P., Pino, M., Strasser, M., Moernaut, J., 2021. What controls the remobilization and deformation of surficial sediment by seismic shaking? Linking lacustrine slope stratigraphy to great earthquakes in South-Central Chile. *Sedimentology*. <https://doi.org/10.1111/sed.12856>.
- Moretti, M., Sabato, L., 2007. Recognition of trigger mechanisms for soft-sediment deformation in the Pleistocene lacustrine deposits of the Sant'Arcangelo Basin (Southern Italy): seismic shock vs. overloading. *Sediment. Geol.* 196, 31–45.
- Moretti, M., Van Loon, A.J.T., 2014. Restrictions to the application of 'diagnostic' criteria for recognizing ancient seismites. *J. Palaeogeogr.* 3, 162–173.
- Moretti, M., Alfaro, P., Caselles, O., Canas, J.A., 1999. Modelling seismites with a digital shaking table. *Tectonophysics* 304, 369–383.
- Morley, C.K., Naghadeh, D.H., 2018. Tectonic compaction shortening in toe region of isolated listric normal fault, North Taranaki Basin, New Zealand. *Basin Res.* 30, 424–436.
- Morley, C.K., von Hagke, C., Hansberry, R.L., Collins, A.S., Kanitpanyacharoen, W., King, R., 2017. Review of major shale-dominated detachment and thrust characteristics in the diagenetic zone: Part 1, meso- and macro-scale. *Earth Science Reviews* 173, 168–228.
- Morsilli, M., Buccì, M.G., Gliozzi, E., Lisco, S., Moretti, M., 2020. Sedimentary features influencing the occurrence and spatial variability of seismites (late Messinian, Gargano Promontory, southern Italy). *Sediment. Geol.* 401, 105628.
- Moscardelli, L., Wood, L., 2008. New classification system for mass transport complexes in offshore Trinidad. *Basin Res.* 20, 73–98.
- Muraoka, H., Kamata, H., 1983. Displacement distribution along minor fault traces. *J. Struct. Geol.* 5, 483–495.
- Nuriel, P., Weinberger, R., Kylander-Clark, A.R.C., Hacker, B.R., Craddock, J.P., 2017. The onset of the Dead Sea transform based on calcite age-strain analyses. *Geology* 45, 587–590.
- Obermeier, S.F., 2009. Using liquefaction-induced and other soft-sediment features for paleoseismic analysis. *Int. Geophys.* 95, 497–564. [https://doi.org/10.1016/S0074-6142\(09\)95007-0](https://doi.org/10.1016/S0074-6142(09)95007-0).
- Ogata, K., Mutti, E., Pini, G.A., Tinterri, R., 2012. Mass transport-related stratal disruption within sedimentary mélanges: examples from the northern Apennines (Italy) and south-central Pyrenees (Spain). *Tectonophysics* 568–569, 185–199.
- Ogata, K., Pogačnik, Z., Pini, G.A., Tunis, G., Festa, A., Camerlenghi, A., Rebesco, M., 2014. The carbonate mass transport deposits of the Paleogene Friuli Basin (Italy/Slovenia): internal anatomy and inferred genetic processes. *Mar. Geol.* 356, 88–110. <https://doi.org/10.1016/j.margeo.2014.06.014>.
- Ogata, K., Festa, A., Pini, G.A., 2020. Submarine landslides: subaqueous mass transport deposits from outcrops to seismic profiles, geophysical monograph 246. In: Ogata, K. (Ed.), *Andrea Festa, and Gian Andrea Pini. 2020 American Geophysical Union, first ed. Published by John Wiley & Sons, Inc., ISBN 978-1-119-50058-2*
- Ogawa, Y., Mori, S., 2021. Gravitational sliding or tectonic thrusting?: examples and field recognition in the Miura-Boso subduction zone prism. In: Wakabayashi, J., Dilek, Y. (Eds.), *Plate Tectonics, Ophiolites, and Societal Significance of Geology: A Celebration of the Career of Eldridge Moores*. Geological Society of America Special, pp. 197–232. [https://doi.org/10.1130/2021.2552\(10\).Paper.552](https://doi.org/10.1130/2021.2552(10).Paper.552).
- Ortner, H., 2007. Styles of soft-sediment deformation on top of a growing fold system in the Gosau Group at Muttekopf, Northern Calcareous Alps, Austria: slumping versus tectonic deformation. *Sediment. Geol.* 196, 99–118.
- Ortner, H., Kilian, S., 2016. Sediment creep on slopes in pelagic limestones: upper Jurassic of northern Calcareous alps, Austria. *Sediment. Geol.* 344, 350–363.
- Owen, G., 2003. Load structures: gravity-driven sediment mobilization in the shallow subsurface. In: VAN RENSBURGEN, R. et al. (Eds.), *Subsurface Sediment Mobilization*, 216 The Geological Society of London, London, pp. 21–34.
- Owen, G., Moretti, M., 2011. Identifying triggers for liquefaction-induced soft-sediment deformation in sands. *Sediment. Geol.* 235, 141–147.
- O'Leary, D.W., Laine, E., 1996. Proposed criteria for recognizing intrastratal deformation features in marine high resolution seismic reflection profiles. *Geo Mar. Lett.* 16, 305–312.
- Palladino, G., Grippa, A., Bureau, D., Alsop, G.I., Hurst, A., 2016. Emplacement of sandstone intrusions during contractional tectonics. *J. Struct. Geol.* 89, 239–249.

- Palladino, G., Alsop, G.I., Grippa, A., Zvirtes, G., Phillip, R.P., Hurst, A., 2018. Sandstone-filled normal faults: a case study from Central California. *J. Struct. Geol.* 110, 86–101.
- Palladino, G., Alsop, G.I., Grippa, A., Seers, T., Hurst, A., 2021. Sandstone intrusions along different types of faults and their effect on fluid flow in siliclastic reservoirs. *Geological Society Special Publication*. In: Silcock, S., Huuse, M., Bowman, M., Hurst, A., Cobain, S. (Eds.), *Subsurface Sand Remobilization and Injection*, vol. 493, pp. 273–286. <https://doi.org/10.1144/SP493-2018-45>.
- Porat, N., Levi, T., Weinberger, R., 2007. Possible resetting of quartz OSL signals during earthquakes – evidence from late Pleistocene injection dikes, Dead Sea basin, Israel. *Quat. Geochronol.* 272–277.
- Posamentier, H.W., Martinsen, O.J., 2011. The character and genesis of submarine mass-transport deposits: insights from outcrop and 3D seismic data. *Mass transport deposits in Deepwater settings: SEPM (Soc. Sediment. Geol.) Spec. Publ.* 96, 7–38.
- Prasad, S., Negendank, J.F.W., Stein, M., 2009. Varve counting reveals high resolution radiocarbon reservoir age variations in palaeolake Lisan. *J. Quat. Sci.* 24, 690–696.
- Pratt, B.R., Rule, R.G., 2021. A Mesoproterozoic carbonate platform (lower Belt Supergroup of western North America): sediments, facies, tides, tsunamis and earthquakes in a tectonically active intracratonic basin. *Earth Sci. Rev.* 217, 103626. <https://doi.org/10.1016/j.earscirev.2021.103626>.
- Ramsay, J.G., 1967. *Folding and Fracturing of Rocks*. McGraw-Hill, New York, p. 568pp.
- Reis, A.T., Araújo, E., Silva, C.G., Cruz, A.M., Gorini, C., Droz, L., Migeon, S., Perovano, R., King, I., Bache, F., 2016. Effects of a regional décollement level for gravity tectonics on late Neogene to recent large-scale slope instabilities in the Foz do Amazonas Basin, Brazil. *Mar. Petrol. Geol.* 75, 29–52.
- Rich, J.L., 1950. Flow markings, groovings, and intrastatal crumplings as criteria for recognition of slope deposits, with illustrations from Silurian rocks of Wales. *Bull. Am. Assoc. Pet. Geol.* 34, 717–741.
- Rossetti, D.F., Goes, A.M., 2000. Deciphering the sedimentological imprint of paleoseismic events: an example from the Aptian Codo Formation, northern Brazil. *Sediment. Geol.* 135, 137–156.
- Sammartini, M., Moernaut, J., Anselmetti, F.S., Hilbe, M., Lindhorst, K., Praet, N., Strasser, M., 2020. An atlas of mass-transport deposits in lakes. In: Ogata, K., Festa, A., Pini, G.A. (Eds.), *Submarine Landslides: Subaqueous Mass Transport Deposits from Outcrops to Seismic Profiles*. American Geophysical Union Monograph Series, vol. 246. John Wiley & Sons Inc. 384pp, ISBN 978-1-119-50058-2, pp. 201–226.
- Sammartini, M., Moernaut, J., Kopf, A., Stegmann, S., Fabbri, S.C., Anselmetti, F.S., Strasser, M., 2021. Propagation of frontally confined subaqueous landslides: insights from combining geophysical, sedimentological, and geotechnical analysis. *Sediment. Geol.* 416, 105877.
- Scarselli, N., McClay, K., Elders, C., 2016. Seismic geomorphology of Cretaceous megaslides offshore Namibia (Orange Basin): insights into segmentation and degradation of gravity-driven linked systems. *Mar. Petrol. Geol.* 75, 151–180.
- Shanmugam, G., 2017. Global case studies of soft-sediment deformation structures (SSDS): definitions, classifications, advances, origins, and problems. *J. Palaeogeogr.* 6, 251–320.
- Sharman, G.R., Graham, S.A., Masalimova, L.U., Shumaker, L.E., King, P.R., 2015. Spatial patterns of deformation and palaeoslope estimation within the marginal and central portions of a basin-floor mass-transport deposit, Taranaki Basin, New Zealand. *Geosphere* 11, 266–306.
- Smith, J.V., 2000. Flow pattern within a Permian submarine slump recorded by oblique folds and deformed fossils, Ulladulla, south-eastern Australia. *Sedimentology* 47, 357–366.
- Sneh, A., Weinberger, R., 2014. Major Structures of Israel and Environs, Scale 1:50,000. Israel Geological Survey, Jerusalem.
- Sobiesiak, M., Kneller, B.C., Alsop, G.I., Milana, J.P., 2017. Sub-seismic scale folding and thrusting within an exposed mass transport deposit: a case study from NW Argentina. *J. Struct. Geol.* 96, 176–191.
- Sobiesiak, M., Kneller, B.C., Alsop, G.I., Milana, J.P., 2018. Styles of basal interaction beneath mass transport deposits. *Mar. Petrol. Geol.* 98, 629–639.
- Sobiesiak, M., Kneller, B.C., Alsop, G.I., Milana, J.P., 2020. Block generation, deformation and interaction of mass-transport deposits with the seafloor: an outcrop-based study of the Carboniferous Paganzo Basin (Cerro Bola, NW Argentina). In: Ogata, K., Festa, A., Pini, G.A. (Eds.), *Submarine Landslides: Subaqueous Mass Transport Deposits from Outcrops to Seismic Profiles*. American Geophysical Union Monograph Series, vol. 246. John Wiley & Sons Inc. 384pp, ISBN 978-1-119-50058-2, pp. 91–104.
- Steventon, M.J., Jackson, C.A.-L., Hodgson, D.M., Johnson, H.D., 2019. Strain analysis of a seismically imaged mass-transport complex, offshore Uruguay. *Basin Res.* 31, 600–620.
- Steventon, M.J., Jackson, C.A.-L., Johnson, H.D., Hodgson, D.M., Kelly, S., Omma, J., Gopon, C., Stevenson, C., Fitch, P., 2021. Evolution of a sand-rich submarine channel-lobe system, and the impact of mass-transport and transitional-flow deposits on reservoir heterogeneity: magnus Field, Northern North Sea. *Petrol. Geosci.* 27 <https://doi.org/10.1144/petgeo2020-095>.
- Tang, W., Zhang, Y., Pe-Piper, G., Piper, D.J.W., Guo, Z., Li, W., 2020. Soft-sediment deformation structures in alkaline lake deposits of Lower Permian Fengcheng Formation, Junggar Basin, NW China: implications for syn-sedimentary tectonic activity. *Sediment. Geol.* 406, 105719.
- Torfstein, A., Goldstein, S.L., Kagan, E., Stein, M., 2013. Integrated multi-site U-Th chronology of the last glacial Lake Lisan. *Geochem. Cosmochim. Acta* 104, 210–231.
- Toro, B., Pratt, B.R., 2015. Eocene paleoseismic record in the Green River Formation, Fossil Basin, Wyoming — implications of synsedimentary deformation structures in lacustrine carbonate mudstones. *J. Sediment. Res.* 85, 855–884.
- Törö, B., Pratt, B.R., 2015b. Characteristics and implications of sedimentary deformation features in the green river formation (Eocene) in Utah and Colorado. In: Vanden Berg, M.D., Resselar, R., Birgenheier, L.P. (Eds.), *Geology of Utah's Uinta Basin and Uinta Mountains*, vol. 45. Utah Geological Association Publication, pp. 371–422.
- Törö, B., Pratt, B.R., 2016. Sedimentary record of seismic events in the Eocene Green River Formation and its implications for regional tectonics on lake evolution (Bridger Basin, Wyoming). *Sediment. Geol.* 344, 175–204.
- Törö, B., Pratt, B.R., Renaut, R.W., 2015. Tectonically induced change in lake evolution recorded by seismites in the Eocene Green River Formation, Wyoming. *Terra. Nova* 27, 218–224.
- Van Daele, M., Moernaut, J., Doom, L., Boes, E., Fontijn, K., Heirman, K., Vandoorne, W., Hebbeln, D., Pino, M., Urrutia, R., Brummer, R., De Batist, M., 2015. A comparison of the sedimentary records of the 1960 and 2010 great Chilean earthquakes in 17 lakes: implications for quantitative lacustrine palaeoseismology. *Sedimentology* 62, 1466–1496.
- Van Loon, A.J., 2014. Seismites and their soft-sediment deformation structures. *Geologos* 20/2, 166.
- Van Loon, A.J., Han, Z., Han, Y., 2013. Origin of the vertically orientated clasts in brecciated shallow-marine limestones of the Chaomidian Formation (Furongian, Shandong Province, China). *Sedimentology* 60, 1059–1070.
- Van Loon, A.J., Pisarska-Jamroz, M., Nartiss, M., Krievans, M., Soms, J., 2016. Seismites resulting from high frequency, high-magnitude earthquakes in Latvia caused by Late Glacial glacio-isostatic uplift. *J. Palaeogeogr.* 5, 363–380.
- Waldron, J.W.F., Gagnon, J.-F., 2011. Recognizing soft-sediment structures in deformed rocks of orogens. *J. Struct. Geol.* 33, 271–279.
- Walker, W., Jobe, Z.R., Sarf, J.F., Wood, L., 2021. Progradational slope architecture and sediment distribution in outcrops of the mixed carbonate-siliclastic Bone Spring Formation, Permian Basin, west Texas. *Geosphere* 17, 1268–1293. <https://doi.org/10.1130/GES02355.1>.
- Watturs, N.J., Rausch, D.E., Cartwright, J., 2003. Soft-sediment deformation in Lake Superior: evidence for an immature polygonal fault system. In: Van Rensbergen, P., Hillis, R.R., Maltman, A.J., Morley, C.K. (Eds.), *Subsurface Sediment Mobilization*, vol. 216. Geological Society, London, Special Publications, pp. 323–334.
- Weinberger, R., Levi, T., Alsop, G.I., Eyal, Y., 2016. Coseismic horizontal slip revealed by sheared clastic dikes in the Dead Sea basin. *Geol. Soc. Am. Bull.* 128, 1193–1206.
- Weinberger, R., Levi, T., Alsop, G.I., Marco, S., 2017. Kinematics of mass transport | Deposits revealed by magnetic fabrics. *Geophys. Res. Lett.* 44, 7743–7749. <https://doi.org/10.1002/2017GL074471>.
- Wetzler, N., Marco, S., Heifetz, E., 2010. Quantitative analysis of seismogenic shear-induced turbulence in lake sediments. *Geology* 38, 303–306.
- Williams, E., 1960. Intra-stratal flow and convolute folding. *Geol. Mag.* 97 (3), 208–214.
- Wils, K., Deprez, M., Kissel, C., Vervoort, M., Van Daele, M., Daryono, M.R., Cnudde, V., Natawidjaja, D.H., De Batist, M., 2021. Earthquake doublet revealed by multiple pulses in lacustrine seismo-turbidites. *Geology* 49. <https://doi.org/10.1130/G48940.1>.
- Woźniak, P.P., Belzyt, S., Pisarska-Jamroz, M., Woronko, B., Lamsters, K., Nartiss, M., Bitinas, A., 2021. Liquefaction and re-liquefaction of sediments induced by uneven loading and glacial earthquakes: implications of results from the Latvian Baltic Sea coast. *Sediment. Geol.* 421, 105944.